University of Thi-Qar Journal Vol.14 No.3 SEP 2019
Web Site: https://jutq.utq.edu.iq/index.php/main
Email: utj@utq.edu.iq

The bacteriological study of *Acinetobacter baumannii* isolated from burn patients in Al- Nasiriyah city - Iraq.

https://doi.org/10.32792/utq/utj/vol114/4/1

Safaa M.kathom **Intidhaar N. Abid***
***Dep. Pathological analysis –College of Science - University of Thi-Qar**
Emails: Intidhaar12ih-pa@sci.utq.edu.iq
alhasnawymary@gmail.com

Abstract

The aim of present study was to investigated some virulence factors of *Acinetobacter baumannii* as well as study their tolerance to some environmental factors. It was identified 20 isolates of *A.baumannii*. burn patients in Al-Hussien Teaching Hospital and other burn care units in Al-Nasiriyah city . The specimens were collected during period from August 2018 to February 2019. It were taken by swabs from pus of the burned area and then inoculated on blood agar and MacConkey agar. The isolates were diagnosed by microscopic examination, biochemical tests , API 20 E and Vitek- 2 system . some virulence factors of bacteria detected such as capsule , biofilm formation , colony factor antigens and gelatin liquification , the results revealed that100%, 85% ,75% and 65% of isolates were positive to capsule, biofilm formation , colony factor antigens producing and gelatin liquification respectively .The effect of some environmental factors on bacterial growth are studied .It is found that the optimal range of pH for bacterial growth is 6-10 ,and the optimal growth of bacteria in a concentration 5% of NaCl , as well as , it shows that all bacterial isolates have the ability to grow in 44 °C. Due to the spread of these bacteria in our hospitale ,especially in the burns unite , this study was doen o detecated its properties and virulence factors .

Keywords: *Acinetobacter baumannii* , Virulence Factors , environmental factors , burn patients

Introduction

Acinetobacter baumannii became wide spread particularly in intensive care units and burn care units because its considered normal flora in human body and change to opportunistic pathogen which have resistance to antibiotics (Poirel *et al.*, 2010 ; Abdel-El-Haleem, 2003) . The most infection that causes by these bacteria are included meningitis , urinary tract infection, peritoneal dialysis , heart disease , arthritis , osteomyelitis , eye infection and skin injuries(Braun,2008 ; Abston , 2000) .

Microbial colonization on open wounds and causes a local infection , it spread to deeper tissues lead to systemic infections, in most time the normal flora that opportunistic pathogens of burn injury (Ahmad *et al.*, 2006).

*Acinetobacter*spp. have thin hair structures on the surface. Pilli are thinner and shorter than the flagella, it facilitates adhesion and colons in host and it considered importing virulent factor of bacteria (Brooks *et al* ., 2004 ; Crouzet *et al*., 2014).

Acinetobacter spp. have two types of pilli ,thick pilli help in motile and thin pilli use by bacteria to adhesion on surface of host (Ishii *et al* .,2004 ; Gohl *et al* .,2006).

The pilli are consisting of lactin and its purified from Enterobacteriaceae , its protein structure consisted of subunit of polypeptide polymers ,these subunits called pillin , pillin is responsible of linking between the pilli and its specific receptor on the host (Gohl*et al* ., 2006).

Capsule the most of important virulence factors in *A. baumannii*, which protects from phagocytosis, dehydration,and make the bacteria more resistant to antibiotic and hosts defense ,this explains the ability of bacteria to survive in medical devices and hospital environment (Tomaras *et al*., 2003; Zhang *et al.*, 2003 ; Braun and Vidotto, 2004).

Although the *Acinetobacter* lives in single form, in most time it form aggregations with others and results mass that resist inappropriate environment and escape from the immune system , these masses are

called biofilm, it can adhere to both living and non-living surfaces (King *et al* .,2009 ; Lewis, 2010).

The biofilm formation assist the cell to tolerate many factors such as pH reduction, nutrient deficiencies, and the host defenses, therefore, it is important for bacteria to continuation causes injury (Sharma *et al.*, 2014).

Several studies indicated that the fimbriae and capsule contributed to forming biofilm membrane , therefore ,these bacteria show resistance against both the host immunity and antibiotics in high degree because the transfer same virulence plasmids that have antibiotic-resistant agents between bacteria cells (Klausen *et al*., 2003) . *A.baumannii* can form the biofilm membrane , therefor it has ability to colonize on medical devices and causes resistance to many antibiotics (Rao *et al.*, 2008). Other studies show the *A.baumannii* have evaluate biofilm production when isolated from 86 different hospitals and from various clinical specimens (Davey and Otool , 2000 ; Henwood *et al* ., 2002).

The gelatin enzyme can analysis gelatin , hemoglobin , casein and the collagen during injury that found in subcutaneous tissue, therefore it can destroy the host cell (Kanemistsu *et al.,* 2001). Other studies show the *A.baumannii* have gelatinase activity when isolated this bacteria from 86 different hospitals and from various clinical specimens (Cevahir., 2008).

The growth of bacteria at 44 °C is a physiological characteristic of the species *A. baumannii* which distinguish them from other species of genus Acinetobacter (Peymani *et al*., 2011 ; Doughari *et al*., 2011).These bacteria are tolerant to a high salt concentration of NaCl and it can grow in the pH range between 5.5 -8.5 (Hood *et al* ., 2010)

Materials and Methods

Specimens collections

Atotal of 205 burn patients of Al-Hussien Teaching Hospital and other burn care units in Al-Nasiriyah city were collected . The specimens were collected during the period from August / 2018 to February /2019. Swabs inoculated on blood agar and MacConkey agar. (Himedia , India) , isolates identification was performed by routine laboratory methods

including API 20 E system(BioMerieux , France) . andVitek- 2 system (GN-ID card to Gram negative identification) (BioMerieux , France)

1-Virulence factors detection

Gelatinase liquefaction

This test was used to detect the ability of bacteria to produce the gelatinase,the gelatin media tubes were seeded with the bacterial inoculms and then incubated at 37 ° C for 24 - 48 hours , after that , the tubes were cooled in refrigerator at 4 °C for 1-2 hours , the gelatin liquification was indicated to positive result (Colleeet *al*., 1996).

Biofilm formation

This test was performed by inoculating trypton soya broth with bacterial growth by the loop an it was incubated at 37 ° C for 48 hours, after that the media were decanted carefully and stained by 1% of crystal violet for 30 minutes, then washed with D.W. and left to dry at room temperature . The results were compared with negative control. The appearance of biofilm layer on tubes surface was indicated to positive result (MacFaddin, 2000).

Detection of Colony factor antigens (CFA)

The agglutination of RBC method was used according to Collee *et al*.,(1996) as the following :

1- RBC suspension was prepared from human blood (group O) in anticoagulant tubes and it was centrifuged at 2000 rpm for 5 minutes , it was washed with normal saline for three times by centrifuge 2000 rpm for 5 minutes , and then discarded the suspension.

2-The precipitate RBC was suspended with 3% normal saline,

3- It was prepared bacterial suspension by taking half of bacterial growth from TSA medium and mixing with 1 ml of 0.15 of NaCl , one drop of bacterial suspension was mixed with one drop of the RBC suspension on a glass slide and mix by stick.The control slides were prepared by using two slides ,one of them was contained bacterial suspension with normal

saline and the other slid was contained RBC suspension with normal saline .

4- The agglutination of RBC with bacteria was detected after 0.5 -2 minutes at room temperature .

Detection of capsule

The Indian ink method was used to detect the ability of bacterial isolates to the formation of the capsule according to MacFaddin(2000).

2-Detection the effect of some environmental factors on bacterial growth

Salt tolerance test

This test was performed by using a series of NaCl salt concentration from 0.5% to 6% in nutrient broth tubes and one tube was control without NaCl for comparison, these tubes were inoculated by bacteria and incubated at 37°C for 24 hours, after that it was determined the NaCl concentration of bacterial growth (Hood *et al* ., 2010).

Test the tolerate of pH change

this test was carried out by using a series tubes of nutrient broth in different values of pH from 1 to 14 , the pH was edited by using HCl and NaOH, these tubes were inoculated by bacterial growth and incubated at 37° C for 24 hours, after incubated period , it was determined the value of the pH in which the bacteria can grow (Garrity *et al* .,2005) .

Test thetolerate of high temperatures

All isolated bacteria of *A.baumannii* were cultured on MacConkey agar media and incubated at44°C for 24 hours (MacFaddin, 2000).

Results

Identification of *Acinetobacterbaumannii* .

*Acinetobacter baumannii*is isolated from bus of burn patients using blood agar and MacConkey agar , the isolates appear white to gray colonies , 2-3 mm in diameter and non-hemolytic ,when they are cultured on blood agar , on MacConkey agar , bacteria isolates appear small , smooth with a high creamy colonies .

*Acinetobacter baumannii*mi croscopically appear as gram-negative ,coccobacilli , non-motile , and encapsulated .

Biochemical test and API20 E kit are used to identification of *Acinetobacter baumannii*,the results show that *Acinetobacter baumannii*isolates are non motile , and give negative result to oxidase , indole ,methel red ,vogesproskauer and avirable to urease and gelatinase . All isolates are positive to catalase and simmons citrate , triple-sugar-iron test was AL-kaline / no change.

It is found that all isolates give negative result to β-galactosidase , arginine dihydrolase ,lysine decarboxylase ,ornithine decarboxylase , production of hydrogen sulfide , tryptophan deaminase , , fermentation of manors , inositol, sorbitol , rhamnose , sucrose ,and amygdalin ,and all isolates give positive results to fermentation of glucose, melibiose , and arabinose by Api20 E test . VITEK-2 system is used to confirmation , to identification of the bacterial isolates .

1-Investigation of some virulence factors of *A.baumannii* (biofilm ,Colony factor antigens and gelatin liquification)

The present study shows that the capacity of bacteria to forming the biofilm appears in 17 (85%) of isolates and 3 (15%) give negative result (Figure 1).

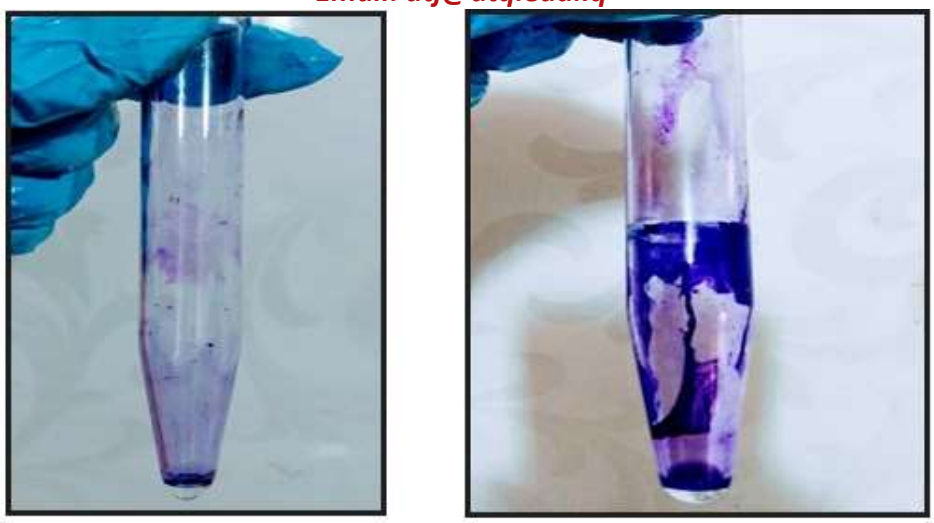

Figure (1): Biofilm formation in *A.baumannii* , the left tube shows the negative result , the right tube shows the positive result.

The results show that the 15 (75%) of isolates have the ability to clotting the RBC (have Colony factor antigens) and 5(25%) of isolates give negative result .

Table (1) shows13 that (65%) of isolates have the ability to gelatin liquification while 7(35 %) are negative to this test , and all isolates (100%) produce the capsule.

Table (1): Production of biofilm ,colony factor antigens and gelatin liquification of *Acinetobacterbaumannii*

Virulence factor	**No .& (%) of positive isolates**	**No .& (%) of negative isolates**
Biofilm	17 (85%)	3 (15%)
Colony factor antigens	15 (75%)	5(25%)
Gelatin liquification	13 (65%)	7(35 %)

Capsule	20(100%)	0(0%)

2-Effect of some environmental factors on bacterial growth .

The isolates of *Acinetobacterbaumannii* are tested for their ability to grow in different degrees of pH are ranged between 1-14 ,the results show that , the optimal range of growth bacteria is between 6-10 .

When tested the isolates to tolerance of different concentration of NaCl , the results show that ,the optimal growth of *Acinetobacterbaumannii*is at 5% of NaCl .

From the results, it is appeared that all bacterial isolates have the ability to grow in high temperature (44 °C) for 24 hr(Table 2).

Table (2): Effect pH, NaCl and temperature on growth of *Acinetobacterbaumannii.*

The factor	Optimal degree or range of bacterial growth	No. & (%)of positive isolates
PH	6-10	20 (100%)
NaCl	5%	20(100 %)
Temperature	44°C	20 (100%)

4.Discussion

The epidemiology of*Acinetobacter baumannii* was different from hospital to another, but in the most cases it became at the fifth rate of epidemiological bacteria in burns patients after *Pseudomonas aeruginosa, Staphylococcus aureus* ,*E. coli* and *Enterobacter*spp. (Karah ,2011) .

The current study shows 85% of *A. baumannii* to have the ability to produce biofilm , these results agree with those obtained by Nahar *et al*., (2012) who found 75% of *A. baumannii*that are able to formation biofilm , Cevahir*et al*. (2008) show that 61 from 86 of *Acinetobacter*spp. are forming biofilm. The reason for the differences in the biofilm formation may be due to several factors, including humidity, temperature and

oxygen (Gotz, 2002). Many studies reported that ,the ability of bacteria to biofilm formation are assist in resistance to antibiotics, phagocytosis, opsonisation and various environmental conditions (Abdulla *et al.*, 2015).

The colony factor antigens are considered from pathogencity factors that aid to adherence of bacteria on mucous surface and epithelial cell of respiratory tract , urinary , genital and gastric tract (Brooks*et al* ., 2004). The results demonstrate that 75% of bacterial isolates are possessed these factors , these percentage are higher than that in results of Cevahir*et al*. (2008) who found 22 out of 86 isolates of *A.baumannii* are able to produce CFA.

Bacteria are capable to adherence on the surface of host cells as well as protecting them from inappropriate environmental conditions. This explains the long-term survival of bacteria in the hospital environment and causes the nosocomial infections (Ramos *et al.*, 2013).

The gelatinase is an important virulence factor of bacteria that uses lysis gelatin and collagen in subcutaneous tissue during wound infection,and assists bacteria to penetrate the cell membrane where infected humans and animals (Abdulla , 2015).

The results of this study show that 65% of *A.baumannii* is a positive for production the gelatin enzyme .These results were agreement with the results of Valli and Gopinath (2016) who found that the percentage of the gelatin enzyme production were 60% while the results were disagree with studies of Cevahir*et al.* (2008) and Nahar*et al.* (2012) they founded the production of gelatinase by their isolates of *A.baumannii* were 14% and 0% respectively .

The results show that , *A.baumannii* can grow in pH ranged between 6-10 .These results identical with Hood *et al* ., (2010) show the *Acinetobacter*spp. can grow in the pH range between 5.5 -8.5 , Garrity*et al* .,(2005) , founded the *Acinetobacter*spp. can grow in the pH ranged between 5 -8.

In palcosol, Hrenovic*et al* .,(2014) show that the isolates of *Acinetobacter*spp. able to survive in a low pH (3.37), desiccation and in a high temperature (50°C).

This difference in results may be due to the acquired the new mutations by bacteria in recent years (Hood *et al* ., 2010) , or the other studies are included other species of *Acintobacter*and the current study was included *A. baumanniii* .

The recent study is founded *A. baumannii* isolates grow at 44°C , The growth of bacteria at 44 °C is a physiological characteristic of the species *A. baumanniii* which distinguish them from other species of genus *Acinetobacter* (Peymani*et al*., 2011).

These bacteria are tolerant to a high salt concentration of NaCl, which has reached 5%. These results similar with both Hrenovic and Ivankovic (2009) and Jasim (2014) who observed that the level of growth is decreased when the NaCl concentration increased . The tolerance of bacteria to high concentration of salts makes it highly resistant to many antibiotics (Hood *et al* ., 2010).

This study shows that the *A. baumannii* isolates are possess many virulence factors such as hemolysin , gelateinase production , Colony factor antigens , capsule and biofilm . *A. baumannii* tolerates some environmental factors such as pH ,NaCl , and a high temperatue . Therefor other studies are necessary to determine other virulence factors in bacteria.

References

- **Abdel-El-Haleem**, D. (2003). *Acinetobacter*: environmental and biotechnological applications. African Journal of Biotechnology, 2(4): 71-75.
- **Abdulla**, A.A.; AL Thahab, A. A.; Abed, T. A.; Mahdi, R. K. and Fadhil, S. (2015). Screening of virulence factors in *Acintobacter*

baumannii isolated from clinical samples. International Journal of Current Research and `Academic Review, 3 (6): 128-134.

- **Abston**, S.; Blakeney, P. and Desai, M. (2000). Post-burn infection and sepsis. Resident Orientation Manual. Galveston Shriners Burn Hospital and University of Texas Medical Branch Blocker Burn Unit.

- **Ahmad**, M.; Shahid, H.S.; Ibrahim, K.M. and Malik, S.A.(2006). Pattern of bacterial invasion in burn patients at the Pakistan institutes of medical sciences, Islamabactt. Annals of burns and fire Disasters. 19 (1).
- **Braun**, G. (2008). Virulence mechanisms of Acinetobacter. In: Bergogne-Berezin E., Friedman H., and Bendinelli M: *Acinetobacter* biology and pathogenesis. Springer p. 145-155.
- **Braun**, G. and Vidotto, M. (2004). Evaluation of Adherence, Hemagglutination, and Presence of Genes Codifying for Virulence Factors of *Acinetobacter baumannii* Causing Urinary Tract Infection.
- **Brooks**, G. F.; Butel, J. S.; and Morse, S. A. (2004) Jawtz, Melnck and Adelberg, s Medical Microbiology. 23th ed.McGrow-hill. New York .
- **Cevahir** , N. ; Demir , M . ; Kaleli , I . ; Gurbuz , M . and Tikvesli , S . (2008) Evaluation of biofilm production, gelatinase activity, and mannose-resistant hemagglutination in *Acinetobacter baumannii* strains . J Microbiol Immunol Infect ., 41:513-518.
- **Collee** , J.C. ; Fraser , A.G. ; Marmiam , B.P. and Simmon , S.A. (1996). Mackie and McCartney; Practical Medical Microbiology. 24th ed. The Churchill Livingstone. Inc. USA.
- **Crouzet**, M.; Lesencha, C.; Brozel, V. S.; Costagelioli, P.; Brath, C. and Bonnen, M. (2014). Exploring early steps in biofilmformation: set-up of an experimental system for molecular studies. Bio Med Central Microbiology, 14:253.

- **Davey**, B. E .and Otoole, G. A. (2000). Microbial Biofilms from ecology to molecular genetics. Microbiology of Molecular Biology Reviews, 64: 847-867.

- **Doughari** H.J., Ndakidemi P.A., Human, I.S., and Benade S. (2011). The ecology biology and pathogenesis of *Acineobacter* spp: An overview. Microbes Environ. 26: 101-112.

- **Garrity**, G. M.; Bell, J. A. J. and Lilburn, T. G. (2005). Taxonomic Outlineof the Prokaryotes, In Bergey's manual of Systemic Bacteriology. Second Edition. New York Berlin Heidelberg .
- **Gohl**, O. ; Friedrich, A.; Hoppert, M. & Averhoff, B .(2006) .The thin pill of *Acintobacter* spp. strains BD413 mediate adhesion to biotic and non biotic surfaces.Appl. Env. Microbiol., 72(2:(1394-1401 .
- **Gotz**, F. (2002). Staphylococcus and biofilms. Molecular of Microbiology, 43(6): 1367-1378.

- **Henwood**, C. J.; Gatward, T.; Warner, M.; James, D.; Stockdale, M. W.; Spence, R. P.; Towner, K. J.; Livermore, D. M. and Woodford, N. (2002). Antibiotic resistance among clinical isolates of *Acinetobacter* in the UK, and invitro evaluation of tigecycline (GAR – 936). Journal of Antimicrobiology Chemotherapy, 49: 479 - 487.

- **Hood** , M .; Jacobs ,A .C.; Sayood ,K.; Dunman ,P.M.; Skaar ,E.P.; (2010).*Acinetobacter baumannii* increases tolerance to antibiotics in response to monovalent cations. Mar;54(3):1029-41. doi: 10.1128/AAC.00963-09. Epub 2009 Dec 22.
- **Hrenovic** ,J.; Durn ,G., Goic-Barisic ,I.; Kovacic, A .(2014).Occurrence of an Environmental *Acinetobacter baumannii* Strain Similar to a Clinical Isolate in Paleosol from Croatia.;DOI: 10.1128/AEM.00312-14.
- **Hrenovic,**J . and Ivankovic, I. (2009). Survival of Escherichia coli and Acinetobacter junii at various concentrations of sodium chloride. DOI: 10.5053/ejobios.2009.3.0.18

- **Ishii** , S.I.; Koki , J.; Unno,H.; and Hori , K.(2004) Tow morphological types of cell appendage on a strongly adhesive bacterium , *Acinetobacter* sp . strain Tol5 . Appl. Env. Microbiol., 7(8): 5026 – 5029 .
- **Jasim** ,E. I.(2014). Comparative study on the effect of chloroxylenol and sodium chloride on *Brucella* and *Acinetobacter* growth.J.A.B.R, VOL. 4(3): 280-282 ISSN 2250 – 3579
- **Kanemitsu**, K.; Nishino, T.; Kunishima, H. and Okmura, N. (2001). Quantitative determination of gelatinase activity among *Enterococci.* Microbiology Methods, 47: 11- 6.
- **Karah,** N., (2011). Identification, molecular epidemiology, and antibiotic resistance characterization of *Acinetobacter* spp. clinical isolates. 109.
- **King** ,L. B., and Swiatlo ,E., *et al*. (2009). Serum resistance and biofilm formation in clinical isolates of *Acinetobacter baumannii*. FEMS Immunol Med Microbiol; 55: 414-421.
- **klausen**, M.; Heydorn, A.; Ragas, P.; Lambertsen, L.; Aaes-Jorgensen, A.; Molin, S. and Nielsen, T. (2003). Biofilm formation by *Pseudomonas aeruginosa* wild type, flagella and type IV pili mutant. Molecular Microbiology, 48(6): 1511-1524.
- **Lewis**, K. (2010). Persister cells. Annual review of microbiology, 64:357-372.
- **MacFaddin**, J. F. (2000). Biochemical tests for identification of medical bacteria (3rd ed.), Lippincott Williams and Wilkins, USA.
- **Nahar**, A.; Anwar, S.; Abu-Saleh, A. and Amin, M. (2012). Virulence factors and Antibiotic Susceptibility Pattern of *Acinetobacter* Species In a tertiary care Hospital in Bangladesh. Ibrahim Medical College Journal, 6(1): 27-30.
- **Peymani ,**A.; Nahaei ,M. R.; Farajnia ,S., *et al*. (2011).High prevalence of metallo-b-lactamase-producing *Acinetobacter baumannii* in a teaching hospital in Tabriz, Iran. Japanese Journal of Infectious Diseases.64:69–71.
- **Poirel**, L.; Naas, T. and Nordmann, P. (2010). Diversity, epidemiology and genetics of Class D100 ß-lactamases. Antimicrob. Agents Chemother. 54:24-38.

- **Ramos**, G.; Rocha, J. and Tuon, F. (2013). Seasonal humidity may influence *Pseudomonas aeruginosa* hospital acquired infection rates .International Journal of Infectious Disease, 17: 757-761.
- **Rao**, R. S.; Karthika, R. U.; Singh, S. P. ;Shashikala, P.; Kanungo, R.; Jayachandran, S. and Prashanth, K. (2008). Correlation between biofilm production and multiple drug resistance in imipenem resistant clinical isolates of *Acinetobacter baumannii*.Indian Journal of Medical Microbiology, 26: 333-337.
- **Sharma**, G.; Rao, S.; Bansal, A.; Dang, S.; Gupta, S. and Gabrani, R. (2014). *Pseudomonas aeruginosa* biofilm: potential therapeutic targets.Journal of Biologicals,42(1):1-7.
- **Tomaras** ,A.P.; Dorsey ,C.W.; Edelmann ,R.E. and Actis ,L.A. (2003). Attachment to and biofilm formation on abiotic surfaces by *Acinetobacter baumannii*: involvement of a novel chaperone-usher pili assembly system. Microbiology, 149: 3473-3484.
- **Valli**, B. and Gopinath, P. (2016). Detection of Gelatinase and Lipase among clinical isolates of *Acinetobacter baumannii*. Journal of chemical and pharmaceutical sciences, 9(4):3245-324.
- **Zhang**, Y. L.; Lau, Y .L.; Arakawa, E. and Leung, K. Y. (2003).Detection and genetic analysis of group II capsule in Aeromonas hydrophila. Microbiology.149 :1051 – 1060.

الخلاصة

تهدف الدراسة الحاليه الى عزل وتشخيص بكتريا *Acinetobacter baumannii* المعزولة من مرضى الحروق والكشف عن بعض عوامل الضراوة وتأثير بعض العوامل البيئية على النمو البكتيري .شملت هذه الدراسة جمع 205 مسحة سريرية من مرضى الحروق في مستشفى الحسين التعليمي ووحدات رعاية مرضى الحروق في مدينة الناصرية خلال الفترة الزمنية من اغسطس2018 الى شباط 2019 تم أخذ المسحات من قيح المناطق المحروقة للمريض ومن ثم زراعتها على أجار الدم وأجار ماكونكي. وقد تم تشخيص العزلات البكتيريه عن طريق الفحص المجهري ،الاختبارات الكيميائية الحيوية ،API 20 E و VITEK – 2.اظهرت الدراسة الحالية وجود 20 عزلة بكتيرية تابعة الى الجنس*A.baumannii* . تمت دراسة العديد من عوامل الضراوة لبكتيريا *A.baumannii* ومن بينها تكوين الغشاء الحيوي ،وإنتاج مستعمرات عوامل المستضدات ،تسييل الجيلاتين ووجود المحفظة ، وقد كانت النتائج 85 ٪ و 75 ٪ و 65 ٪ 100 ٪ على التوالي. تم دراسة تأثير بعض العوامل البيئية على نمو البكتيريا ومن بينها الرقم الهيدروجيني وتحمل الملوحة ودرجات الحرارة العالية . فقد وجد أنها تنمو في مدى يتراوح 6-

10 رقم هيدروجيني، وتنمو حتى تركيز 5 ٪ من كلوريد الصوديوم ، وكذلك لديها القدرة على النمو في درجات حرارة عالية تصل الى 44 درجة مئوية.

الكلمات المفتاحية : *Acinetobacter baumannii* ,عوامل الضراوة , عوامل البيئة , مرضى الحروق

The Frequency and Sensitivity Pattern of *Pseudomonas aeruginosa* among Otitis Media patients in Nasiriyah City

Zahraa A. Fadhel , Saad S. Hamim
Pathological analysis Department, Science College, Thi-Qar University, Iraq
Email: Saadalsalman1122@gmail.com

ABSTRACT

Otitis Media considered as one of the most common types of ear infections, as well as the most blamed etiology is bacterial. *Pseudomonas aeruginosa* is the most diagnosed pathogens causing these infections. *P. aeruginosa* has virulence factors that lead to damage to the mucosa of the middle ear. A total of two hundred and ten (210) samples collected from Otitis media patients whom consulting the Ear, Nose, and Throat (ENT) section in AL-Habbobi Teaching Hospital in Al-Nasiriyah City, Southern-Iraq. During the period from August 2018 to January 2019. *P. aeruginosa* accounted for 65 samples (30.95%). Almost of isolates were sensitive to Carbapenem. The present study concludes females constitute a high percentage of infection with Otitis media (P-value= 0.01) and younger ages are more exposed to the risk of Otitis media (P-value = 0.36). The present study aimed to detect the relationship between the prevalence of Otitis media and the parameters associated with patients like gender, age, housing, and the study period. Also studying the pattern of antibiotics Sensitivity for the targeted bacteria and detection of some virulence factors.

Keywords: Otitis media, *Pseudomonas aeruginosa,* Sensitivity test, Nasiriyah.

INTRODUCTION

Otitis Media

Otitis Media (OM) is a term referring to an infection of the middle ear. It is mostly caused by an accumulation of the fluid behind the eardrum, that result of obstruction the Eustachian tube. It is considered one of the most common infections in children because the Eustachian tube in children is shorter and more horizontal than adults, which it is formed of more flaccid cartilage, that it makes opening easily [1]. Clinically, Otitis Media (OM) include a broader range of disease, Acute Otitis Media (AOM), Chronic Suppurative Otitis Media (CSOM), and Otitis Media with Effusion (OME) [2]. The pathogenesis and the etiology of Otitis media are multiple including infections, allergy, genetic, racial, environmental, and social factors [3]. *P. aeruginosa* has the ability to colonize several sites because it contains effective adhesion mechanisms, Multidrug resistance, Biofilm formation and ability to survive in low nutritional requirements [4]. The incidence of the disease differs between the children and the adults. Children tend to develop AOM because the anatomical structure and the immune system are immature. While the ear infections in the adult are usually chronic infection [5]. Otitis media if untreated or left with incomplete treatment may be lead to complications, due to for many reasons like antimicrobial-resistant bacteria, or unknown causes. Other factors may be lead to complications such as immunological or anatomical factors, congenital malformations and the soft bony structures of kids may be more exposed to infection [6].

P. aeruginosa is infrequently found in nasopharynx by comparison with other types of bacteria. It is very rarely isolated from a healthy person ear canal [7, 8]. *Pseudomonas aeruginosa* can grow in strict conditions like the absence of special nutrition and can proliferate at the room temperature, and it has highly resistant to the antibiotic, all these causes making it difficult to treat [9]. A previous study in Baghdad

province isolated *P. aeruginosa* from Otitis media with a percentage of (30%) [10]. Globally, *P. aeruginosa* was isolated from these infections in Nigeria with a percentage of (28.8%) [11].

Virulence factors have a significant pathological role in adhering, colonization, the survival of microbe and lastly in the invasion of tissues [12]. Hemolysin is an enzyme produced by Gram-negative bacteria and Gram-positive such as *Pseudomonas aeruginosa*, *Staphylococcus aureus*, *Streptococcus pyogenes*, *Escherichia coli*, *Vibrio Vulnificus*, *Salmonella enterica*, *Proteus vulgaris* and *Proteus mirabilis* [13].

Pyocyanin is a blue-green pigment considered one of the most notable phenotypic characteristics of *P. aeruginosa*. Pyocyanin created in big quantities, particularly when bacteria are cultivated in low-iron media [14]. This pigmentation result from the excretion of phenazine compound pyocyanin (PCN), that acts as an important virulence factor in this bacteria, phenazine compound pyocyanin is readily isolated from the ear discharges and the sputum from *P. aeruginosa* infections [15].

The present study aimed to:

1- Detection of the relationship between Otitis media prevalence and the parameters associated with patients like gender, age, housing, and the study period.
2- Studying the pattern of antibiotic Sensitivity of *P. aeruginosa.*
3- Detected of some virulence factors of *P. aeruginosa* such as Hemolysin, and Pyocyanin.

Materials and Methods

Specimens

A total of 210 of middle ear swab samples were collected from Otitis media patients attending to the ENT Department in AL-Habbobi Teaching Hospital in Thi-Qar province, which includes both sexes of different ages. 99 males and 111females. The age groups of the patients ranged from less than ten years to more than fifty years. During the period from August (2018) to January (2019). These samples were collected by the ENT physicians by using a sterile swab. The information for each

patient was recorded in a special form, including name, age, gender, housing.

Isolation and identification

P. aeruginosa isolates culturing on Blood agar, MacConkey agar, and Cetrimide agar. Also diagnosed with different biochemical tests, including Oxidase test, Catalase test, gram staining, and phenotypic characteristics, the diagnosis was confirmed with VITEK-2 compact System (BioMerieux, France) at probability level between 98%-99%. *P. aeruginosa* in blood agar appears as a large, gray to dark colonies and some isolates were beta hemolysis. While in MacConkey agar *P. aeruginosa* was non-lactose fermenter with pale colonies, All *P. aeruginosa* isolates were grown on cetrimide agar as a selective medium for this bacteria to distinguish it from other species in this genus [16].

Detection of some Virulence Factors

Hemolysin production

A blood agar plate (5%) was inoculated with bacteria and incubated at (37 °C) for (24 h) for detection of beta hemolysis. Hemolysin production was detected by the presence of a clear zone around the colonies (complete lysis for RBCs) [17].

Pyocyanin production

Young colonies at (18-24 h) were inoculated on Muller-Hinton agar and incubated at (37°C) for (24 h). This medium is used for detection the

ability of *Pseudomonas aeruginosa* to produce pyocyanin pigment, which considered as an important diagnostic for this bacteria [18].

Antibiotic sensitivity test

In this study used 12 antibiotics from different classes (Bioanalyse, Turkey and Mast Group, England) Amikacin (10 µg), Aztreonam (30 µg), Cefepime (30 µg), Ceftazidime (30 µg), Ciprofloxacin (10 µg), Gentamicin (10 µg), Imipenem (10 µg), Levofloxacin (5 µg), Meropenem (10 µg), Ofloxacin (5 µg), Piperacillin (100 µg), Tobramycin (10 µg). Antibiotic sensitivity test was performed using Kirby Bauer disc diffusion method [19]. A bacterial suspension was prepared by inoculated 2-3 fresh colonies at (24 h) into test tube contains (3 ml) of normal saline. The suspension turbidity was compared with McFarland turbidity (0.5) that equal to 1.5×10^{8} CFU/ml. The bacterial suspension for each isolate was streaked in three different directions on Muller-Hinton agar plates by using a sterile cotton swab after pressed the swab several times on the inside wall of the tube to remove the excess inoculum. The plates were left to dry for (10 minutes) at room temperature. The antibiotic discs were applied to the medium surface by using a sterile forceps and the plates were incubated at (37°C) for (24 h). The diameter of the inhibition zone for each antibiotic disc was measured by using a plastic ruler (mm), and the results were interpreted based on CLSI, 2018 [20].

Statistical Analysis

The results in the present study were evaluated statistically via Chi-square by using Statistical Package for Social Sciences (SPSS) program version 23 at a probability of ($P \leq 0.05$) as a significant level between the parameters of the present study like gender, age, the study period, residency and some of virulence factors.

Results

After samples collection and performing all the diagnostic tests, the positive culture of *P. aeruginosa* was 65 samples (30.95%). The present study results for total samples revealed females more infected with Otitis media with111 cases (52.86%) and 99 cases (47.14%) for males. with regard to the relationship between *P. aeruginosa* rate infections with gender. Females recorded with 40 cases (61.54%), compared to males with 25 cases (38.46%), there was a significant difference (P-value= 0.01) in gender distribution (Figure 1).

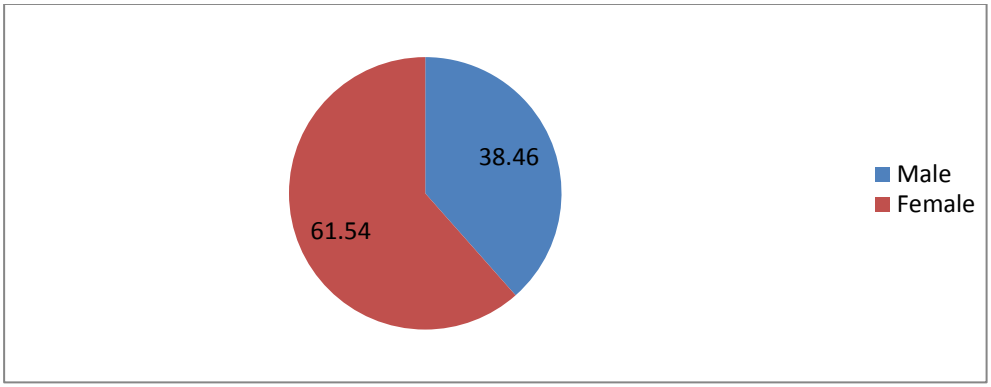

Figure (1): Patients distribution according to the gender.

With regard to the age, the present study showed the predominance the third group of age (21-30) years for total samples with percentage (21.43%). The highest incidence of Otitis media caused by *P. aeruginosa* also was in the age group of (21-30) years with 15 patients (23.08%). While the lowest occurrence was noticed with patients in the groups of (41-50) and more than 50 years with a percentage of (12.31%) for both. Statistically, have not a significant difference among these groups (P-value = 0.36) (Table 1).

Table 1: Patients distribution according to age groups

No.	Age	No. of Total Isolates	%	No. of *P. aeruginosa* Isolates	%
1	<10	37	17.62	10	15.38
2	11-20	39	18.57	12	18.46
3	21-30	45	21.43	15	23.08
4	31-40	39	18.57	12	18.46
5	41-50	21	10	8	12.31
6	>50	29	13.81	8	12.31
	Total	210	100	65	100

The relationship between the study period parameter and Otitis media for total samples revealed the highest percentage of Otitis media was in November (24.76%). Also, this study showed the highest percentage for *P. aeruginosa* targeted infections with 19 patients (29.23%) in November. While the lowest rate of infection was in January (3.08%), there was a significant difference (P-value = 0.00) between *P. aeruginosa* infections rates and the months of years (Table 2).

Table 2: Patients Distribution according to the study period

Month	No. of Total Isolates	%	No. of *P. aeruginosa* Isolates	%
August	28	13.33	9	13.85
September	31	14.76	10	15.38
October	45	21.43	14	21.54
November	52	24.76	19	29.23
December	40	19.05	11	16.92
January	14	6.67	2	3.08
Total	210	100	65	100

According to the residency, the total samples revealed the highest percentage of Otitis media was in urban 130 patients (61.90%) and in rural 80 patients (38.10%), with respect to *P. aeruginosa* infections were 36 patients (55.38%) in urban and lower in rural with 29 patients (44.62%), there have not a significant difference according to the otitis

media occurrence with *P. aeruginosa* and the residency (P-value = 0.31) (Figure 2).

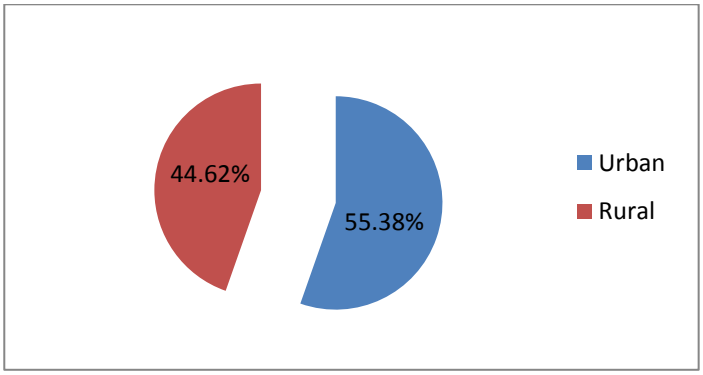

Figure 2: Distribution of the patients according to residency

Virulence factors

The present study results showed the ability of *P. aeruginosa* isolates to hemolysin production in 49/65 (75.38%) of the isolates, there was a significant difference in the production of this enzyme (P-value= 0.00). Pyocyanin production was detected on Muller Hinton agar, 32/65 (49.23%) isolates were Pyocyanin Production, there was a non-significant difference in the production of pyocyanin (P-value= 0.84) (Figure 3).

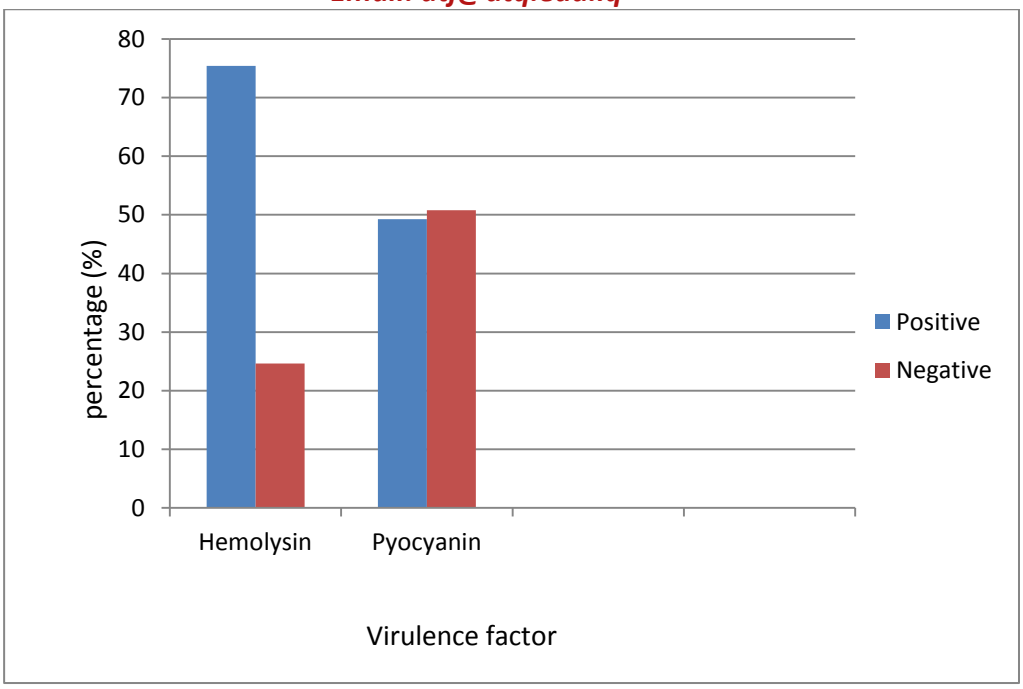

Figure (3): Percentages of virulence factors of *P. aeruginosa* isolates

Antibiotic sensitivity test of *Pseudomonas aeruginosa*

The antibiotic sensitivity results showed a high sensitivity of *P. aeruginosa* isolates to Carbapenems, 63/65 (96.92%) were sensitive to Imipenem. Followed by Meropenem with 61/65 (93.84%). *P. aeruginosa* showed high resistance to Cephalosporins 64/65 (98.46%) and 62/65 (95.38%) isolates were resistant to Ceftazidime and Cefepime, respectively (Figure 4).

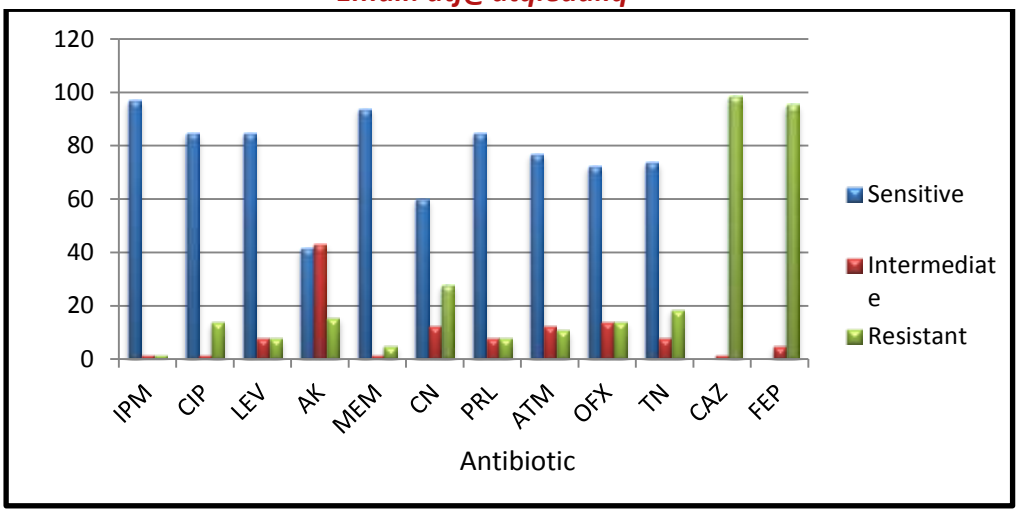

Figure (4): Antibiotic sensitivity of *P. aeruginosa*

Discussion

The results of the present study showed *P. aeruginosa* was the most common cause of Otitis media with the highest ratio of isolation. *P. aeruginosa* considered a ubiquitous microbe which exists in wide ranges of environments, developing mechanisms to antibiotic resistance persistently, ability to compete with other organisms, and widely distributed in the swimming water [21]. The present study results were inconsistent with other studies in Diyala and Baghdad provinces with a percentage of (30.6%, and 33.33%), respectively [22, 23]. Also agree with another previous study in Palestine, that showed the percentage of *P. aeruginosa* was (32.5%) [24]. On the other hand, the present study results conflicts with many former studies in Thi-Qar, and Kufa Cities, where recorded the percentage of *P. aeruginosa* as following (53.14%, 18%), respectively [25, 26]. The variations in the percentages of bacterial type

depend on the geographical regions, the environmental factors, and the health state of people [27].

The present study results revealed the percentage of Otitis media was higher in females compared with males. Higher rates of infections in females may be due to many reasons such as females constitute a higher percentage of the population surveyed in Iraqi society, based on the latest statistical account in Iraq was found that the females comprise 55% of the Iraqi population [28]. Other reasons may include direct contact with the polluted environment, and polluted water, as well as exposed to trauma that affect the ear due to rapid change in the pressure between the middle ear and the surrounding air [29, 30]. The present study results agree with a previous study in Baghdad province where mention the rates of infection in females (25%) compared with males (19%) [31].

The present study results showed the highest rates of Otitis media were located in the third group in the age (21-30) year. The high percentage of Otitis media in this age group, due to this group of the population are more exposed to several factors like environmental factors, practicing swimming in polluted water, smoking and different lifestyles [27]. *P. aeruginosa* is considered from the Contaminants of the water of the river, and using of these water in swimming is an important way of infection with this bacteria especially otitis media [32]. The present data discrepancy with a former study performed in India, where revealed the highest percentage of Otitis media was in the age (11-20) with 31 cases, while in the age (21-30) with 14 cases [33]. Also, a previous study in Korea showed the percentage of infection with *P. aeruginosa* in (21-30) age group was (4.1%) [34].

The current study data showed that the occurrence of Otitis media was the highest in November. In the present study the highest rates of infection in the Autumn season, especially in November due to the nasal allergy that is considered as a risk factor for occurrence otitis media. The role of inflammatory mediators like cytokines and colony stimulatory factors that secreted by mast cells in response to an allergen resulting in mucosal damage and increased secretions. 30-45% of patients with allergic rhinitis also suffering from otitis media. The allergic rhinitis patients have increased secretions in eustachian tubes and middle ear, that may be resulting in the development of otitis media [35]. This result seems to be approximated with a study conducted in Korea was reported the highest percentage of otitis media in Autumn season, the percentage of chronic suppurative Otitis media with *P. aeruginosa* in November was (24.5%) [36].

In the current study, the percentage of patients with Otitis media that caused by *Pseudomonas aeruginosa* was higher in urban than a rural area. Most patients attending the hospital from urban areas and the polluted environment compared with the rural area that considered predisposing factors for Otitis media, an earlier study performed in Al- Hawija City recorded a higher percentage of Otitis media in urban area (71.6%) compared with the rural area [37].

The present study showed a bit high beta hemolysis activity of the targeted bacteria. Hemolysin causes disrupting of tissue and releasing the host nutrients like iron this improves the ability of bacteria to grow and multiply within the host cell [38]. A predate study performed in Babyl

province reported (30%) of *P. aeruginosa* isolates have the ability to hemolysin enzyme production [39].

The present study showed that about half of *P. aeruginosa* isolates were positive to Pyocyanin Production. *P. aeruginosa* has a single polar flagellum is important to mediate chemotactic signaling when occurring changes in the environment as a response process for these changes, flagellum-deficient mutant strains are suffering from an inability to regulate Quorum sensing-signalling molecules that are basic for pyocyanin production [40, 41]. A previous study isolated *P. aeruginosa* from different clinical isolates included otitis media cases showed (78.66%) of isolates have the ability of Pyocyanin Production [42].

Antibiogram results for the studied isolates showed high sensitivity to Imipenem and Meropenem (Carbapenems). The penems (Meropenem and Imipenem) antibiotic structure differs a little of the penicillins structure. These antibiotics possess a wider spectrum of activity against gram-positive and gram-negative bacteria. Due to they are more reluctant to beta-lactamase hydrolysis [43]. The present study agrees with a previous study in Najaf province found the percentage of Imipenem sensitivity was (100%) [44].

The current study result reported high sensitivity of Ciprofloxacin, Levofloxacin, and Ofloxacin (Fluoroquinolones). Fluoroquinolones group have a broad spectrum of activity for microbes and active against *P. aeruginosa*. This group targets the bacterial topoisomerase II, and DNA gyrase and consequent inhibition the DNA replication. The resistance to fluoroquinolones is developed as a reflection of a mutation that resulting

from the selective pressure of the random usage of these antibiotics [45]. The present study results approximated with an earlier study in Basrah City showed the percentage of Ciprofloxacin sensitivity (75%) [46]. A quondam study was performed in Diala province found all isolates were sensitive to Ofloxacin [22].

The sensitivity results of Amikacin, Gentamicin, and Tobramycin (Aminoglycosides) in the present study showed a low percentage by comparison with other studies. The current study results disagree with a previous study in Baqubah City that showed the percentages of Gentamicin and Amikacin sensitivity were (81%, and 85%), respectively [47]. A former study carried out in Baghdad province revealed Tobramycin active against (67.7%) of isolates [48]. In the present study, Amikacin sensitivity percentage disagrees with most previous studies,that revealed high sensitivity to Amikacin. Whereas with regard to our study revealed (43.07%) were intermediate isolates, this means most isolates tend to become more resistant.

The present study showed the majority of isolates were sensitive to Piperacillin (which belongs to Penicillins) and Aztreonam (Monobactams). Aztreonam is a monobactam antibiotic, it has great activity against gram negative, and also active against β-lactamase producing bacteria [49]. This result came differently from a predate study in Najaf province that found from total 40 isolates only (19 and 14) isolates were sensitive to Piperacillin and Aztreonam, respectively [44].

The current study results showed high resistance to Cephalosporine generations. The development of resistance to Cephalosporin generations

is considered a warning sign to stop the random antibiotic using. Because these groups are considered a potent anti-Psuedomals [50, 51]. A previous study performed in Baghdad province found the sensitivity percentages of Ceftazidime and Cefipime (81.8%, and 0.0%), respectively [48].

Conclusion

Pseudomonas aeruginosa seems to be the predominant pathogen in Otitis media patients. Patient's gender may consider as a risk factor in Otitis media infections. Younger ages were the most infected with Otitis media by *P. aeruginosa*. The majority of isolates were resistant to Cephalosporins.

References

[1] Bluestone, C. D., & Klein, J. O. (2001). Microbiology. In: Bluestone, C. D., Klein, J. O. (eds.). Otitis Media in Infants and Children. (3rd ed.). W. B. Saunders. Philadelphia, USA., Pp. 1014.

[2] Lieberthal, A. S., Carroll, A. E., Chonmaitree, T., Ganiats, T. G., Hoberman, A., Jackson, M. A., ... & Schwartz, R. H. (2013). The diagnosis and management of acute otitis media. Pediatrics, 131(3), e964-e999.

[3] Maharjan, M., Bhandari, S., Singh, I., & Mishra, S. C. (2006). Prevalence of otitis media in school going children in Eastern Nepal. Kathmandu University Medical Journal, 4(4), 479-482.

[4] Fricks-Lima, J., Hendrickson, C. M., Allgaier, M., Zhuo, H., Wiener-Kronish, J. P., Lynch, S. V., & Yang, K. (2012). Differences in biofilm formation and antimicrobial resistance of

Pseudomonas aeruginosa isolated from airways of mechanically ventilated patients and cystic fibrosis patients. International Journal of Antimicrobial Agents, 37(4), 309-315.

[5] Bluestone, C. D. (2008). Impact of evolution on the eustachian tube. The Laryngoscope, 118(3), 522-527.

[6] Stenfeldt, K., Enoksson, F., Stalfors, J., Hultcrantz, M., Hermansson, A., & Groth, A. (2014). Infants under the age of six months with acute mastoiditis. A descriptive study of 15 years in Sweden. International Journal of Pediatric Otorhinolaryngology, 78(7), 1119-1122.

[7] Stroman, D. W., Roland, P. S., Dohar, J., & Burt, W. (2001). Microbiology of normal external auditory canal. The laryngoscope, 111(11), 2054-2059.

[8] van Dongen, T. M., Venekamp, R. P., Wensing, A. M., Bogaert, D., Sanders, E. A., & Schilder, A. G. (2015). Acute otorrhea in children with tympanostomy tubes: prevalence of bacteria and viruses in the post-pneumococcal conjugate vaccine era. The Pediatric Infectious Disease Journal, 34(4), 355-360.

[9] Mansoor, T., Musani, M. A., Khalid, G., & Kamal, M. (2009). Pseudomonas aeruginosa in chronic suppurative otitis media: Sensitivity spectrum against various antibiotics in Karachi. Journal of Ayub Medical College Abbottabad, 21(2), 120-123.

[10] Aldhaher, Z. A., Hassan, H. F., Al-Jassim, Z. G., & Mahmood, M. A. (2018). Bacterial isolates and antibiotic susceptibility of ear infections in Iraqi patients. International Journal of Biosciences, (13)1, 292-297.

[11] Onifade, A. K., Afolayan, C. O., & Afolami, O. I. (2018). Antimicrobial sensitivity, extended spectrum beta-lactamase (ESBL) production and plasmid profile by microorganisms from Otitis media patients in Owo and Akure, Ondo State, Nigeria. Karbala International Journal of Modern Science, 4(3), 332-340.

[12] Hogardt, M., & Heesemann, J. (2013). Microevolution of *Pseudomonas aeruginosa* to a chronic pathogen of the cystic fibrosis lung. Current Topics in Microbiology and Immunology, 358, 91-118.

[13] Tiwari, R. P., Deol, K., Rishi, P., & Grewal, J. S. (2002). Factors affecting haemolysin production and Congo red binding in *Salmonella enterica* serovar Typhimurium DT 98. Journal of Medical Microbiology, 51(6), 503-509.

[14] Barakat, R., Goubet, I., Manon, S., Berges, T., & Rosenfeld, E. (2014). Unsuspected pyocyanin effect in yeast under anaerobiosis. MicrobiologyOpen, 3(1), 1-14.

[15] Lau, G. W., Hassett, D. J., Ran, H., & Kong, F. (2004). The role of pyocyanin in *Pseudomonas aeruginosa* infection. Trends in Molecular Medicine, 10(12), 599-606.

[16] MacFaddin, J. F. (2000). Biochemical test for identification of medical bacteria. (3rd ed.). Lippincott Williams & Wilkins. USA., Pp. 555-565.

[17] Kayser, F. H., Bienz, K. A., Eckert, J., & Zinkernagel, R. M. (2005). Medical Microbiology. (9th ed.). Thieme. Stuttgart. New York, Pp. 698.

[18] Brown, P. D., & Izundu, A. (2004). Antibiotic resistance in clinical isolates of *Pseudomonas aeruginosa* in Jamaica. Revista Panamericana de Salud Publica, 16, 125-130.

[19] Bauer, A. W., Kirby, W. M. M., Sherris, J. C., & Turck, M. (1966). Antibiotic susceptibility testing by a standardized single disk method. American Journal of Clinical Pathology, 45(4), 493-496.

[20] Clinical and laboratory standards institute. (2018). Performance standards for antimicrobial susceptibility testing. (28th ed.). Clinical and Laboratory Standards Institute Document, M100: Wayne, USA.: Pp. 39-40.

[21] Hailu, D., Mekonnen, D., Derbie, A., Mulu, W., & Abera, B. (2016). Pathogenic bacteria profile and antimicrobial susceptibility patterns of ear infection at Bahir Dar Regional Health Research Laboratory Center, Ethiopia. SpringerPlus, 5(1), 466.

[22] Mubarak, K. I., Farhan, A. A., & Razuki, B. M. (2011). Bacterial Otitis Media in Diyala. Journal of Technique, 24(7), A19-A30.

[23] Hamid, A. N., Al Maeny, S. A. L., & Nader, M. I. (2017). Relationship of Lectins *Pseudomonas aeruginosa* bacteria with some other virulence factors. Al-Anbar Journal of Veterinary Sciences, 10(1), 108-118.

[24] Elmanama, A. A., Tayyem, N. E. A., & Allah, S. A. N. (2014). The bacterial etiology of otitis media and their antibiogram among children in Gaza Strip, Palestine. Egyptian Journal of Ear, Nose, Throat and Allied Sciences, 15(2), 87-91.

[25] Jafat, N. N. (2013). Isolation and identification of some bacteria that causes inflammation of otitis media in Thi-Qar. Journal of Thi-Qar Science, 3(4), 11-16.

[26] Al-Mohana, A. M., Al-Yasiri, I. K., & Al-Toriahi, T. S. A. D. (2008). ß-Lactamase Producing Bacteria Isolated From Patients Infected With Otitis media. Kerbala Journal of Medicine, 2(3), 289-294.

[27] Jreemich, S. K. (2014). Isolation of Some Bacteria from Chronic Otitis Media. Al-Qadisiyah Medical Journal, 10(18), 159-163.

[28] Alrubaiee, A. R. H., & Abdulwahed, A. G. (2013). Chronic Suppurative Otitis media risk factors in our society. Basrah Journal of Surgery, 19(2), 40-47.

[29] Poorey, V. K. (2002). Study of bacterial flora in CSOM and its clinical significance. Indian Journal of Otolaryngology, Head and Neck Surgery, 54(2), 91-95.

[30] Hassooni, H. R., Fadhil, S. F., Hameed, R. M., Alhusseiny, A. H., & Jadoo, S. A. A. (2018). Upper respiratory tract infection and otitis media are clinically and microbiologically associated. Journal of Ideas in Health, 1(1), 29-33.

[31] Alkhlifawi, I. J. (2013). Isolation & Identification of Bacteria Causes Otitis Media in Children, Study the Resistance to Antimicrobials and The Effect of Cerumen and Xylitol on Selected Isolated Bacteria. Journal of Karbala University, (11)1, 12-19.

[32] Magtooph, M. G., & Kredy, H. M. (2006). Secretion ß-lactamase Enzyme from some Gram negative Bacteria Causing Chronic

Otitis Media disease In Nassriya. Tikrit Journal of Pure Science, 11(1), 1-4.

[33] Deshmukh K. A., & Manthale D. (2017). Prevalence and antibiotic susceptibility of *Pseudomonas aeruginosa* isolated from chronic suppurative Otitis media. International Journal of Otorhinolaryngology and Head and Neck Surgery, 3(1), 56-60.

[34] Kim, S. H., Kim, M. G., Kim, S. S., Cha, S. H., & Yeo, S. G. (2015). Change in detection rate of methicillin-resistant *Staphylococcus aureus* and *Pseudomonas aeruginosa* and their antibiotic sensitivities in patients with chronic suppurative otitis media. The Journal of International Advanced Otology, 11(2), 151-156.

[35] Acuin, J., & Browning, G. G. (2002). Clinical review Chronic suppurative otitis media Commentary: Interpreting the evidence. British Medical Journal, 325(7373), 1159-1160.

[36] Lee, S. K., Lee, M. S., Jung, S. Y., Byun, J. Y., Park, M. S., & Yeo, S. G. (2010). Antimicrobial resistance of *Pseudomonas aeruginosa* from otorrhea of chronic suppurative otitis media patients. Otolaryngology-Head and Neck Surgery, 143(4), 500-505.

[37] Ali, M. J. (2011). Isolation and Identification the bacterial causes agent of otitis media in patients with otitis media in AL-Hawija City. Tikrit Journal of Pure Sciences, 16(1), 106-111.

[38] Bnyan, I. A., & Ahmed, H. F. (2013). Effect of some factors on extracellular hemolysin filtrate from bacterial *Pseudomonas aeruginosa* isolated from burn infection in Hilla city. Research in Pharmacy, 3(2), 26-32.

[39] Razzak, M. S. A., Muhsin, M. A., & Al-wae'li, N. k. K. H. (2009). Study of Some Characteristics of the Bacteria Isolated from Patients with Otitis Media in Babylon Province. Medical Journal of Babylon, 6(2), 225-234.

[40] Juhas, M., Eberl, L., & Tummler, B. (2005). Quorum sensing: the power of cooperation in the world of *Pseudomonas*. Environmental Microbiology, 7(4), 459-471.

[41] Kuang, Z., Hao, Y., Hwang, S., Zhang, S., Kim, E., Akinbi, H. T., Schurr, M. J., Irvin, R.T., Hassett, D. J., & Lau, G. W. (2011). The *Pseudomonas aeruginosa* flagellum confers resistance to pulmonary surfactant protein- A by impacting the production of exoproteases through quorum- sensing. Molecular Microbiology, 79(5), 1220-1235.

[42] Abdullah, R. M., & Mehdi, A. F. (2016). Identification of *Pseudomonas aeruginosa* from clinical specimens by using 16S rDNA gene. Journal of Biotechnology Research Center, 10(1), 45-49.

[43] Clinical and Laboratory Standard Institute (2006). Performance standards for antimicrobial susceptibility testing. (16^{th} ed.). Informational Supplement. Clinical and Laboratory Standard Institute Document, M100-S16: Wayne, Pennsylvania.

[44] Al-zubaidy, I. (2014). Microbiological assessment of chronic suppurative otitis media. Kufa Journal for Nursing Scinces, 3(4), 101-105.

[45] Sheng, W. H., Chen, Y. C., Wang, J. T., Chang, S. C., Luh, K. T., & Hsieh, W. C. (2002). Emerging fluoroquinolone-resistance for common clinically important gram-negative bacteria

inTaiwan. Diagnostic Microbiology and Infectious Disease, 43(2), 141-147.

[46] Alsaimary, I. E., Alabbasi, A. M., & Najim, J. M. (2010). Antibiotics susceptibility of bacterial pathogens associated with otitis media. African Journal of Bacteriology Research,2(4),41-50.

[47] Muhammed, N. K., & Hamood, H. J. (2016). Role of Bacteria in chronic Suppurative Otitis Media and Sensitivity pattern in Baqubah Teaching Hospital. Diyala Journal of Medicine, 10(2), 25-33.

[48] AL-Ataar, Z. I. (2015). The prevalence and antimicrobial resistance of *Pseudomonas* species in patients with chronic suppurative otitis media. Al-Kindy College Medical Journal, 11(1), 49-52.

[49] Gul, A. A., Ali, L., Rahim, E., & Ahmed, S. (2007). Chronic suppurative otitis media: frequency of *Pseudomonas aeruginosa* in patients and its sensitivity to various antibiotics. Professional Medical Journal, 14(3), 411-5.

[50] Kumar, H., & Seth, S. (2011). Bacterial and fungal study of 100 cases of chronic suppurative otitis media. Journal of Clinical and Diagnostic Research, 5(6), 1224-1227.

[51] Suhail, Z., Ashrafi, A. K., Malik Iqbal, S. S., Khambaty, Y., Khan, A. F., & Sajjad Qaiser, M. S. (2012). Microorganism and Anti-Microbial Resistance of Bacterial Agents in Chronic Suppurative Otitis Media Patients at Abbasi Shaheed Hospital. Pakistan Journal of Otolaryngology, 28, 92-94.

University of Thi-Qar Journal Vol.14 No.3 SEP 2019
Web Site: **https://jutq.utq.edu.iq/index.php/main**
Email: utj@utq.edu.iq

تواتر ونمط الحساسية للزائفة الزنجارية بين مرضى التهاب الاذن الوسطى في مدينة الناصرية

المستخلص

يعد التهاب الأذن الوسطى أحد أكثر أنواع التهابات الأذن شيوعا. بالاضافة الى ان المسببات الاكثر هي بكتيرية. الزائفة الزنجارية هي أكثر الممرضات المشخصة التي تسبب هذه العدوى. تمتلك الزائفة الزنجارية عوامل ضراوة تودي الى تلف الغشاء المخاطي المبطن للاذن الوسطى. تم جمع مئتان وعشرة عينة من المرضى الذين راجعوا قسم الانف والاذن والحنجرة في مستشفى الحبوبي التعليمي في مدينة الناصرية جنوب العراق. خلال الفترة من شهر أب 2018 الى شهر كانون الثاني 2019. شكلت الزائفة الزنجارية 65 عينة بنسبة (30.95%) . وكانت معظم العزلات حساسة لصنف الكاربابينيم. وخلصت الدراسة الحالية الى ان الاناث يشكلن نسبة عالية من الاصابة بالتهاب الاذن الوسطى (P-value= 0.01). وان الشباب هم الاكثر تعرضا لخطر الاصابة (P-value = 0.36). تهدف الدراسة الحالية الى تحديد العلاقة بين نسبة التهاب الاذن الوسطى وبعض العوامل المرتبطة بالمرضى مثل الجنس والعمر ومنطقة السكن وفترة الدراسة وكذلك تحديد بعض عوامل الضراوة للبكتريا المستهدفة.

الكلمات المفتاحية: التهاب الاذن الوسطى, الزائفة الزنجارية, أختبار الحساسية ,الناصرية.

University of Thi-Qar Journal Vol.14 No.3 SEP 2019
Web Site: https://jutq.utq.edu.iq/index.php/main
Email: utj@utq.edu.iq

Contaminants of Nasiriyah thermal power station and its impact on the Euphrates River in Thi Qar city

A.Y.Makah AL-Ardy[(1)] A.G.AL-Shatravi[(2)] R.A.Ali AL-Fatlawi[(3)]

[(1)]Department of Physics, College of Science, University of Thi-Qar, amiryaser557@gmail.com

[(2)]Department of Physics, College of Science, University of Thi-Qar,

[(3)]Department of Physics, College of Science, Mustansiriyah University

Abstract:

The research included the study of environmental pollution in the Euphrates River in the vicinity of the power plant in Thi Qar city and its impact on the quality and environment of the river water. The study showed the high values of most physical and chemical properties in the river water, which confirms the effect of the electric station. The samples were taken during the months of February and April of 2019. Six stations were chosen along the river in the study area, two stations before the electric station and two stations next to the station and two stations after the electrical station. The samples were taken from the edge of the river and from the middle and at a depth of (30) cm. The laboratory tests were conducted to calculate the electrical conductivity ,PH and the calcium and magnesium ion rates. The study of properties showed that all levels except PH are not in accordance with the Iraqi and global determinants of potable water as shown in Table (2). We also noticed that these rates were higher in February than in April due to the rain that swept the country and consequently the rise in the water level of the river, which led to a decrease in the percentage of pollutants.

Keywords: environmental pollution, river water environment, pollutant ratio

الخلاصة :

تضمن البحث دراسة التلوث البيئي في مياه نهر الفرات في المناطق القريبة من محطة توليد الطاقة الكهربائية في محافظة ذي قار وأثره في نوعية وبيئة مياه النهر . أظهرت الدراسة ارتفاع معدلات قيم أغلب الصفات الفيزيائية والكيميائية في مياه النهر , مما يؤكد تأثير المحطة الكهربائية . حيت تم اخذ العينات خلال شهري شباط ونيسان من عام 2019 . وقد اختيرت ستة محطات على امتداد النهر في منطقة الدراسة بواقع محطتين قبل المحطة الكهربائية ومحطتين بجانب المحطة ومحطتين بعد المحطة الكهربائية , وقد اخذت العينات من حافة النهر ومن منتصفه وعلى عمق (30) سم , واجريت الفحوصات المختبرية لحساب معدلات التوصيلية الكهربائية والأس الهيدروجيني وكذلك تم حساب معدلات العسرة الكلية ومعدلات ايوني الكالسيوم والمغنيسيوم , وبينت دراسة الخواص أن معدلاتها جميعا ما عدا الاس الهيدروجيني غير مطابقة للمحددات العراقية والعالمية لمياه الشرب كما مبين في الجدول (2) , ولاحظنا كذلك تفوق تلك المعدلات خلال شهر شباط عنها في شهر نيسان وذلك بسبب موجة الامطار التي اجتاحت البلاد وبالتالي ارتفاع منسوب مياه النهر مما أدى الى تقليل نسبة الملوثات .

1. Introduction

Water is an indispensable source of life in all fields. It is considered the source of life and the basis for development. It is one of the most important essentials for the continuation of life, especially freshwater, which is a limited and endangered resource due to the sovereignty of the desert climate and drought. Different. Therefore, it must be given priority in planning to study, develop and develop it in accordance with its importance. The Euphrates River is particularly important in the province of Thi Qar because it is the main source of water in the governorate. As a result of the sovereignty of dry desert climate and the development of different development requirements. As a result of the continuous decrease in water resources of Iraq. In general, thus reducing its water share, it suffers from changes in its water quality [1].

Pollution is a global problem that is of interest to researchers at present, as it has a clear risk to the components of the environment. Pollution can generally be defined as (a change in the concentration of the physical, chemical or pyelogical properties of the major environmental constituents of soil, water and air beyond the limit as a result of various human activities)[2].

As for water pollution, many scientists have defined it as "adding human material to the aquatic environment sufficient to cause harm to human health or other living organisms or ecosystems, including rest and recreation"[3] . This definition is broad and comprehensive, can be determined by (the introduction of solid, liquid, gaseous or any form of energy such as heat, sound or radiation to the environment which makes it unsafe to live in excess of the rates that the environment can be absorbed, analyzed or converted into harmless materials).

The environment is that important part of the world in which people are affected and effected. That is, the part that it uses, exploits, influences and adapts to it[4], the human environment means all that affects the human physical, chemical and life, which have clear results on the health of the citizen. Since waste disposal is a natural result of any natural activity, how to get rid of these wastes or to benefit from them has remained one of the greatest human problems in modern times. Therefore, several methods of disposal of sewage (from cities or laboratories) have been found and most commonly discharged into natural waterways without treatment. That the presence of pollutants in these water contribute to the poor quality of water and make it unsuitable for any human use.

Since the rivers, including the Euphrates River, are the main source of human water needs, which receive and reduce man-made pollutants[5],and to determine the validity of its water for different investments, the qualitative properities of river water were assessed through the Raman spectroscopy study, physical and chemical properties to detect the extent of water pollution in Thi Qar city, and then compare the results with local and international standards for the quality of river water and drinking water. And thus assess these waters to determine their suitability for various uses of life.

2.Physical and chemical factors

2-1. Power of hydrogen (PH)

The Ph of the water was measured using the pH-meter (inoLab Ph7110) was produced by the German WTW company and after calibration with the standard buffer solution of pH 4, 7, 9 before work.

PH meter

2-2.Electrical conductivity and salinity

The electric conductivity of the water samples was measured using the E.C-meter E.C-Heter (Sens. Ion5) and expressed the output with micromenzyme / cm. In terms of electrical conductivity results, the salinity values were calculated in the samples according to Mackereth et al. , 1978). According to the following equation:

Salinity % = E.C × 640 × 10^{-6}

Where E.C is the value of the electrical conductivity and the salinity output is expressed in ppt.

Electrical conductivity measuring device

Total hardness (T.H) :

The method described by Lind (1979) was followed by the titration of 25 mL of the sample with EDTA-2Na solution (0.02 N) after adding 1-2 ml of the regulator solution and using the Erichrome Blak T detector and expressed in mg / L.

Calcium and Magnesium (Ca , Mg) :

The method described by the American Public Health Association (APHA, 2003) was applied for Calcium Calculation with EDTA-2Na (0.02 N) after adding 1-2 cm 3 of NaOH solution (1N) to pH to pH 12 and using Murexid revealing and expressing the results in mg / l.

Magnesium concentration in water can be obtained from the results of both total calcification and calcium using the following equation:

Mg(mg/L) = (T.H as $caco_3$ × 2.5) × 0.244

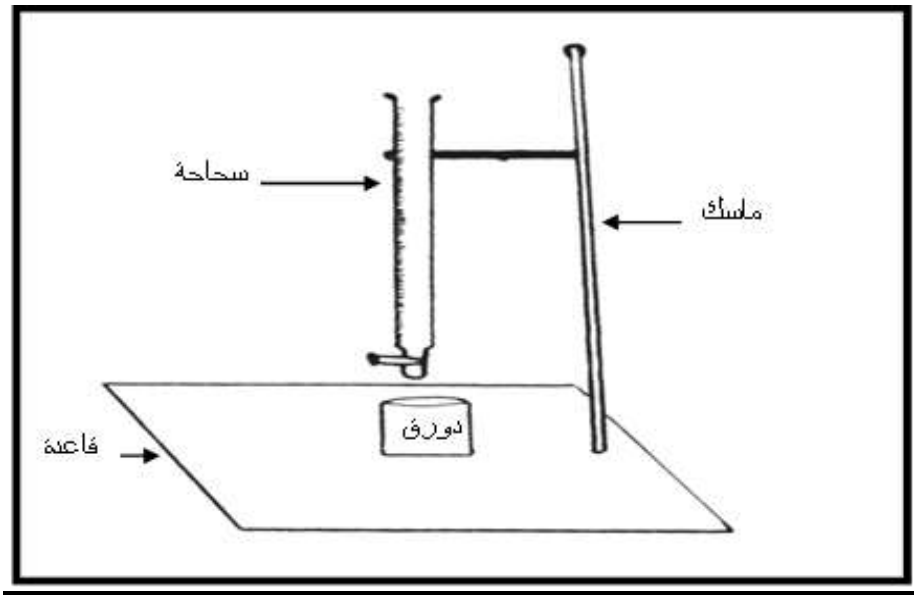

The main parts to determine the ions of salts and chlorine

Results and Discussion

Table (1)

Rate of physical and chemical properties of pH, total hardness, electrical conductivity, calcium and magnesium ions for study sites during the study period.

المحطات	month	PH	T.H	Ca	Mg	E.c
St.1	**Feb.**	8.1	1118	204	148	4537
St.2		8.1	1121	207	147	4546
St.3		7.9	1129	210	147	4561
St.4		8	1136	214	146	4580
St.5		8.1	1092	189	151	4408
St.6		7.8	1104	192	152	4419
St.1	**Apr.**	7.9	881	158	118	3506
St.2		8.1	873	150	121	3497
St.3		8.1	878	152	121	3499
St.4		7.9	874	152	120	3496
St.5		7.9	907	168	118	3541
St.6		7.8	910	170	118	3541
RO		6.7	42	11	3	146
Asals		7.8	579	151	49	1644
Determinants		6.5-8.5	500	200	150	1000

Specific electrical conductivity(E.C) :

The electrical conductivity of the water samples showed a clear difference between the various stations, as shown in diagram (1), where the highest values in the fourth station and the lowest in the fifth station, ranging between (4408 - 4580) micro-Siemens cm^{-1} respectively in February, while we notice a remarkable change between the fourth station and the sixth station during the month of April, where values have ranged between (3496 - 3541) micro-Siemens cm^{-1}, respectively.

The sample of drinking water (RO) recorded values for specific electrical conductivity up to (146) micro-Siemens. cm^{-1}. While the tap water sample values (Asala) I reached (1644) micro-Siemens. cm^{-1}.

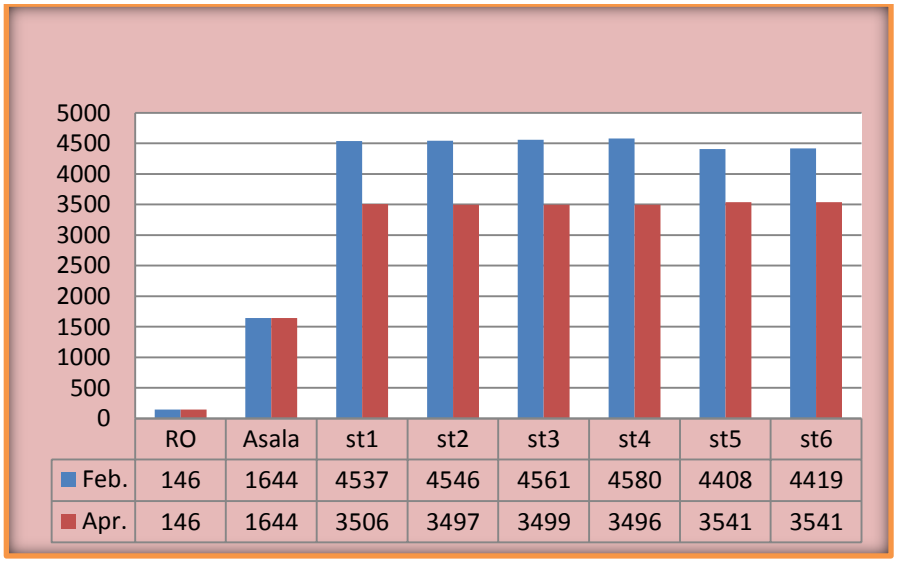

	RO	Asala	st1	st2	st3	st4	st5	st6
Feb.	146	1644	4537	4546	4561	4580	4408	4419
Apr.	146	1644	3506	3497	3499	3496	3541	3541

diagram (1) Monthly and Local Changes the values of electrical conductivity in the studied stations.

Power of hydrogen (PH) :

It was observed from this study that the pH values of the water samples for all the sites are relatively basic where the pH value did not decrease from (7.0) regardless of location. The pH values for the stations ranged from (1) to (6) in February between (7.8) and 8.1 and the

variability of the values of these stations did not exceed (0.3) units of pH. The variability of the stations was constant for the same stations in April Where the same pH range was observed, as shown in diagram (2). The drinking water sample (RO) found that the pH rate was (6.7) while the tap water sample gave a rate of " (7.8).

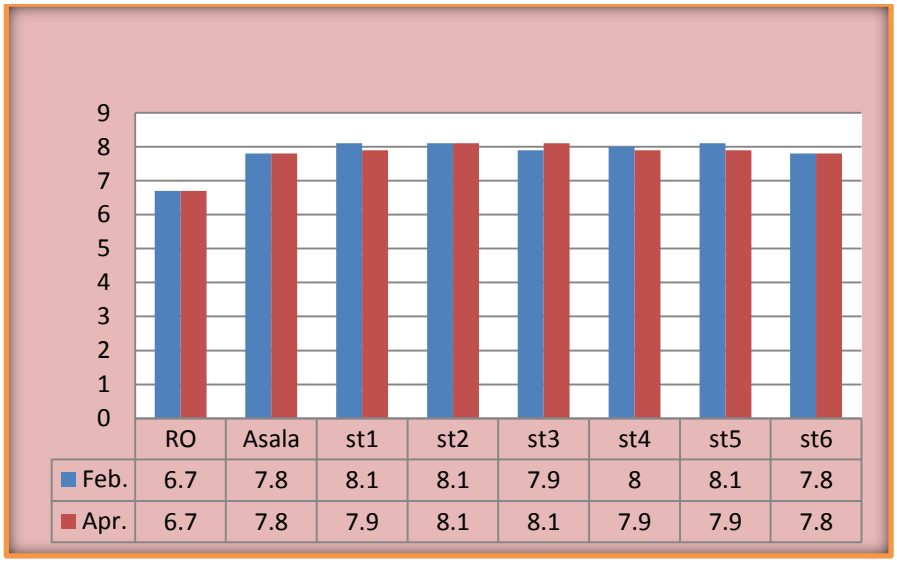

	RO	Asala	st1	st2	st3	st4	st5	st6
Feb.	6.7	7.8	8.1	8.1	7.9	8	8.1	7.8
Apr.	6.7	7.8	7.9	8.1	8.1	7.9	7.9	7.8

diagram (2) Monthly and local changes of PH values in the studied stations.

Total hardness (T.H) :

Total hardness of water was measured at all stations of study and found that the water is very difficult, especially at the third and fourth stations located near the cooling water discharge stations of the power station on the Euphrates River, where the average values of concentrations between (1129 - 1136) mg. L1-calcium carbonate, respectively, during February.

In the second and fourth stations, the average concentration of the total mass was lower than that of the other stations during the month of April as in diagram (3). The drinking water sample (RO) was the average value (42) mg. L1 - calcium carbonate while the value rate (579) mg. L1-Calcium carbonate for the tap water sample.

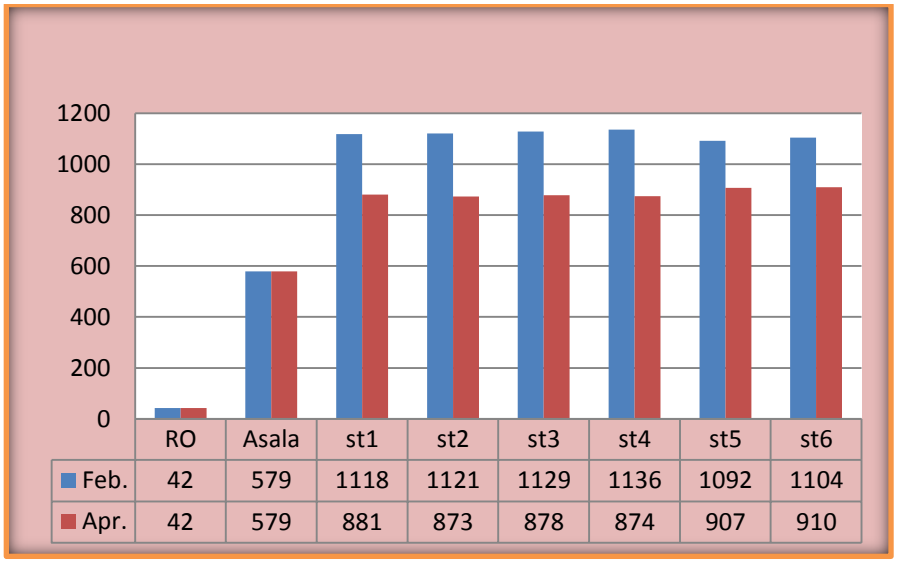

	RO	Asala	st1	st2	st3	st4	st5	st6
Feb.	42	579	1118	1121	1129	1136	1092	1104
Apr.	42	579	881	873	878	874	907	910

diagram (3): Monthly and local changes of the Total Hardness values in the studied stations.

Ionic of Calcium and Magnesium. (Ca , Mg) :

Calcium concentrations showed a significant difference in the course of all study sites. The concentration of calcium ion decreased from (214) mg. L1. In the fourth station during the month of February to (150) milligrams. The concentration of magnesium was observed as the highest value in the sixth station during February and the lowest value was in the same station during the month of April, where the values ranged between (152 - 118) Mg. As shown in diagram. (5), for the sample of drinking water (RO) it was found that the calcium ion concentration (11) mg. L1 - magnesium ion (3) mg. L1, and the sample of water tap (Asala) has given a rate (151) and (49) mg. L1, for Ionic calcium and magnesium respectively.

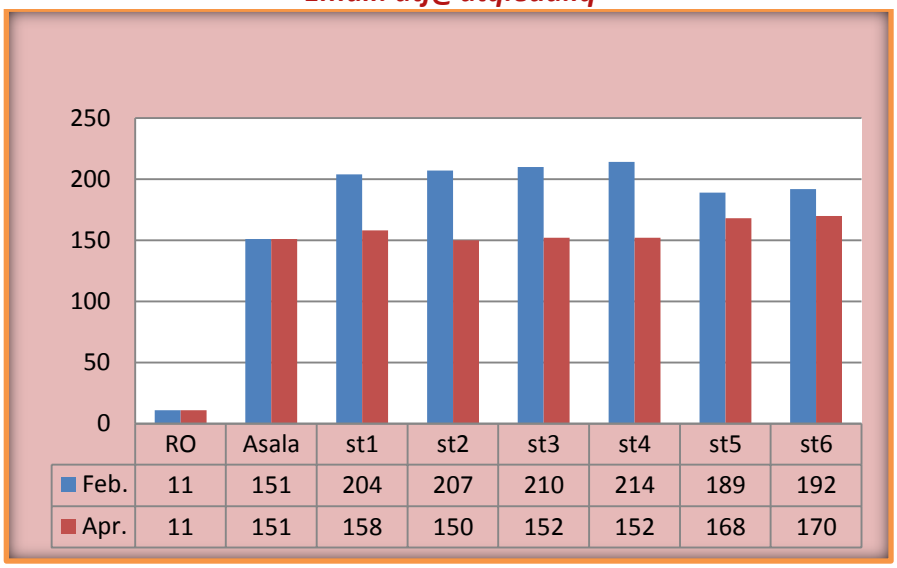

diagram (4) Monthly and local changes of calcium values in the studied stations.

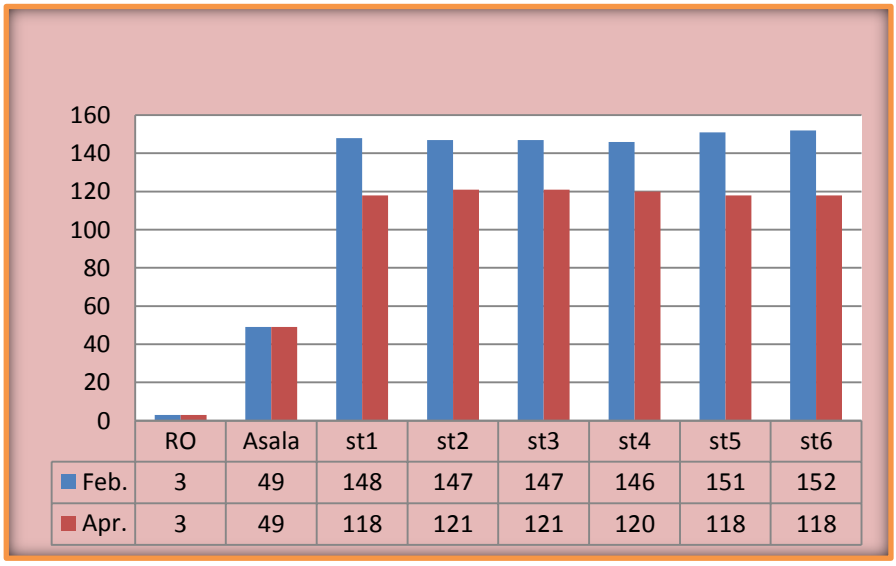

diagram (5) Monthly and local changes of the magnesium values of the studied stations.

Table (2)Iraqi determinants of the quality of water suitable for the aquatic environment And drinking water for the World Health Organization (WHO) Compared to the specifications of the Euphrates water per mg / liter except for the indicator in front of it[6,7]

Case	WHO determinants of drinking water	Iraqi determinants of the aquatic environment	Concentration of elements in the Euphrates River	Element
Non Identical	1000	1000	4010	(µs/cm) Electrical conductivity
Identical	6.5-8.5	6.5-8.5	7.9	PH
Non Identical	100-500	160-480	1001	Total Hardness
non identical in drinking only	75	Less than 200	180	Calcium
Non Identical	10-25	50	133	Magnesium

Conclusions:

- The quality of the Euphrates River in the province of Dhi Qar is constantly changing, the rates of electrical connection (4508) and (3513) while the average value of the total severity (1116) and (887) during the months of February and April, respectively. This change reflects the intensity of the volume of contaminants and the resulting, as well as the lack of maintenance projects and poor efficiency, which

can leave these changes have negative effects on several aspects of development, for example, aspects of agricultural development, where these changes contribute to the decline of cultivated areas and leave a significant proportion of the labor force on agricultural land from work leading to increased rural unemployment. For the purpose of maintaining the quality of water resources in the Euphrates River and developing its efficiency for investment, the following measures are required :

1- The need to regulate the volume of running water in the Euphrates River according to different investment requirements.

2- The need to encourage studies and research and benefit from the expertise, skills and experience in the field of river conservation and development of quality, in line with its importance as a major resource for development in various fields.

3- Control the sources of pollution of all kinds.

4- That the governmental institutions have a role in this area through the formation of joint committees between the various departments involved in this matter to address the problems experienced by the river.

المصادر :

1- العبد الله, نجم عبدالله رحيم, "الخصائص الفيزيائية والكيميائية لترب محافظة ذي قار وتأثيراتها في الإنتاج الزراعي", أطروحة دكتوراه, كلية الاداب , جامعة البصرة , (2006) .
2- أنماروهبي صبري, التلوث الصناعي وأثاره البيئية , مجلة الأرض والتنمية , العدد 2 , بغداد , (1995) .
3- Mason , C.F .Biology of Fresh water pollution Longman Group Limited. London. (1981).
4- ميللينبي، كينيت. بايولوجيا التلوث. ترجمة كامل مهدي التميمي. بغداد: مطبعة دار الشؤون الثقافية، (1994)، ص –7.
5- الخفاف, عبد المعطي, ندوة حماية البيئة والتلوث الصناعي, الاتحاد العربي للصناعات الهندسية الامانة العامة, (1997) .
6- التشريعات البيئية , نظام صيانة الأنهار من التلوث رقم 3 , دائرة حماية وتحسين البيئة , (1998).
7- World health organization (WHO) ,International standards for drinking water .

University of Thi-Qar Journal Vol.14 No.3 SEP 2019
Web Site: https://jutq.utq.edu.iq/index.php/main
Email: utj@utq.edu.iq

Study of Mixed Spin (1, 3/2) in Ferrimagnetic Ising Nanowire

Omar M. Nabil[1] Hadey K. Mohamad[2] Hassan A.Yasser[3]
Emails: Omaralh 725 @ gmail . com

abc-2002@mu.edu.iq

Hassan.yasser_ph@sci.utq.edu.iq

[1]Alwaqfalsheai in Thi-Qar, Presidency of the Council of Ministers, College of Science, Thi-Qar University.
[2]Physics Science Department, ,college of Science,

Al Muthanna University.

[3]Physics Science Department, College of Science,

Thi-Qar University.

Abstract

A ferrimagnetic mixed spin square Blume-Capel Ising nanowire system depend of spin-1 core and spin-3/2 outer shell have been investigated. The general formula for the temperature dependence of the equilibrium magnetization of the system is presented. The ferrimagnetic core-shell nanosystem shows a compensation point when the exchange interactions are changed at various values of the single-ion anisotropies of shell sublattices and core ones, respectively. So, one can examine interesting phenomena are compensation behaviors and the free energy of the nanosystem, where these phenomena found that the mixed-spin square Blume-Capel Ising nanosystem which is being considered has two spin compensation temperatures in the range of $-0.8 \le D_B|J_1| \le -0.4$, when $J_3 = -0.7$, for two different values of core anisotropy for sublattices of atoms A, $D_A|J_1| = 0$, and $D_A|J_1| = 1.0$, respectively.

Keywords: Magnetization , Ising Model , Compensation point , Crystal field , Square lattice.

1.Introduction

Recently, I drew a lot of attention towards understanding the magnetization processes and related applications. Thus, magnetic wires have provided ground very successful test to understand the microscopic mechanisms that determine the important parameters ostensibly in different applications [A.K. Srivastava andA.DakhamaN]. It revealed the development of nanowire arrays of tiny magnetic different extraordinary properties relevant applications in data storage devices and in high-density bio-engineering applications [E. Vatansever]. B. Deviren and Y. Sener studied magnetic properties of nanoparticles mixed Ising spin with the basic structure / shell using the effective field with links theory. The researchers found that the system gives new behaviors under the domain crystal effect, core and shell interactions and coupling interface on phase diagrams. In this paper we have investigated the magnetic properties of a ferrimagnetic mixed spin-1 and spin-3/2 square Blume-Capel Ising nanowire system, for a series of molecular based magnets, which is numerically solved by using the mean-field approximation(MFA), in order to clarify the physical background for the characteristic phenomena observed in the ferrimagnetic mixed nanowire models. It is contained in the work as follows. In Section 2, we offer briefly the basic framework of the theory of the average field and give Hamilton of mixed ferrimagnetic spin-(1,3/2) square Blume-Capel Ising nanowire system. In Section 3, numerical results for phase diagrams, the study of the magnetization of the system in detail. Finally, the conclusion is offered in Section 4.

2. Model and Formalism

The proposed model contains of a ferrimagnetic square nanowire consists of the spin-1 core for atoms A and spin-3/2 outer shell for atoms B, respectively, as shown in Figure(1):

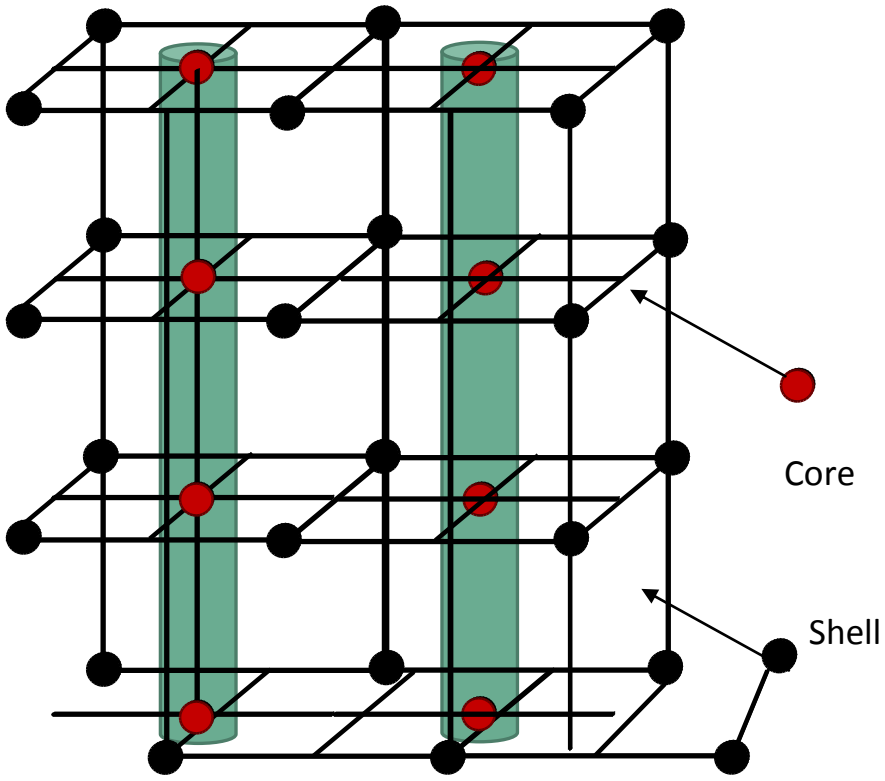

Figure1: Square Blume-Capel Ising nanowire with core-shell structure. Each square represents a plaquette consisting of one core spin and four shell spins.

The Hamiltonian of the nanosystem, in the absence of external magnetic field, is written as [4]

$$H = -J_1 \sum S_i^A S_j^B - J_2 \sum S_i^A S_i^A - J_3 \sum S_j^B S_j^B - D_A \sum S_i^{A^2} - D_B \sum S_j^{B^2} \quad (1)$$

where $\left(S_i^A, S_j^B\right)$ takes the values $\left(\pm 1, \pm \frac{3}{2}\right)$; and D_A is a magnetic anisotropy acting on A-atoms(core anisotropy), D_B is a magnetic anisotropy acting on B-atoms (shell anisotropy). J_1 is the near neighbor exchange parameter between magnetic atoms across the core and the outer shell. J_2 is the nearest neighbor

exchange parameter between magnetic atoms in the core. J_3 is the exchange interaction at the outer shell.

The free energy of the nanosystem is obtained from a mean field calculation of the Hamiltonian based on the Bogoliubov inequality [D. J. Sellmyer5]:

$$A \le \Phi = A_0 + \langle H - H_0 \rangle_0 \quad (2)$$

where A is the Gibbs free energy of H given by relation (1), that:

$$A = -k_B T \ln Z \quad (3)$$

A_0 is the Gibbs free energy of a paramagnetic phase and H_0 a trial Hamiltonian depend on variation parameters, that:

$$A_0 = -k_B T \ln Z_0 \quad (4)$$

Z, Z_0 are the true partition function and trial one respectively.

In this research we consider one of the possible choices of H_0, namely:

$$H_o = -\sum_i [\lambda_1 s_i^A + \gamma_A (s_i^A)^2] - \sum_j [\lambda_2 s_j^B + \gamma_B (s_j^B)^2] \quad (5)$$

S_i^A taking the values of spins for core-atoms, and S_j^B taking the values of spins for shell-atoms. Whereas λ_1, λ_2, γ_A, and γ_B are the variational parameters related to the different spins and the anisotropies of the two sublattices proposed(i.e., the core and shell anisotropies), respectively. Then, the approximated free energy can be obtained by minimizing the right side of equation (2) with respect to variational parameters mentioned above. Thus, Eq.(2) can be expressed as,

$$f \equiv \frac{\Phi}{N} = -\frac{1}{\beta}\{\ln(a+1) + 4\ln b\} + J_1 z_1 m_A m_B + J_2 z_2 m_A^2 + 4 J_3 z_3 m_B^2 \quad (6)$$

with,

$$a = 2e^{\beta D_A} \cosh \beta\lambda_1 \ ; \ \lambda_1 = J_1 z m_B + 2 J_2 z m_A \ ; \ z_1 = z_2 = z_3 = z$$

and,

$$b = 2e^{\frac{9}{4}\beta D_B}\cosh\frac{3}{2}\beta\lambda_2 + 2e^{\frac{1}{4}\beta D_B}\cosh\frac{1}{2}\beta\lambda_2 \;;\; \lambda_2 = \frac{1}{4}J_1 z m_A + 2J_3 z m_B$$

with,

$$m_A = \frac{2\sinh\{t_1 z_1 m_B + t_2 z_2 m_A\}}{2\cosh\{t_1 z_1 m_B + t_2 z_2 m_A\} + 2e^{-\beta D_A}} \tag{7}$$

$$m_B = \frac{1}{2}\frac{3\sinh\{\frac{3}{2}t_1 z_1 m_A + \frac{3}{2}t_3 z_3 m_B\} + e^{-2\beta D_B}\sinh\{\frac{1}{2}t_1 z_1 m_A + \frac{1}{2}t_3 z_3 m_B\}}{\cosh\{\frac{3}{2}t_1 z_1 m_A + \frac{3}{2}t_3 z_3 m_B\} + e^{-2\beta D_B}\cosh\{\frac{1}{2}t_1 z_1 m_A + \frac{1}{2}t_3 z_3 m_B\}} \tag{8}$$

where, $\beta = \frac{1}{K_B T}$, z is the coordination number of the lattice.

It is worth mentioning that the case ferrimagnetic shows that signs magnetizations different sublattice, and there can be a point of compensation, which total longitudinal magnetization of each site is equal to zero [Fathi Abubrig].

3. Results and discussion

The magnetic phase transitions has been investigated numerically by the use of mean-field approximation (MFA), in order to clarify the physical background for the characteristic phenomena observed in the ferrimagnetic mixed nanowire models. The effect of single-ion anisotropies (i.e., crystal fields) on the compensation phenomenon have been taken into consideration. Besides, we have shown the effect of exchange interactions on the magnetization curves and the phase transition of these systems. Let us consider the thermal variation dependence of the total magnetization for a mixed spin-1 and spin-3/2 square Blume-Capel Ising nanowire as shown in Figure2, Figure3, respectively.

We found some compensation behaviors for square-type nanowire, at different values of $D_A|J_1|$ and $D_B|J_1|$, when $J_1 = -1, J_2 = -1, J_3 = -0.75$, respectively. Fig. 2. reveals interesting phenomena regards compensation temperatures in the range of $0 \le D_A|J_1| \le 3$, for different values of $D_B/|J_1| = -1.0, -0.9, -0.8, -0.7, -0.6, -0.5$. One can observe, Fig.2, when $1 \le D_A|J_1| \le 3$, shows a multi-compensation behavior for different $D_B/|J_1| = -1.0, -0.9, -0.8, -0.7, -0.6, -0.5$, respectively. It is worth to note that the compensation point caused by the presence of magnetic variation of atom- B, it is only possible is in the magnetic phase. This magnetizations sublattice undergo to cancel but it is still incomplete so there is spontaneous magnetization of the remaining in the system(M≠0), this is evidence to the antiferromagnetic near neighbor interactions[T. Kaneyoshi].

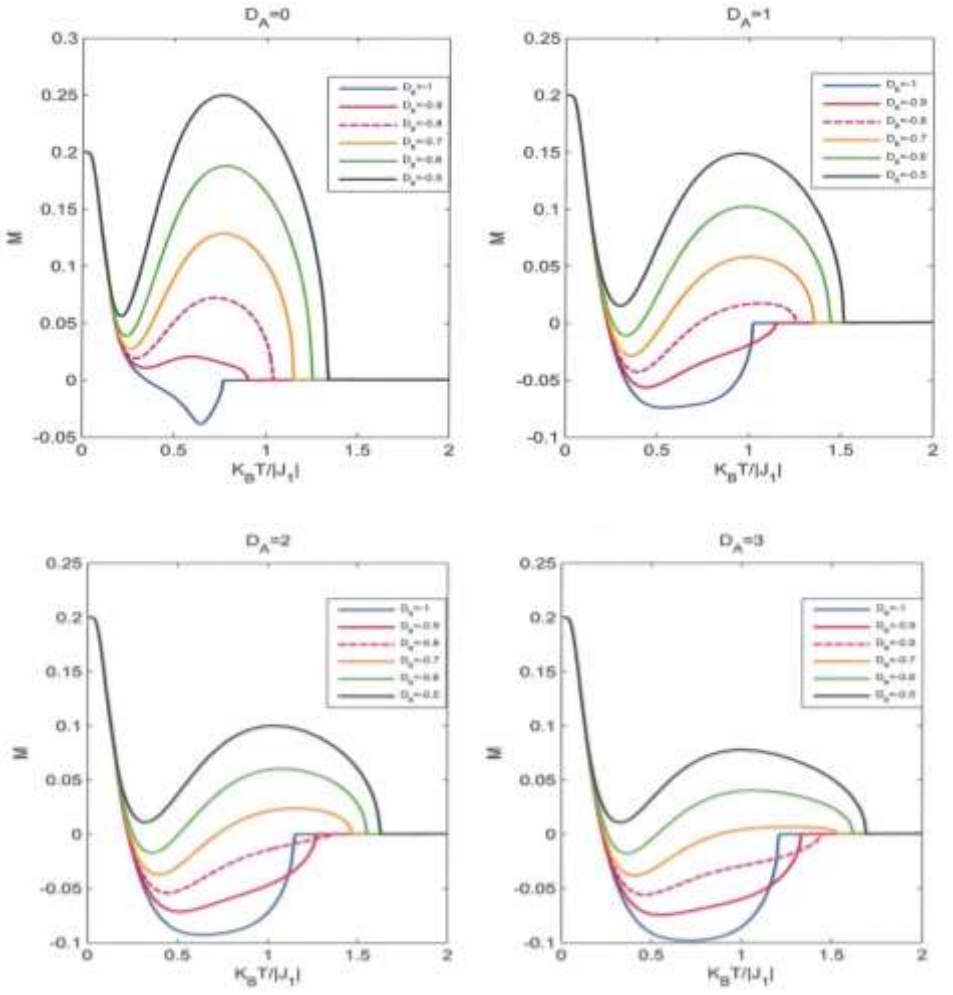

Figure2: The temperature dependences of the total magnetization M for a ferrimagnetic mixed-spin square Ising nanowire with, $J_1 = -1, J_2 = -1$, $J_3 = -0.75$

This interaction tends to align the spins adjacent in opposite directions as the rising temperature of the system, and therefore the direction of this residual magnetization can switch because of the thermal excitation. The compensation

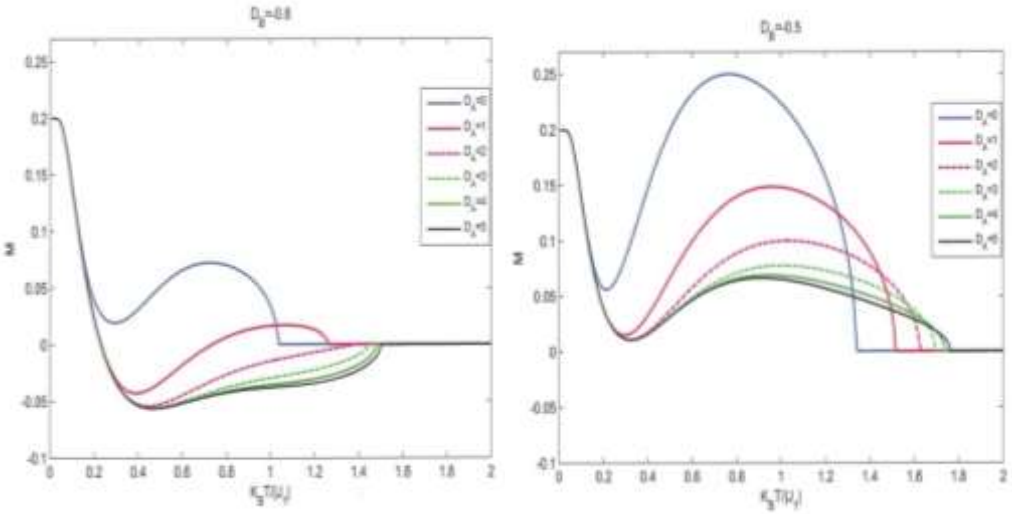

Figure 3: The temperature dependences of the total magnetization M for a ferrimagnetic mixed-spin square Ising nanowire at different values of D_A and, D_B when $J_1 = -1,\ J_2 = -1,\ J_3 = -0.75$.

behaviors shown in Figuress.(2,3) indicate the crossing points between the magnitudes of m_A and m_B which prove the eligibility of Eqs.(7) and (8).

B. Boughazi et al studied a hexagonal nanowire consisting of a ferromagnetic spin-1/2 core and spin-3/2 outer shell coupled with ferrimagnetic interlayer coupling by the use of Monte Carlo simulation. The authors draw a total magnetization versus temperature for some specific values of $R_S(J_S / J)(0,0.05, and 0.10)$, respectively. As is clear from these criteria that the system displays the temperature and one compensation. One can compare our results interesting with those [T. Kaneyoshi].

On the other hand, Figure 3, shows the temperature dependence of the total magnetization M for a ferrimagnetic mixed spin Ising nanowire system, with $J_1 = -1, J_2 = -1, J_3 = -0.75$. One can be observe that nanosystem has two compensation points when $D_A|J_1| = 1.0$, and $D_B|J_1| = -0.8$, for $J_1 = -1, J_2 = -1, J_3 = -0.75$. This is in good agreement with the possibility of

compensation in the other two points of nanosystem that have been discussed in the reference.[T. Kaneyoshi and V. F. Puntes].

Now let us discuss the temperature dependence of the total magnetization M for the mixed spin Ising nanowire ferrimagnetic system with , J_1=-1, J_2= - 1, for J_3= - 1.0, and J_3= - 0.7, respectively. In Fig.4, that the system has two compensation points at a fixed value of $D_A|J_1| = 0$ and different values of $D_B|J|$, in particular for J_3= - 0.7. This is in good agreement with the possibility of compensation in the other two points nanosystem that are discussed as in reference.[V. F. Puntes].

From the two figures(5,6), one can found interesting features, i.e., the possibility of multicompensation temperatures are particularly induced, when $D_A|J_1| = 0$, $J_3 = -0.7$, in the range of $-0.8 \le D_B|J_1| \le -0.6$, respectively.

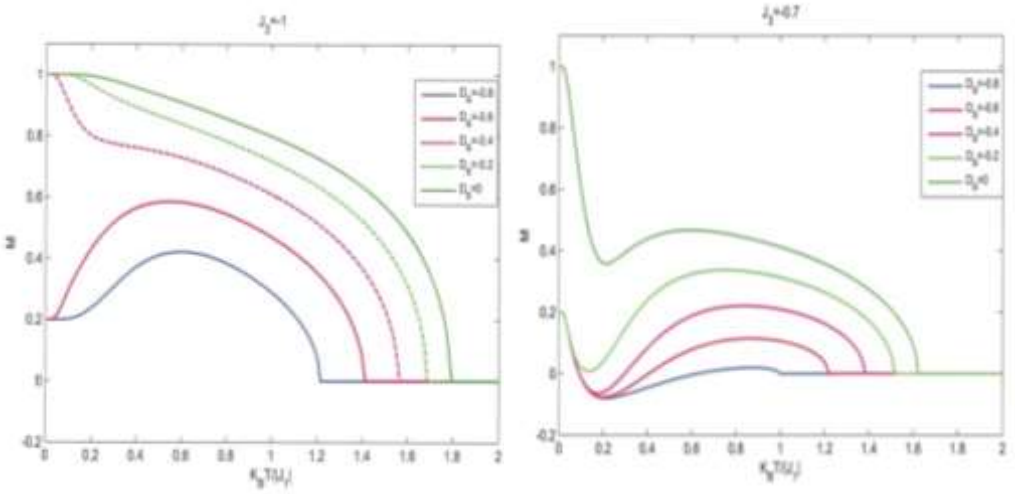

Figure 4 : The temperature dependences of the total magnetization M at constant values of $D_A = 0$ and different values of D_B for $J_1 = -1, J_2 = -1$

Conclusions

We have investigated a ferrimagnetic mixed spin-(1,3/2) square Blume-Capel Ising nanowire system by using the mean-field treatment. The effect of single-ion anisotropies(i.e., crystal fields) on the compensation phenomenon have

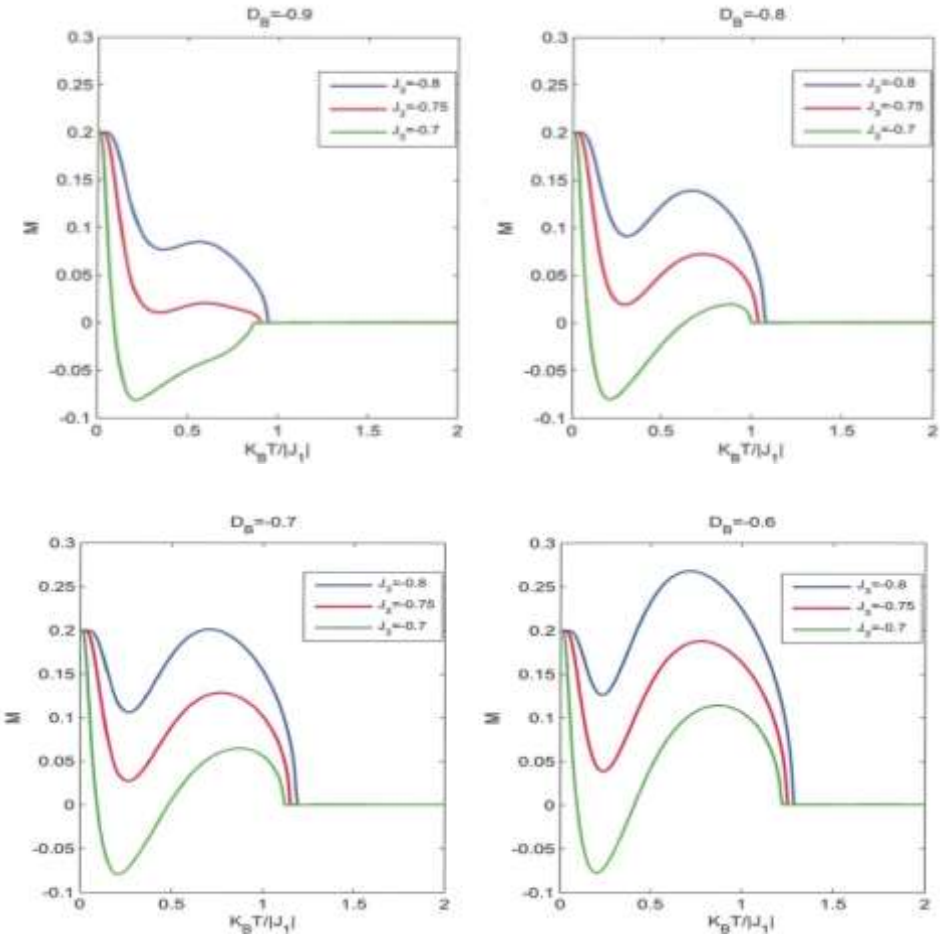

Figure5: The temperature dependences of the total magnetization m at constant values of $D_A = 0$ and different values of D_B, when $J_2 = -1$, for $J_3 = -0.8, -0.75, -0.7$, respectively.

been taken into consideration. It has carefully changed the magnetic anisotropies so that one can study the phenomena of interest are the behaviors of compensation in which these phenomena are found that the mixed-spin square Blume-Capel Ising nanosystem which is being considered has one compensation temperature when the core anisotropy is in the range $1.0 \le D_A/|J_1| \le 5.0$ at $D_B/|J_1| = -0.8$, for J_1=-1, J_2=-1, J_3=-0.75. Besides, our nanosystem has two spin compensation temperatures in the range of $-0.8 \le D_B|J_1| \le -0.4$, when $J_3 = -0.7$, for two different values of core anisotropy for sublattices of atoms A, $D_A|J_1| = 0$, and $D_A|J_1| = 1.0$, respectively. It have been shown that the appearance of spin compensation points is independent of D_A; however D_A influences the magnitudes of these points in the temperature space. On the other hand, from the point of view of the pilot, it was synthesized quasi-one-dimensional heterotrinuclear complex $[NiCr_2(bipy)_2(C_2O_4)_4(H_2O)]H_2O$, which shows a rare case of antiferromagnetism between $Ni(II)S = 1$ and $Cr(III)S = 3/2$.

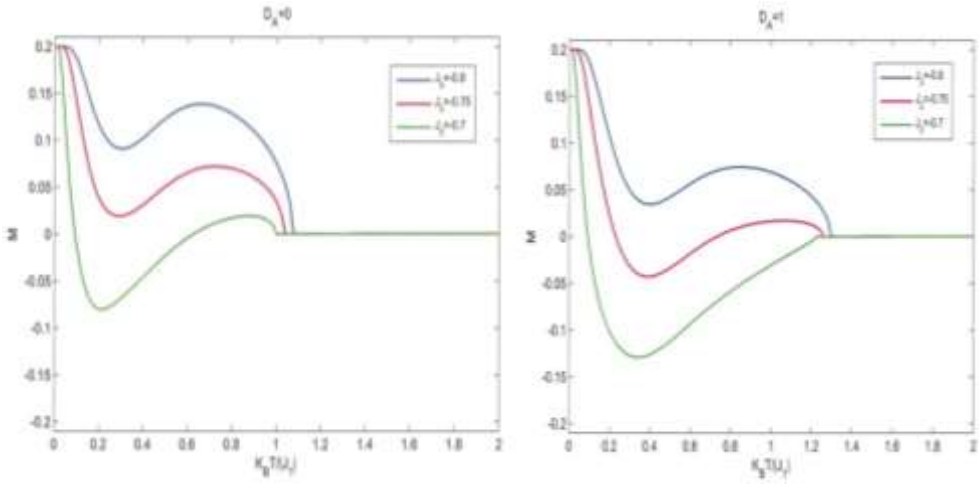

Figure 6: The thermal dependence of the total magnetization m at constant values of D_B=- 0.8and different values of D_A, when $J_2 = -1$, for $J_3 = -0.8, -0.75, -0.7$, respectively.

References

[A] A.K. Srivastava, R.S. Singh, K.E. Sampson, V.P. Singh and R.V. Ramanujan, Metallurgical and Materials Transactions A ,38A, 717. 2007.

[A] A.DakhamaN.Benayad, J.Magn.Magn.Mater,213,117(2000).

[B] B. Boughazi, M. Boughrara, M. Kerouad, Physica A, 465, 628(2017).

[E] E. Vatansever, H. Polat, J.Magn.Magn. Mater.,343,221, 2013.

[D] D. J. Sellmyer, M. Zheng, R. Skomski, J. Phys.: Condens. Matter ,213, ,R433. 2001.

[F] Fathi Abubrig, Open J. Applied Sciences, 3,270. 2013.

[T] T. Kaneyoshi, J. Phys. Chem. Solids, 87, 104(2015).

[T] T. Kaneyoshi, Solid Stat. Commun., 244,51(2016).

[V] V. F. Puntes, K. M. Krishnan and A. P. Alivisatos, Science, 291, ,2001,2115.

عمر محمد نبيل[1] **هادي قاسم محمد[2]** **حسن عبد ياسر[3]**

Omaralh 725 @ gmail . com **abc-2002@mu.edu.iq**
Hassan.yasser_ph@sci.utq.edu.iq

[1]Alwaqfalsheai in Thi-Qar, Presidency of the Council of Ministers, College of Science, Thi-Qar University.
[2]Physics Science Department, ,college of Science,

Al Muthanna University.

[3]Physics Science Department, College of Science,

Thi-Qar University.

الخلاصة:

تم دراسة نظام ايزنك نانوي فيريمغناطيسي مختلط يتكون من عزوم 1 في النواة وعزوم 3/2 في الغلاف لشبيكة مربعة تخضع لقوانين بوم كايبل. تم تقديم العلاقة الاساسية لتمغنط التوازن المعتمد على درجة الحرارة الخاصة بالنظام. النظام النانوي الفيريمغناطيسي المتكون من نواة-غلاف يظهر نقطة تعادل عندما تكون قيم معامل التفاعل المتبادل متغيرة ولعدة قيم من المجالات البلورية الخاصة بغلاف الشبيكة الفرعية ونواتها. من الممكن ان نلاحظ ظاهرة مهمة سلوك التعادل بالاضافة للطاقة الحرة للنظام النانوي حيث وجدنا ان هذه لظاهرة الموجودة بنظام ايزنك لبرم مختلط والخاضعة لقوانين بلوم كيبل قيد دراسة بحيث يملك نقطتيان تعادلتين لمدى من القيم المجالات البلورية وهي $-0.8 \le D_B|J_1| \le -0.4$ عندما تكون قيم $J_3 = -0.7$, لقيمتين مختلفتين من المجالات البلورية النوي للشبيكة الفرعية من نوع $D_A|J_1| = 0$ A و $D_A|J_1| = 1.0$, بالتتابع.

الكلمات المفتاحية: التمغنط , نموذج ايزنك , درجة حرارة التعادل , المجال البلوري , الشبيكة المربعة.

University of Thi-Qar Journal Vol.14 No.3 SEP 2019
Web Site: https://jutq.utq.edu.iq/index.php/main
Email: utj@utq.edu.iq

Serological and Molecular detection of *Staphylococcus aureus* isolated from UTI patients

Ahmed A. R. Abbas* Saad S. Hamim*
hamim_pa@sci.utq.edu.iq
***Ministry of health-Thi-Qar health office.**
***Department of pathological analysis-College of science-Thi-Qar University.**

Abstract

Urinary tract infections (UTIs) are one of the commonest infections encountered by clinicians despite the widespread availability of antimicrobial agents. Such Infections caused by different bacterial pathogens that can be acquired through both hospitals and the community. The present study is aimed to isolation and diagnosis of *Staph. aureus* , detecting the optimal antimicrobial for the treatment of these infections. A total of (600) mid-stream urine samples were collected during the period from August to December, 2018 from patients who were complained from UTIs at AL-Hussain Teaching Hospital in AL-Nasiriyah City, Southern Iraq. The study included isolation and diagnosis of *Staph. aureus* based on morphological, microscopic characterization, biochemical tests and confirmed by API-20 and Vitek2 systems. In addition , all *Staph. aureus* isolates were subjected to the serological diagnosis of protein A by using a latex agglutination test and convention PCR technique was used to detect the presence of the 16S rRNA gene (353bp). 380 (63.33%) were positive isolates for bacteriological examination, the *Staph. aureus* was identified with 50 samples (13.5 %). In addition, all *Staph. aureus* isolates were assayed for antimicrobial susceptibility against 14 selected antibiotic discs by using the disc diffusion method. All isolates were completely resistant to Penicillin (P), Oxacillin (Ox), and Ampicillin (Amp). While the most effective antibiotics were Nitrofurantoin, Gentamycin, isolates were susceptible to these antibiotics in 76%, and 60%, respectively. Also, In the analysis of the nucleotides sequence of the partial 16S rRNA gene, the results were showed that these bacteria actually related to *Staph. aureus* ,according to

current result, three of these isolates registered globally in the NCBI Gen bank, and the accession numbers of these isolates are (MK910079.1),(MK910080.1), and (MK910081.1).

Keywords: *Staphylococcus aureus*, Urinary tract infections, Identification, Serological and Molecular diagnosis

1. Introduction

Urinary tract infections (UTIs) are infections caused by the presence and growth of microorganisms anywhere in the urinary tract and may be the single most common human bacterial infections [1]. The urinary tract includes the organs that collect, store and release urine from the body, including kidneys, ureters, bladder, and urethra. UTIs are among the most common human bacterial infections in the community or hospital settings and has been reported in both sexes in all age groups [2]. The prevalence and incidence of UTI in women are higher than in men, which is probably the result of several clinical factors, including anatomical differences, hormonal effects and behavioral patterns [3]. About 150 million people worldwide develop UTI each year, with high social costs [4]. UTI accounts for a large portion of the workload in clinical microbiology laboratories and enteric bacteria (*Escherichia coli* in particular) remain the most common cause of UTI, although the distribution of UTI - allowing pathogens is changing [5]. Some other pathogens are associated with UTIs like *Staphylococcus*, *Staph. aureus* which is a major human pathogen and a widespread contaminant in hospitals. Although *Staph. aureus* isolation from urine samples is often secondary to Staphylococcal bacteremia that occurs elsewhere (e.g. endocarditis cases), In some patients, *Staph. aureus* causes colonization and infection in the urinary tract. Instrumentation of the urinary tract and presence of an indwelling catheter increase the risk of *Staph. aureus* carriage of the urinary tract. Majority of cases *Staph. aureus* bacteriuria is not associated with symptoms of urinary tract infection because bacteriuria nearly universally occurs concomitantly with long-term urinary catheterization [6]. The susceptibility of *Staph. aureus* to the penetration of the body's defenses and tissue invasion and possession of virulence factors such as toxin and

enzyme production, including high antibiotic resistance [7]. In the past few decades, *Staph. aureus* is considered as one of the most common nosocomial infections due to various virulence factors, acquisition of antibiotic resistance genes, poor sanitation, and hygiene of health care setting and discriminate use of antibiotics [8]. Also, *Staph. aureus* has a number of identifying properties, including free coagulase, clumping factor (bound coagulase), thermonuclease, and protein A [9]. The present study aimed to investigate the molecular characterization of 16S RNA gene in *Staph. aureus* isolates from UTI patients.

2. Materials and Methods

2.1 Samples collection

Samples were collected from 600 UTI patients from both sexes with different ages, based on the symptoms and which diagnosed by physician and microscopic examination of urine, Patients had taken care and medications in AL- Hussein Teaching Hospital in AL- Nassiriyah City South of Iraq , during the period from August to December, 2018.

2.2 Isolation, Identification & biochemical tests of *Staph. aureus*

Collected specimens were inoculated on several types from culture media which included blood agar, mannitol salt agar, and *Staph* 110 agar base according to standard methods. *Staph. aureus* was identified depending on the morphological features of culture media. Isolates were stained by Gram stain to detect their response to stain, shapes and their arrangement[10]. The biochemical tests used include Catalase, Coagulase, Oxidase and Novobiocin [11].The bacterial diagnosis was confirmed by API system and Vitek2 compact (BioMerieux, France).

2.3 Antibiotic susceptibility test for *Staph. aureus* isolates

All *Staph. aureus* isolates were subjected to antibiotic susceptibility by using disc diffusion method [12]. The inhibition zone diameters were measured and interpreted according to [13].

2.4 Serological diagnosis

All isolates were subjected to a serological diagnosis of protein A by using a latex agglutination test. This test consists of yellow latex particles that have been coated with fibrinogen and rabbit immunoglobulin G (IgG)

specific for *Staph. aureus* . This test was performed according to the directions of the manufacturing company (Remel, UK).

2.5 Molecular detection

1. DNA extraction and purification: DNA was extracted and purified according to the company manufacturer instructions (Geneaid / Korea).

2. *Staph. aureus* isolates were subjected to the detection of the 16S rRNA gene by conventional PCR technique using specific primer pairs (Table 1). The amplification was conducted in a thermal cycler (BioRad / USA) which has been programmed with the following conditions: an initial denaturation step for 5 min. at 95°C with one cycle, 30 cycles of amplification were performed as follows: denaturation at 95°C for 30 sec annealing at 58°C for 30 sec and extension at 72°C for 1 min followed by a final extension step at 72°C for 5 min. These conditions were designed by the researcher in this study.

3. DNA sequencing: Three PCR products of the 16S rRNA gene were selected for the sequencer. The sequencing of gene reverse and forward primers was done in Macrogen, Korea outside of Iraq. Basic Local Alignment Search Tool analysis (BLAST) was lead to a blast algorithm. The sample sequences designated as (No1, No2 and No3) were edited, aligned and compared with the reference sequences by using Unweighted Pair Group Method with Arithmetic Mean (UPGMA tree) with MEGA6 software. Thus, the MEGA version 6.0 was used to construct phylogenetic tree**.**

The PCR primers were designed online and provided by (Macrogen, Korea) using NCBI Gene Bank and primers 3 plus[14]as follows (Table1).

Table 1 : Primer sequences of 16S rRNA gene in *Staph. aureus* .

Gene		Primer Sequences (5'-3')	Product size (bp)
16S rRNA *Staph. aureus*	F*	GTTGACTGCCGGTGACAAAC	353
	R*	GCTGTTACGACTTCACCCCA	

F: forwared, *R: reverse, T: thymine, C: cytosine, G: guanine, A: adenine

*

3. Results

3.1 Isolation of *Staph. aureus*

From a total of 600 urine samples from both sexes who suffered from UTI infections with different ages. During the period from August to December, 2018, were collected and tested. The results of the present study showed that 380 (63.5%) isolates noted positive growth of pathogen collected from UTI patients while 220 samples (36.5%) showed no significant growth. Only (50) samples were given growth *Staph. aureus* with 13.5% while 50% were other types of bacteria and 36.5% did not grow, as in figure (1)**.**

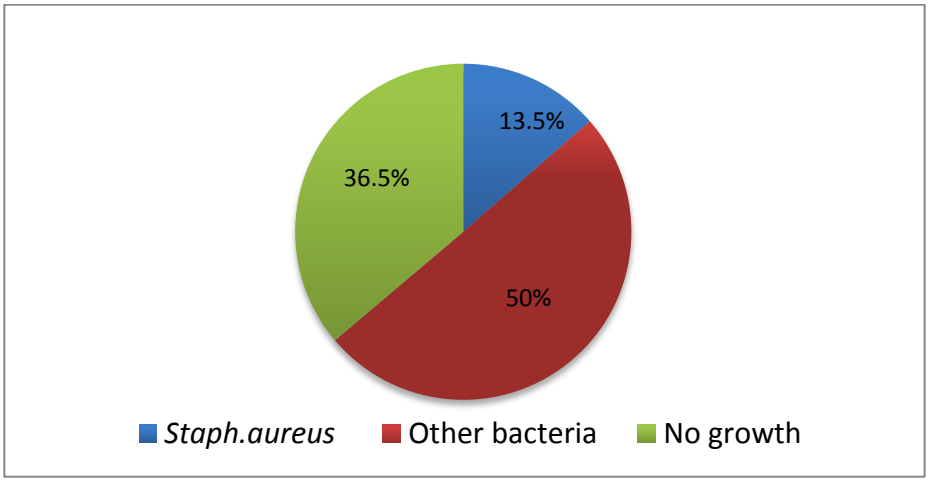

Figure (1): The percentage of *Staph. aureus* and other bacteria isolated from 600 UTI patients.

3.2 Macroscopic & Microscopic examination

Morphology characteristics of *Staph. aureus* grow on different media, such as Blood agar, Mannitol salt agar and Staph 110 meduim, then microscopic examination was applied to all 50 isolates after being stained by gram stain to detect their reaction. The cells appeared as gram-positive cocci, mostly arranged in grapes like irregular clusters.

3.3 Conventional Biochemical tests & Api-20 system identification

In the initial stage of identification, all isolates were identified by biochemical tests such as Catalase, Coagulase**,** Oxidase and Novobiocin. All these tests positive for *Staph. aureus*. Then, used the API 20 *Staph* to confirm the diagnosis of isolates from *Staph. aureus* and to complete important biochemical tests. The result of API-20 *Staph* test has reveals that only 50 isolates identified as *Staph. aureus.*

3.4 Serological diagnosis

All of *Staph. aureus* isolates were diagnosed by Staphaurex Plus which is a rapid latex agglutination test for the identification of Staphylococci which possess clumping factor, protein A and surface antigens characteristic of *Staph. aureus* . When a drop of the reagent is mixed on a card with *Staph. aureus* organisms, rapid agglutination occurs, indicates a positive result. As illustrated in figure (3).

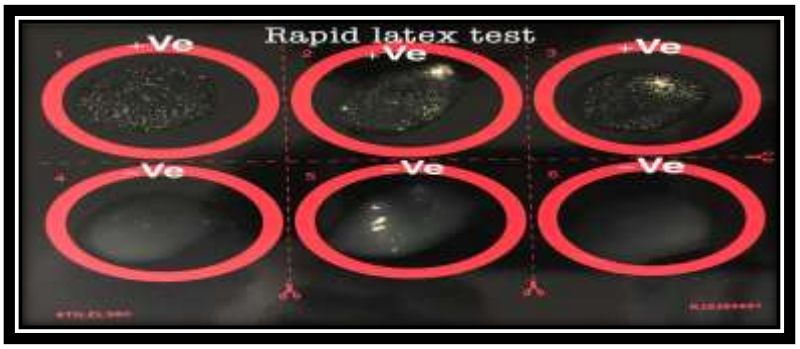

Figure (3): Latex agglutination test for *Staph. aureus*

3.5 Antibiotic susceptibility profile of *Staph. aureus*

All *Staph. aureus* (n=50) was assayed for antibiotic susceptibility test against 14 type of antibiotics. The results showed that there was a variation in resistance rates of the tested bacteria. All *Staph. aureus* isolates were completely resistant to penicillin (P), Oxacillin (Ox), and Ampicillin (Amp) with (100%) for the three antibiotics and highly resistant to Trimethoprim-Sulfamethoxazole, Tetracycline (TE) and Rifampicin (RA) with a percentages of (75.0%),(62.0%), and (52.0%), respectively. While the most effective antibiotics for *Staph. aureus* were

Nitrofurantoin, Gentamycin where isolates were susceptible to these antibiotics in 76%, and 60%, respectively. As shown in figure (2).

3.6 Molecular diagnosis of *Staphylococcus aureus* by 16S rRNA

Fifty isolates of *Staph. aureus* which were identified by biochemical test, API 20, Vitek 2 system and serological diagnosis were subjected to DNA extraction, PCR assay for sequencing of 16S rRNA gene approximately size (353bp). All the isolates were positive for that gene (100%), as in figure (4). The DNA sequences and phylogenetic tree analysis are accurate and highly sensitive diagnostic methods and can be used in many aspects of life and practice.

Figure (2): The percentage of antimicrobial susceptibility of *Staph. aureus* against isolates 14 types of antibiotic.

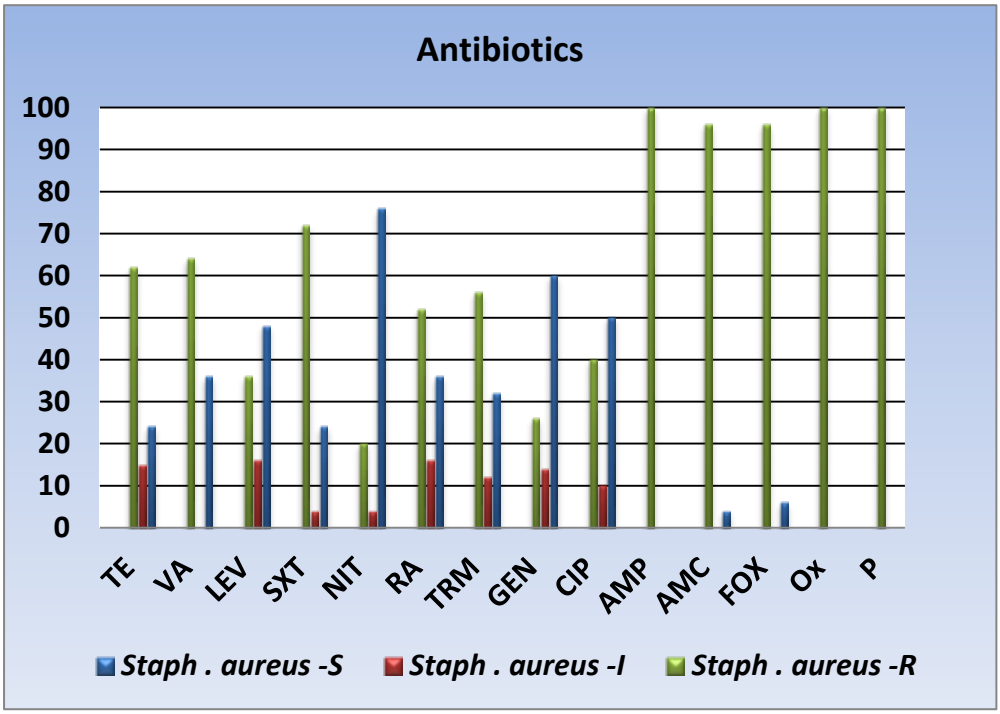

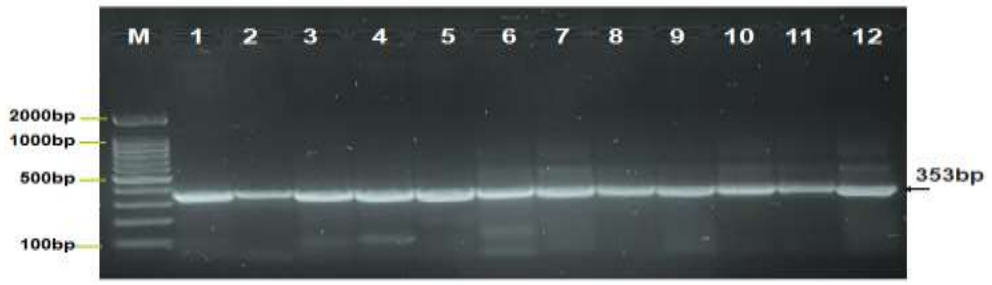

Figure (4): A garose gel electrophoresis presented the analysis of PCR product in *Staph. aureus* 16S ribosomal RNA gene. M represents the Marker ladder with (100-2000bp) while lane (1-12) showed positive *Staph. aureus* isolates at approximately (353bp) product size**.**

Figure (5): Phylogenetic tree analysis based on 16 ribosomal RNA gene

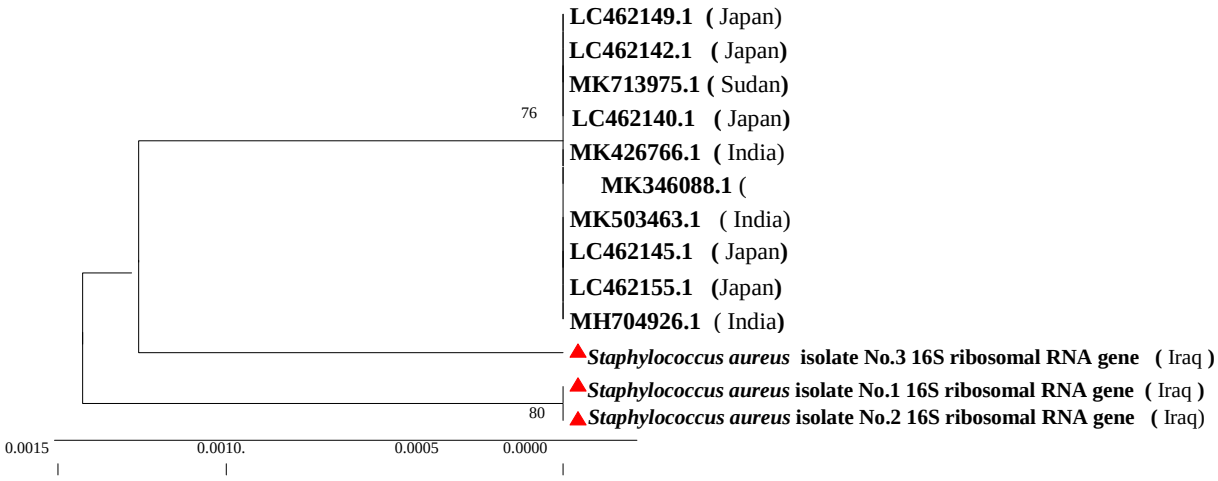

partial sequence in local *Staph. aureus* human urine isolates that used for genetic *Staph. aureus* genetic analysis. The phylogenetic tree was constructed using the Unweighted Pair Group Method with Arithmetic Mean (UPGMA tree) in (MEGA version 6.0).

4. Discussion

4.1 Isolation of *Staph. aureus*

Problems in managing urinary tract infections are attributed to factors related to the host and those related to the causative agents of urinary tract infections. UTIs can occur due to the pathogenicity of the organism, susceptibility of the host, or a combination of both factors[15]. The results of the present study showed that *Staph. aureus* was the most predominant gram-positive species isolated from all UTI cases with a total number of 50/380 (13.15%). Inside Iraq, the current results agreed with [16,17] who recorded both of them (11%) and [18] whom recorded (14.29%) for *Staph. aureus*. Outside Iraq, the present results agreed with results of study [19] who document that (13.71%), of isolates identified as *Staph. aureus* that isolated from UTI patients. On the other hand, the results of the present study were incompatible with [20,21] where *Staph. aureus* accounted for only 0.5%, and 1.5% of isolates respectively, also the results of this study are disagree to other studies, like the results of [22,23], that described a *Staph. aureus* incidence in UTI with a percentages of 28.9%, and 33.3%, respectively. Prior studies suggest that isolation of *Staph. aureus* from the urine is often secondary to Staphylococcal bacteremia originating at another site (e.g., in cases of endocarditis) [24]. This is probably due to the fact that *Staph. aureus* is a member of the normal flora of both asymptomatic carriers and sick persons thus takes advantage of the weak immune system. This organism can be spread by the hands, expelled from the respiratory tract or transmitted by animate or inanimate objects [25].

4.2 Antibiotic susceptibility of *Staph. aureus*

Antimicrobial resistance represents a serious problem in the treatment of infectious diseases including UTI. Antibiotics are the main treatment for all UTIs. A variety of antibiotics are available, and choices depend on many factors, including whether the infection is complicated or uncomplicated or primary or recurrent [26]. Where worldwide data show that there is increasing resistance among urinary tract pathogens to conventional drugs. Antibiotic resistance by Staphylococci is on the increase [27]. The results of antibiotics susceptibility test for *Staph. aureus* isolates showed that there were a high rate of resistance to most

of Penicillin drugs. Inside Iraq, the result of the current study seems to be in agreement with [16,28], who recorded that the same resistance to this antibiotics. Outside Iraq, the results of the present study were compatible with[29], whom recorded high a resistance rate to Oxacillin (100%), Amoxicillin (91.7%), followed by Penicillin (83.3%). Penicillin resistance may be due to the structural modification of enzymatic action (β-lactame action) or the prevention of access to target by altering the outer membrane permeability and may be due to the alternation of the antibiotic target site and sometimes the resistance is due to efflux pump which pumps out the antibiotic [30]. *Staph. aureus* develops resistance very quickly and successfully to different antimicrobials over some time. The present study showed that *Staph. aureus* isolates were highly susceptible to Nitrofurantoin and Gentamycin, a finding that was consistent to that reported by [31,32] where they recorded a sensitive rate of (79.5% ,52.3%), and (85%, 80%), respectively. On the other hand, these results were incompatible with similar studies performed by [33] who founded completely sensitivity of *Staphylococcus* spp. to gentamycin with a percentage of (100%). Also, do not agree with the [18] where the isolates were (75.6%) resistant to gentamycin.

4.3 Serological diagnosis

Protein A was tested for all isolates of *Staph. aureus* under study. The method used in this research is easy to apply as well as sensitive. *Staph. aureus* isolates showed significant variation in their containment of protein A associated with the cell wall. Some isolates of *Staph. aureus* were found to possess this protein. It is the result of having high protein A content that is part of its wall, but the lack of possession of some isolates of *Staph. aureus* of this protein these are due to many reasons, the most important reasons, where the type of culture medium and its components is of great importance in the production of protein A. Research on the effect of carbon source in the production of protein A indicates that the presence of mannitol in the culture medium leads to inhibition of protein production. The presence of high concentration salt affects the production of protein A inhibits its production and affects the correlation efficiency between protein A and the fraction of FC of IgG [34].

4.4 Molecular detection of *Staph. aureus*

Using of Polymerase Chain Reaction (PCR) technique increases the accuracy and speed of *Staph. aureus* identification and validation [35]. The DNA sequences and phylogenetic tree analysis are accurate and highly sensitive diagnostic methods and can be used in many aspects of life and practice [36]. All isolates gave a positive reaction to the 16S rRNA gene. This finding agrees with other local studies [37,38,39] who revealed the complete percentage of the 16SrRNA gene. Outside Iraq, some results agreed to go for from what was recorded [40,41] who recorded that all isolates had 16S rRNA. Also, the results of this study disagree with[42]. These differences may be due to many factors; such as the sources and number of the clinical samples used, geographical dependency, and the sensitivity of different techniques used. This gene was used for diagnosis and through this tree we found that the isolates of the study were genetically identical by 99% with those found in the genebank. The isolates of the three studies are genetically far from the genes taken from the genebank because they appeared in the out group, especially isolates No.1 and No.2 that appeared genetically identical while isolate No. 3 has a genetic relationship with the genes taken from the genebank this is confirmed by the value of the boot strap, which amounted to 76%. The value of the boot strap that appeared among the study isolates was good. The constructed phylogenetic tree showed that *Staph. aureus* MK910079.1 and MK910080.1 were highly relative to each other in comparison with *Staph. aureus* MK910081.1 that revealed a close relatedness to *Staph. aureus* from India, Sudan and Japan, at total genetic changes (0.0005-0.0015%) (Fig. 5).

Conclusions

Staphylococcus aureus consider as one of important Gram positive causative agents of UTI infections and has become one of the most successful adaptable human pathogens.

References:

[1] Negussie, A.; Worku, G., and Beyene, E. (2018). Bacterial identification and drug susceptibility pattern of urinary tract infection in pregnant women at Karamar Hospital Jigjiga, Eastern Ethiopia. African Journal of Bacteriology Research, 10(2): 15-22.

[2] Hassan, H. E. M.; Altayb, H. N.; El Hassan, M. M., and Elmekki, M. A. (2018). Genotypic detection of the virulence factors of uropathogenic *Escherichia coli* isolated from diarrheic and urinary tract infected patients in Khartoumn State, Sudan.African Journal of Microbiology Research,12(9): 230-236.

[3] Griebling, T. L. (2018). How Often do Clinically Diagnosed Catheter-Associated Urinary Tract Infections in Nursing Homes Meet Standardized Criteria?. The Journal of urology, 200(6): 1141-1144.

[4] Flores-Mireles, A. L., Walker, J. N., Caparon, M., and Hultgren, S. J. (2015). Urinary tract infections: epidemiology, mechanisms of infection and treatment options. Nature reviews microbiology, 13(5): 269.284.

[5] Bradley, C. W.; Flavell, H.; Raybould, L.; McCoy, H.; Dempster, L.; Holden, E., and Garvey, M. I. (2018). Reducing *Escherichia coli* bacteraemia associated with catheter-associated urinary tract infections in the secondary care setting. Journal of Hospital Infection, 98(3): 236-237.

[6] Muder, R. R.; Brennen, C.; Rihs, J. D.; Wagener, M. M.; Obman, A.; Obman, A., and Yu, V. L. (2006). Isolation of *Staphylococcus aureus* from the urinary tract: association of isolation with symptomatic urinary tract infection and subsequent Staphylococcal bacteremia. Clinical infectious diseases, 42(1): 46-50.

[7] Brooks, G. F.; Carroll, K. C.; Butel, J. S.; Morse, S. A., and Mietzner, T.A(2013). Medical Microbiology, (26th ed.). New York. USA: McGraw-Hill Education, p.880.

[8] Kumosani, T. (2014). Nosocomial Infections in Saudi Arabia Caused by Methicillin Resistance *Staphylococcus aureus* (MRSA). Clinical Microbiology: Open Access, 03(03): 2–5.

[9] Smith, D. S.; Siggins, M. K.; Gierula, M.; Pichon, B.; Turner, C. E.; Lynskey, N. N., and Sriskandan, S. (2016). Identification of commonly expressed exoproteins and proteolytic cleavage events by proteomic mining of clinically relevant UK isolates of *Staphylococcus aureus*. Microbial genomics, 2(2).

[10] Benson, J. H. (2001). Microbiological Applications: Laboratory Manual in General Microbiology. (8th ed). McGraw-Hill Higher Education, New York, PP: 125-130.

[11] MacFaddin, J. F. (2000). Biochemical tests for identification of medical bacteria, (3rd ed.). USA: Lippinocott Williams and Wilkins, p. 912.

[12] Bauer, A. W.; Kirby, W. M. M.; Sherris, J. C., and Turck, M. (1966). Antibiotic susceptibility testing by a standardized single disk method. American journal of clinical pathology, 45(4): 493-496.

[13] Clinical and Laboratory Standards Institute (2018). Performance standards for antimicrobial susceptibility testing of anaerobic bacteria: informational supplement. CLSI document M100, (28th ed.) Wayne, PA USA.: 258p.

[14] Untergasser, A.; Nijveen, H.; Rao, X.; Bisseling, T.; Geurts, R., and Leunissen, J. A. (2007). Primer3Plus, an enhanced web interface to Primer3. Nucleic acids research, 35(2): W71-74.

[15] Flores-Mireles, A. L.; Walker, J. N.; Caparon, M., and Hultgren, S. J. (2015). Urinary tract infections: epidemiology, mechanisms of infection and treatment options. Nature reviews microbiology, 13(5): 269-284.

[16] Al-Jebouri, M. M., and Mdish, S. A. (2013). Antibiotic resistance pattern of bacteria isolated from patients of urinary tract infections in Iraq. Open Journal of Urology, 3(02): 124-131.

[17] Abdulrahman, I. S. (2018). Antimicrobial Susceptibility Pattern of Pathogenic Bacteria Causing Urinary Tract Infections at Azadi Hospital In Duhok City\Kurdistan Region of Iraq. Science Journal of University of Zakho, 6(2): 46-50.

[18] Alsamarai, A. G. M.; Khorshed, S. A., and Ali, H. (2016). Urinary tract infection in female in Kirkuk, Iraq: impact of younger aged women compared to diabetic and pregnant women. World Journal Of Pharmacy and Pharmaceutical Sciences, 5(11), 73-86.

[19] Mollick, S.; Dasgupta, T.; Hasnain, M. J., and Ahmed, M. (2016). Isolation and characterization of pathogens responsible for urinary tract infection in Bangladesh and determination of their antibiotic susceptibility pattern. Journal of Applied Pharmaceutical Science, 6(04): 072-076.

[20] Barrett, S. P.; Savage, M. A.; Rebec, M. P.; Guyot, A.; Andrews, N., and Shrimpton, S. B. (1999). Antibiotic sensitivity of bacteria associated with community-acquired urinary tract infection in Britain. Journal of Antimicrobial Chemotherapy, 44(3): 359-365.

[21] Mane, M. S.; Sandhya, B. K.; Priya, R .L., and Magdalene, J. (2015). Prevalence and antibiotic susceptibility pattern of bacterial isolates from urinary tract infection in a tertiary care hospital in Tamilnadu. Journal of medical and dental sciences, 14 (7): 59-65.

[22] Okonko, I. O.; Ijandipe, L. A.; Ilusanya, A. O.; Donbraye-Emmanuel, O. B.; Ejembi, J., Udeze, A. O., and Nkang, A. O. (2010). Detection of urinary tract

infection (UTI) among pregnant women in Oluyoro Catholic Hospital, Ibadan, South-Western Nigeria. Malaysian journal of Microbiology, 6(1): 16-24.

[23] Alwash, S. J., and Saleh, D. S. (2013). Comparison between Cefoxitin disk diffusion, Crome agar and EPI-M Screening Kit for Detection of Methicillin-Resistant *Staphylococcus aureus*. Iraqi Journal of Science, 54(4): 847-850.

[24] Muder, R. R.; Brennen, C.; Rihs, J. D.; Wagener, M. M.; Obman, A.; Obman, A., and Yu, V. L. (2006). Isolation of *Staphylococcus aureus* from the urinary tract: association of isolation with symptomatic urinary tract infection and subsequent Staphylococcal bacteremia. Clinical infectious diseases, 42(1): 46-50.

[25] DeLeo, F. R.; Diep, B. A., and Otto, M. (2009). Host defense and pathogenesis in *Staphylococcus aureus* infections. Infectious disease clinics of North America, 23(1): 17-34.

[26] Zahera, M.; Rastogi, C.; Singh, P.; Iram, S.; Khalid, S., and Kushwaha, A. (2011). Isolation, identification and characterization of *Escherichia coli* from urine samples and their antibiotic sensitivity pattern. European Journal of Experimental Biology, 1(2): 118-124.

[27] Khan, R. A.; Khan, F. A.; Iqbal, M., and Nigar, H. (2019). Prevalence and antibiotic susceptibility of multi-drug resistant *Staphylococcus aureus* and *Acinetobacter baumannii* in clinical samples from intensive care unit patients in a tertiary care hospital at Peshawar (Pakistan). Anaesthesia, Pain and Intensive Care, 231-236.

[28] Hussein, N. R.; Daniel, S.; Salim, K., and Assafi, M. S. (2018). Urinary Tract Infections and Antibiotic Sensitivity Patterns Among Women Referred to Azadi Teaching Hospital, Duhok, Iraq. Avicenna Journal of Clinical Microbiology and Infection, 5(2): 27–30.

[29] Chandrasekaran, D.; Venkatesan, P.; Tirumurugaan, K. G.; Nambi, A. P.; Thirunavukkarasu, P. S.; Kumanan, K., and Ramesh, S. (2014). Pattern of antibiotic resistant mastitis in dairy cows. Veterinary World, 7(6): 389-394.

[30] Chakraborty, S. P.; KarMahapatra, S.; Bal, M., and Roy, S. (2011). Isolation and identification of vancomycin resistant *Staphylococcus aureus* from postoperative pus sample. Al Ameen Journal of Medical Sciences, 4(2): 152-168.

[31] Hammoudi, A. A. (2013). Urinary tract infection of adults in Baghdad City. International Journal of Current Microbiology and Applied Sciences, 2: 1-6.

[32] Sujatha, R., and Pal, N. (2015). Antibiotic Resistance Pattern Of The Hospital And Community Acquire Isolates Of Uropathogens In A Teritiary Care Centre at Kanpur" Rama Univ. Journal of Medical Sciences, 1(1): 10-17.

[33] Bendahou, A.; Lebbadi, M.; Ennanei, L.; Essadqui, F. Z., and Abid, M. (2008). Characterization of *Staphylococcus* species isolated from raw milk and milk products (lben and jben) in North Morocco. The Journal of Infection in Developing Countries, 2(03): 218-225.

[34] Cheung, A. L.; Nishina, K. A.; Trotonda, M. P., and Tamber, S. (2008). The SarA protein family of *Staphylococcus aureus*. The international journal of biochemistry and cell biology, 40(3): 355-361.

[35] Rallapalli, S.; Verghese, S., and Verma, R. S. (2008). Validation of multiplex PCR strategy for simultaneous detection and identification of methicillin resistant *Staphylococcus aureus*. Indian Journal of Medical Microbiology, 26(4): 361-364.

[36] Didelot, X.; Bowden, R.; Wilson, D. J.; Peto, T. E., and Crook, D. W. (2012). Transforming clinical microbiology with bacterial genome sequencing. Nature Reviews Genetics, 13(9): 601-612.

[37] Ibed, A. N., and Hamim, S. S. (2014). Molecular detection of methicillin resistant *Staphylococcus aureus* isolated from burns infection in Al-Nasiriyah City. World Journal of Pharmaceutical Sciences, 2: 950-954.

[38] Degaim, Z. D.; Shani, W. S., and Hamim, S. S. (2015). Virulence factors of Methicillin Resistant *Staphylococcus aureus* (MRSA) isolated from burn patients. International Journal of Current Microbiology and Applied Sciences, 4: 898-906.

[39] Hashim, I. A.; Wdaah, Q. H., and Atya, A. A. (2019). Potential effect of antimicrobial agents against *Staphylococcus aureus* and *Pseudomonas aeruginosa* strains from patients with skin infections. University of Thi-Qar Journal of Science, 7(1): 7-14.

[40] Makgotlho, P. E.; Kock, M. M.; Hoosen, A.; Lekalakala, R.; Omar, S.; Dove, M., and Ehlers, M. M. (2009). Molecular identification and genotyping of MRSA isolates. Federation of European Microbiological Societies Immunology and Medical Microbiology, 57(2): 104-115.

[41] Al-Talib, H.; Yean, C. Y.; Al-Khateeb, A.; Hassan, H.; Singh, K. K. B.; Al-Jashamy, K., and Ravichandran, M. (2009). A pentaplex PCR assay for the rapid detection of methicillin-resistant *Staphylococcus aureus* and Panton-Valentine Leucocidin. BMC microbiology, 9(1): 113-119.

[42] Zhang, K.; Sparling, J.; Chow, B. L.; Elsayed, S.; Hussain, Z.; Church, D. L., and Conly, J. M. (2004). New quadriplex PCR assay for detection of methicillin and mupirocin resistance and simultaneous discrimination of *Staphylococcus aureus* from Coagulase-Negative Staphylococci. Journal of clinical microbiology, 42(11), 4947-4955

University of Thi-Qar Journal Vol.14 No.3 SEP 2019
Web Site: https://jutq.utq.edu.iq/index.php/main
Email: utj@utq.edu.iq

الكشف المصلي والجزيئي للمكورات العنقودية الذهبية المعزولة من مرضى التهاب المسالك البولية

احمد عبدالرزاق عباس * سعد سلمان هميم **
hamim_pa@sci.utq.edu.iq
*** مكتب وزارة الصحة ذي قار**
**** قسم التحليلات المرضية ، كلية العلوم ، جامعة ذي قار ، العراق**

المستخلص:

تعتبر التهابات المسالك البولية واحدة من أكثر الإصابات شيوعًا التي يواجهها الأطباء على الرغم من توفر الأدوية المضادة للميكروبات على نطاق واسع. الالتهابات ناجمة عن مسببات بكتيرية مختلفة تنتشر بصورة واسعه ويمكن الحصول على العدوى بهذا المرض من خلال كل من المستشفى والمجتمع. هدفت الدراسة الحالية التحري عن بكتيريا المكورات العنقودية الذهبية المعزولة من مرضى التهاب المسالك البولية بحالاته المختلفة البسيطة والمعقدة، والكشف عن مضادات الميكروبات الأمثل لعلاج هذه الالتهابات. حيث تم جمع 600 عينة ادرار من منتصف مجرى البول خلال الفترة من أغسطس إلى ديسمبر 2018 من المرضى الذين يشتكون من التهاب المسالك البولية في مستشفى الحسين التعليمي في مدينة الناصرية, جنوب العراق. الدراسة شملت عزل وتشخيص المكورات العنقودية الذهبية على أساس الوصف المظهري والمجهري والأختبارات الكيميائية الحيوية وتأكيدها بواسطة أنظمة API-20 و Vitek2. اضافة إلى ذلك ، تعرضت جميع عزلات المكورات العنقودية الذهبية للتشخيص المصلي للبروتين A باستخدام اختبار تراص اللاتكس واستخدمت تقنية انزيم تفاعل البلمرة التقليدية للكشف عن وجود جين 16s RNA(353 زوج قاعدي). حيث تم تسجيل (380) عزلة موجبة ، وتم تحديد المكورات العنقودية الذهبية ب 50 عزلة (13.5%). ايضا خضعت جميع عزلات المكورات العنقودية لفحص الحساسية الدوائية ضد 14 نوع من المضادات الحيوية المختارة بأستخدام طريقة الأنتشار عبر الأقراص. حيث كانت جميع عزلات المكورات العنقودية الذهبية مقاومة تمامًا لمضادات البنسلين (P) والأوكساسيلين (Ox) والأمبيسيلين (Amp). بينما المضادات الحيوية الأكثر فعالية للمكورات العنقودية الذهبية كانت هي نيتروفورانتوين (NIT)و جنتاميسين (GN) ، حيث أظهرت العزلات حساسية لهذه المضادات بنسبة 76 ٪ و 60% تواليا .اما فيما يخص تحليل تسلسل النيوكليوتيدات لجين 16s RNA ، أظهرت النتائج أن هذه البكتيريا مرتبطة فعليًا بالبكتريا العنقودية الذهبية، ووفقًا للنتيجة الحالية ، ثلاثة من هذه العزلات سجلت عالميًا في بنك الجينات،وأرقام الانضمام إلى هذه العزلات هي (MK910079.1و MK910080.1 و MK910081.1).

الكلمات المفتاحية: المكورات العنقودية الذهبية ، التهابات المسالك البولية ، التشخيص ، الكشف المصلي والجزيئي.

University of Thi-Qar Journal Vol.14 No.3 SEP 2019
Web Site: https://jutq.utq.edu.iq/index.php/main
Email: utj@utq.edu.iq

Theoretical study for Coronene and Coronene-Al, B, C, Ga, In and Coronene-O interactions by using Density Functional theory

Abbas Sh. Alwan, Sadiq Kh. Ajeel, Mohammed L. Jabbar
Physics Department, College of science, Thi-Qar University, Iraq
Emails: abbasshwaa_ph@sci.utq.edu.iq
abbasalwan@hotmail.com

Abstract

Molecular structure geometry have been investigated for Coronene and Coronene-Al, B, C, Ga, In and Coronene-O by using Gaussian software at basis set 3-21G, B3LYP level, density functional theory (DFT). Adding the atoms Al, B, C, Ga, In or Oxygen to Coronene change electrons density distribution. Study of the magnetic characterstics shows that some systems like Coronene-Carbon and Coronene-oxygen has the antiferromagnetic charactersti, this type of magnetic properties stands for open shel system which has two type of orbital α and β orbitals. Individual atoms calculations was achieved in order to make a comparison between Coronene and the atoms to demonstrate which of them will behave as a donor or an acceptor. E_{HOMO}, E_{SOMO}, E_{LUMO}, total energy electronegativity and electrophilicity were evaluated for all paradigms under the study. Using DFT to study the symmetry shows that there are two types of point group symmetries C_{6h}/C_1 and Cs/C_1. Coronene-Corbon posseses the highest dipole moment value among the samples, it has the value (5.5873 Debye), dipole moment credit is very important to give sight about the internal structure of substances. Calculations of chemical potential shows clearly Al, Ga and In behave as donors, while B, C and O behave as acceptors. Also binding energy study exhibits that Coronene is going to physisorbe on the surface of the atoms B, C and O.

Keywords: DFT, Contours, Symmetry, Dipole moment, Binding energy.

Introduction

One can investigate the electronic structure of particular atoms, molecules, nanoclusters, nanoribons, nanoballs and substances by using

quantum mechanics methods such as Hartree-Fock approximation, post Hartree-Fock methods and density functional theory [1]. Density functional approaches form the basics of a variety and very active sciences nowadays computational atomic, molecular, nuclear and even solid state physics [2]. Density functional theory treats with the systems that have many particles throughout the electron density [3]. Electron density is the likelihood of determining existence places of the electrons at certain space[4]. Density functional theory suppose the electron density instead of the wave function, and also it assumes the electron density only depends on three spatial coordinates without regarding how the electrons are existed in the systems, while the wave function approximation considers 3N variables, three spatial coordinates, one coordinate for spin by assumption the nuclei location is fixed [5]. Density functional theory seek on ground state energy, ane also say it seach on approximation solution to schrodinger equation of many electrons system [6]. In DFT many electrons system can described by functionals [7]. DFT calculation agree tremendously with the practical results. Gaussian orbitals in density functional approximations can expressed as a Gaussian function vary exponentially with the square of the position of the electrons [8]. Using B3LYP basis set in density functional theory gives precisely consequences than other approaches [9]. Exchange correlation functionals are from the important instruments in the computations of density functional theory [10]. Total atom charge is calculated depending on Mullkin method when on use density functional theory for studying properties of many electrons system [11]. Computations of density functional approximations take in account inner shell electrons, inner valence electrons and outer valence electrons [12].

Results and Discussion

Molecular Geometry

Molecular structure point out arrangement of atoms in the molecule, it denotes to positions of atoms in the substance[13]. Molecular structure maps clarify the optimized parameters, bond lengths, bond angles and dihedral angles [14]. Optimization of Coronene and Coronene-Al, Coronene-B, Coronene-C, Coronene-Ga, Coronene-In and Coronene-O interactions have been carried out with Gaussian 09 software package.

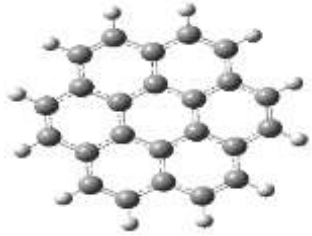

Figure (1) Molecular structure of Coronene

Coronene-Al

Coronene-B

Coronene-C

Coronene-Ga

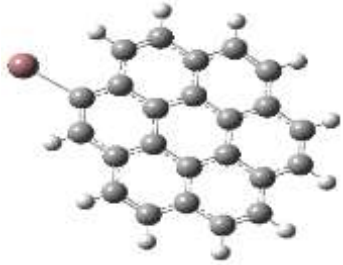

Coronene-In

Coronene-O

Figure (2) Molecular structure of Coronene-Al, B, C, Ga, In and Coronene-O

From Figure (1) one can say the molecular structure of Coronene and Coronene-Al, Coronene-B, Coronene-C, Coronene-Ga, Coronene-In and Coronene-O have been gained throughout the geometry optimization procedure that search on stationary points on the potential surfaces. Molecular structure describe the topological properties, bond angles among any three atoms and dihedral angles among any four atoms. In order to get the optimized molecular structure the geometry optimization seek on the lowest energy.

Contours

One can express the electrons density throughout the contours [15]. Contours have been implemented at electrostatic potential (ESP). Contour maps explain mechanism of the reaction throughout determination the active sites in the molecule. Contour maps is very useful in the study of charge exchange and energy transfer procedures, also the contours maps yield the spatial distribution with the surface [16]. Electrostatic potential maps have been investigated for Coronene and Coronene – Al, B, C, Ga, In, O interactions.

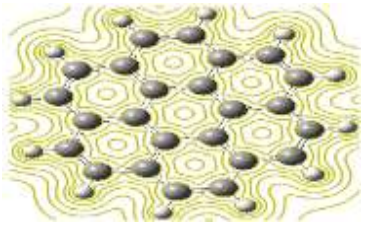

Figure(3)

Contours for Coronene

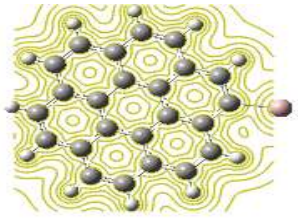

Coronene-Al

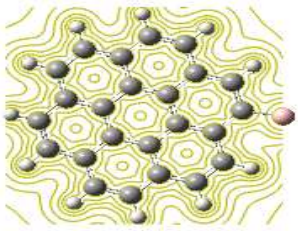

Coronene-B

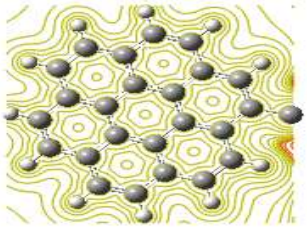

Coronene-C

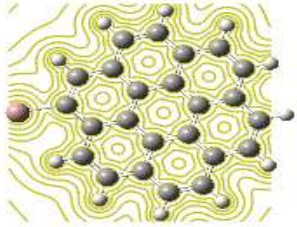

Coronene-Ga

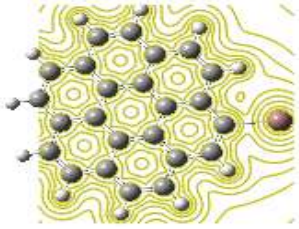

Coronene-In

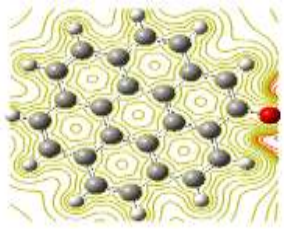

Coronene-O

Figure(4)

Contours of Coronene-Al, B, C, Ga, In and Coronene-O

In Figures (3) and (4) one can remark electronical density contours, contour maps show clarity charge density distribution around atoms. Adding atoms of Aluminume, Boron, Carbon, Gallium, Indium and Oxygen to Coronene make distortion in contour maps, this refers to the interaction of those atoms with Coronene surface. Also contour diagrams give informations about interaction behavior and the probability to come about. Wave packet propagation of electrons tremendously associated with contour schemes. Charge distribution around Oxygen atom is the maximum among all atoms

that adding to Coronene, also one can see contour distortion as a result to addition of Carbon atom to Coronene is higher than all of Aluminume, Boron, Gallium and Indium, that is to say charge distribution about the other atoms (Aluminume, Boron, Gallium and Indium) except Oxygen.

Magnetic Properties

Magnet is very important in many useful devices, such as electric generators, electric transformers and also computers. Solid substances are divided according to response to the magnet into many types:paramagnetic, diamagnetic, ferromagnetic, anti-ferromagnetic and ferrimagnetic [17]. Magnetic credits for Coronene and Coronene- Al, B, C, Ga, In, O were investigated through geometrical optimization process.

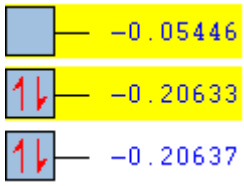

Figure(5)

Magnetic properties for Coronene

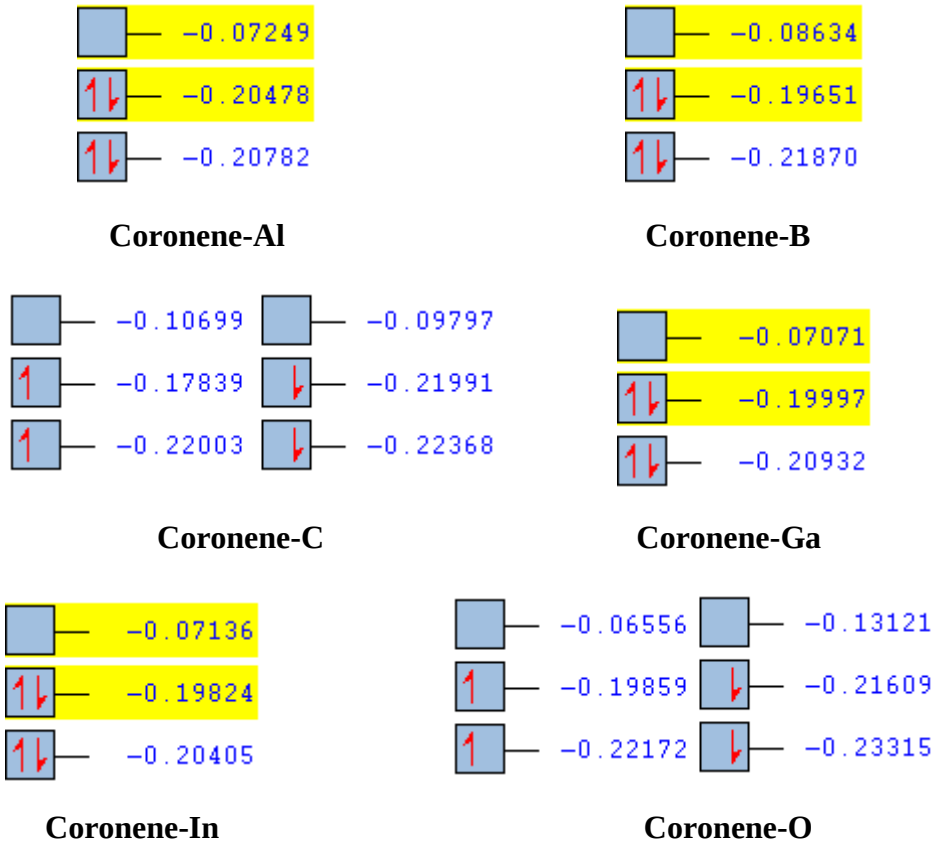

Figure(6)

Magnetic properties for Coronene and Coronene-Al, B, C, Ga, In, O

One can see in figure(5) and Figure(6) the difference in magnetic properties for samples under the study spin property demonstrate if the sample is closed or open system. Coronene, Coronene-Al, Coronene-B, Coronene-Ga and Coronene-Al are of the type closed because the occupied ultimate orbital is perfectly filled, but the occupies final orbital in Coronene-C and Coronene-O is partially filled with electrons, ie. those systems open systems. Open system describe the anti-ferromagnetic characterstic, Coronene-C and Coronene-O anti-ferromagnetic systems.

Individual atoms Calculations

Computations of individual atoms is very important for discussion some properties materials. Some of these properties are total energy, electronegativity and electrophilicity as in table (1).

Table (1) shows individual atoms(Al, B, C, G, In and O) calculations.

atom	HOMO (eV)	LUMO (eV)	Total energy (eV)	Electronegativity	Electrophilicity
Al	-3.5484561	2.0766672	-6558.802772	0.73589445	0.096271782
B	-4.900521	-2.4361113	-667.1519136	3.66831615	5.460351571
C	-5.153574	-3.4834242	-1022.359854	4.3184991	11.16632441
Ga	-3.3242457	-1.9308216	-52117.89136	2.62753365	4.954653132
In	-3.2262897	-2.0129958	-155575.2965	2.61964275	5.656113607
O	-8.6565894	-6.4993806	-2028.639308	7.577985	26.62044428

Symmetry

In general there are seven elements of the symmetries that molecular systems own, those seven elements are identity, proper axis, horizontal plane, vertical plane, dihedral plane, improper axis and inversion center or center of symmetry [18]. All element contains symmetry operation. Point group symmetries in the present study were obtained for Coronene and Coronene and Coronene-Al, B, C, Ga, In, O through the geometry optimization procedure of the studying systems.

Table (2) shows the point group symmetries of Coronene and Coronene and Coronene-Al, B, C, Ga, In, O.

System	Symmetry
Coronene	C6h/C1

Coronene-Al	Cs/C1
Coronene-B	Cs/C1
Coronene-C	Cs/C1
Coronene-Ga	Cs/C1
Coronene-In	Cs/C1
Coronene-O	Cs/C1

In Table (2) one can show that Coronene has the symmetry C_{6h}/C_1 , one can say the rotation in Coronene obtains by 60^o since Coronene of the kind of that has rotation repeats the same molecule by (360/n) degrees, also, Coronene has horizontal mirror plane (h). All other systems (Coronene, Coronene-Al, Coronene-B, Coronene-Ga and Coronene-Al Coronene-C and Coronene-O) have two elements identity and mirror plane, Also all those systems repeat themselves throughout 360^o. Symmetry is very important credit, it gives informations obout the molecular structures without calculations.

Dipole moment

Dipole moment represents charge multiplying by the displacement between two signal different charges one is positive and the other is negative. Dipole moment illustrates in hetronuclear molecules. It can be described by the following relation[19]

$$P = q\, r$$

Table (3) shows the dipole moments for Coronene and Coronene – Al, B, C, Ga, In, O interactions.

System	Dipole moment (Debye)
Coronene	0.0000
Coronene-Al	1.4223

Coronene-B	5.0211
Coronene-C	5.5873
Coronene-Ga	1.9236
Coronene-In	0.2504
Coronene-O	4.5746

From Table (3) on can visualize that Coronene has zero value of the dipole moment although it has two type of atoms Carbon and Hydrogen, this occurs because of many factors such as the molecular structure and symmetry. Adding Boron atom to Coronene makes it has value of dipole moment equal to (5.0211 Debye) because the system Coronene-Boron Hetronuclear, Also this happen because of the hybridization procedure. So Coronene-Aluminume, Coronene-Carbon, Coronene-Oxygen and Coronene-Gallium Hetronuclear, therefore they have nonzero values of dipole moment. Coronene-Indium has semi-zero value of the dipole moment although it is hetronuclear system this also takes place because of many factors like the molecular structure, symmetry and hybridization.

Donor Acceptor property

Electronegativity show trend of an atom for attracting a bonding pair of electrons. It is a property show tendency of the electrons to escape from equilibrium system, this system perhaps atoms or molecules system. The mathematical description of the electronegativity as follows[20]

$$\mu = \left(\frac{\partial E}{\partial N}\right)_{V(r)} \approx -\chi$$

Electrophilicity is the property that measure the energy lowering which result from maximum electron flow between donor and acceptor. The following equation show how the electrophilicity is calculated [21]

$$\omega = \frac{\mu^2}{2\eta}$$

Table (4) shows the electronegativities and electrophilicities for Coronene and Coronene – Al, B, C, Ga, In, O interactions.

System	Electronegativity	Electrophilicity
Coronene	3.54804795	1.291590487
Coronene-Al	3.77225835	1.551508697
Coronene-B	3.84817425	1.774579507
Coronene-C	3.8825949	2.217892895
Coronene-Ga	3.6826014	1.513845256
Coronene-In	3.667908	1.520773863
Coronene-O	3.59376075	1.431294708

According to Table (4) one can classify Coronene and the adding atoms if it behave as a donor or an acceptor. With consideration to this table in Coronene-Al, Coronene-Ga and Coronene-In, the adding atoms (Al, Ga and In) behave as donors while Coronene became an acceptor, electrons of Al, Ga and In atoms adsorbed on Coronene surface. While in Coronene-B, Coronene-C and Coronene-O come about the contrary, Coronene behaves as a donor, but Boron atom, Carbon atom and Oxygen atom become acceptors, electrons of coronene will physisorbe on B, C and O atoms.

Binding energy

In general binding energy denotes to the work done against the electric attraction. Sometimes it is called the separation energy, because it is the energy required to decompose atom, molecule or nucleus into its constituent particles [22]. Mathematically it has the formula [23]

$$E_B = nE(X) + mE(Y) - E(X_nY_m)$$

$E(X)$ is the energy of the molecule X, $E(Y)$ is the energy of the molecule Y, $E(X_nY_m)$ is the energy of the molecule X_nY_m, n is number of atoms for the molecule X, m is Number of atoms for the molecule Y.

Table (5) shows the binding energies for Coronene and Coronene – Al, B, C, Ga, In, O.

System	Binding Energy(eV)
Coronene-Al	-481936.5177
Coronene-B	17486.05166
Coronene-C	26796.05177
Coronene-Ga	1366009.933
Coronene-In	4077628.521
Coronene-O	53170.63626

Table (5) exhibits the binding energy of the ground state, binding energies shows how (Al, Ga and In) physisorbs on Coronene surface, so visualize that Coronene atoms can adsorbed on B, C and O atoms surfaces. Binding energies between Coronene surface and (Al, Ga, In, B, C and O) indicates to that the interaction between Coronene surface and those atoms takes place at certain distances represents the bond lengthes. The binding energies refer to a physical interaction between (Al, Ga, In, B, C and O) and Coronene surface. The linear combination of the atomic orbitals between Coronene and (Al, Ga, In, B, C and O) forms the binding energies in Coronene-Al, Coronene-Ga, Coronene-In, Coronene-B, Coronene-C and Coronene Oxygen.

Conclusions

Molecular geometry maps clarify that the distances (bond angles), bond angles and dihedral angles between Coronene surface and the adding individual atoms are different, that is to say charge transfer between theatoms and Coronene surface obtain at different optimized parameters. Contour maps diagrams demonstrate the distortion in the wave function of electrons, electrons density distributions and electrostatic potential. Electrons density distribution in the samples Coronene-C and Coronene-O is clear tremendously largerger than the other samples through Contour diagrams. Only alpha orbitals result in Coronene and Coronene- Al, Ga, In, B, but alpha and beta orbitals consequent in the samples Coronene-C and Coronene-O, those two paradigms has the E_{SOMO} and E_{LUMO}, one can assert those two patterns have antiferromagnetic characterstics. It is very clear that adding any atom to Coronene in this study make the symmetry properties different. Coronene-In has the minimum value of dipole moment, but Coronene-C hasthe maximum valueof dipole moment. Coronene behave as a donor in the paradigms Coronene-Al, Ga, In, but it behaves as an acceptor in Coronene-B, C, O through charge transfer procedures. Also computations of electronegativity characterstic shows clearly Al, Ga and In behave as donors, while B, C and O behave as acceptors. Coronene-Al has negative value of the binding energy because of the nature of bonding which gets throughout geometry optimization procedure.

Acknowledgements

Our thankful for Prof. Dr. Hamid I. Abboud, Prof. Dr. Falah H. Hannon and Asst. prof Fouad N. Ajeel.

References

[1] Assadi, M.H.N, *et al*. Theoretical study on copper's energetic and magnetism in TiO2 polymorphs. (2013).
[2] Van Maurik, Tanjia, Gdanitz, Robert J. Acritical note on density functional theory studies on rare-gas dimmers. Journal of Chemical Physics 116 (22): 9620-9623. (2002).
[3]] Zimmerli., Urs., Parrinello., Michele., Koumoutsakos., Petros., Dispersion corrections to density functionals for water aromatic interactions, Journal of Chemical Physics 120 (6): 2693-2699. (2004).
[4] Parr, Robert G., Yang, Weitao, Density-Functional Theory of Atoms and Molecules, Oxford University Press, (1994).

[5] C.J. Carmer, Essential of Computational Chemistry, Chichester, John Wiley and Sons, Ltd,
154-168. (2002).
[6] C.J. Carmer, Essential of Computational Chemistry, Chichester: John Wiley and Sons, Ltd,
(2002), 154-168.
[7] Wolfram Koch, Max C. Holthausen, A Chemist's Guide to Density Functional Theory, 2nd Edition, Wiley–VCH Verlag GmbH, Germany, (2001).
[8] G. Robert, D.Yang, Weitao, Density-Functional Theory of Atoms and Molecules, Oxford University Press, (1994).

[9] C. Lee, W. Yang, R.G. Parr, Development of the Colle-Salvetti correlation-energy formula into a functional of the electron density, Phys. Rev. B 37, 785, (1988).

[10] Jack Simons, An Introduction to Theoretical Chemistry, Salt Lake City, Utah, University of Utah, Chemistry Department, (2000).
[11] Ali A. M., Investigations Of Some Antioxidant Materials By Using Density Functional And Semiempirical Theories, P.hD. Thesis, University of Basrah, College of Science, Department of Physics, (2009).
[12] Jensen, Frank, Introduction to computational chemistry. JohnWiley and Sons. Pp. 68-77. (1999).
[13] M. J. Frisch, G.W. Trucks, H. B. Schlegel, G. E. Scuseria, M. A. Robb, J. R. Cheeseman, G.Scalmani, V. Barone, B. Mennucci, G. A. Petersson, H. Nakatsuji, M. Caricato, X. Li, H. P. Hartchain, A. F. Izmaylov, J. Bloino, G. Zheng, J. L. Sonnenberg, M. Hada, M. Ehara, K. Toyota, R. Fukuda, J. Hasegawa, M. Ishida, T.Nakajima, Y. Honda, O. Kitao, H. Nakai, T. Vreven, J. A. Montgomery, Jr., J. E. Peralta, F. Ogliaro, M. Bearpark, J. J. Heyd, E. Brothers, K. N. Kudin, V. N. Staroverov, R. Kobayashi, J. Normand, K. Raghavachari, A. Rendell, J. C. Burant, S. S. Iyengar, J. Tomasi, M. Cossi, N. Rega, J. M. Millam, M. Klene, J. E. Knox, J. B. Cross, V. Bakken, C. Adamo, J.Jaramillo, R. Gomperts, R. E. Stratmann, O. Yazyev, A.J. Austin, R. Cammi, C. Pomelli, J. W. Ochterski, R. L. Martin, K. Morokuma, V.G. Zakrzewski, G. A. Voth, P. Salvador, J.J. Dannenberg, S. Dapprich, A. D. Daniels, O.Farkas, J. B. Foresman, J. V. Ortiz, J. Cioslowski and D. J. Fox, "*Gaussian 09*", revision A. 1, Gaussian, Inc., Wallingford CT, (2009).

[14] H. I. Abood., Density Functional Theory Calculations of Di-amino naphthalene, Journal of Babylon university, Pure snd Applied Science, 3(22). (2014).
[15] Frisch M. J., G. W. Trucks, H. B. Schlegel et al., Gaussian 09, Revision A.02, Gaussian, Inc., PA, Wallingford CT. (2009).
[16] A. G. Borisov, A. K. Kazansky, and J. P. Gauyacq, Phys.Rev. B,59, 16 10 935 (1999).
[17] Charles Kittel., Introduction to solid state physics, (1991).
[18] A.M. Lesk, Introduction to symmetry and group theory for chemists, Kluwer Academic Publishes, London, (2004).
[19] Mc Grow-Hill, Fundamentals of molecular spectroscopy, (1972).
[20] Szabo, A.; Ostlund, N. S. Modern Quantum Chemistry:Introduction to Advanced Electronic Structure Theory, Dover Publications, Inc.:New York, (1989).
[21] P. Udhayakala, T. V. Rajendiran, S. Seshadri, and S. Gunasekaran, Quantum chemical vibrational study, molecular property and HOMO-LUMO energies of 3-bromoacetophenone for Pharmaceutical application, J. Chem. Pharm. Res., 3, 610-625, (2011).
[22] R.G. Pearson, Recent advances in the concept of hard and soft acids and bases, Journal of
Chem. Edu., 64(1987), 561-567.
[23] Vipin Kumar, Esha V. Shah, Debesh R. Roy, Physica E, Low-dimensional Systems and Nanostructures, (2015).

University of Thi-Qar Journal Vol.14 No.3 SEP 2019
Web Site: https://jutq.utq.edu.iq/index.php/main
Email: utj@utq.edu.iq

An analytical study of some trace elements in water and plants using an atomic absorption spectrophotometer in Thi-Qar governorate

Asst. Prof. Dr. Sajid Hassan Guzar
Hawraa Chassib Bukhaibukh
College of science, chemistry department,
University of Thi-Qar
Emails: Sajid.h@uokerbala.edu.iq
hawraamaster99@gmail.com

Abstract

The present study was conducted to measure concentrations of six trace elements (Cu ,Pb ,Zn ,Cr ,Ni and Cd) in water and plants (*Apium graveolens* , *Lepidium sativum* and *Raphanus sativus*). The samples were collected during winter 2016 from different places of Thi-Qar province. Levels of trace elements were determined by aflame atomic absorption spectroscopy (FAAS). The means concentrations of Cu ,Pb ,Zn ,Cr ,Ni and Cd in the water were 1.687, 3.052, 1.634, 4.082, 0.341 and 0.879 ppm respectively. In plants, their means concentrations in the A. graveolens plant were 3.288 , 1.930 , 2.850, 3.440 , 0.375 and 0.715 ppm dry weight respectively, in the L. sativum plant were (4.745 , 1.724 , 3.213 , 2.789 , 0.375, 0.750) ppm dry weight respectively, and in the R. sativus plant were 4.677, 1.559, 2.348 , 2 .483, 0.373 and 0.679 ppm dry weight respectively.It was found that most concentrations of trace elements in the water samples were exceeded the allowed limits for irrigation. Moreover, in A. graveolens, L. sativum and R. sativus plants, elements Pb,Cr and Cd exceeded the allowed limits by Food and Agricultur organization (FAO) and World Health Organization (WHO).

Keyword s: trace elements , water, Apium graveolens , Lepidium sativum , Raphanus sativus ,Atomic absorption spectroscopy .

1. Introduction

The trace elements are dangerous environmental pollutants, it accumulate in the body of living organisms and it bio concentrated through their transition to different levels of the food chain to pass on to humans or other organisms at the end of food chain. It threat life and sometimes causing death [1]. Because it do not turn and do not decompose and also not affected by the sun when they exist in the environment . It can combine to form complexes and many other compounds [2]. Plants are one of the main links in the food chain and the trace elements affect significantly the effectiveness of the plant [3]. The plants have high sensitivity to the toxicity of trace elements and are effective as the first stage in the food chain works on the accumulation of pollutants in their textures compared with organism that are at higher food levels [4]. The increase in concentration of these elements in plants over permissible limits can put the consumer's life in danger [6.5] The reason of the concentrations increase of trace elements was attributed to irrigation water contaminated with sewage, household wastes and centesis water [8,7], the concentration of trace elements in water was studied by many researchers [9,10,11, 12]. Ibrahim(2015) [13] investigated of concentrations Cd,Zn,Pb, Mn,Ni and Cu of Put up water from Baiji /the North refinery Company, this water used for irrigation purposes. His results showed trace element effect on celery plant and some other plants , that the water was led to a reduction in the percentage of germination and natural growth and

high concentration of lead in celery, it exceeded the permitted limit..The concentrations of trace elements in A. graveolens , L. sativum and R. sativus plants were studied by many other researchers [14,15]. The objective of the present study was to measure concentrations of six trace elements (Cu ,Pb ,Zn ,Cr ,Ni and Cd) in water and plants (*A. graveolens* , *L.sativum* and *R.sativus*) and assess water validity for irrigation and plants validity for human consumption by compare them with the allowed global limits.

2. Materials and methods

2.1 The Study station description

In the present study, four stations were selected in Thi-Qar province, these are:

Station 1 was located in Sdnawia area, water of this station receives polluted water directly from the sewage drainage station.

Station 2 was located in Al-Shawalish area in Suq al-Shuyukh, the water of this station was polluted by the sewage and human waste of people in this area..

Station 3 was located in five thousand area in Al Gharaf , also the water of this station was polluted with sewage and agricultural waste .

Station 4 was located in al-Shatrah District and surrounded by agricultural land.

The Stations were showed in Image 2-1 .

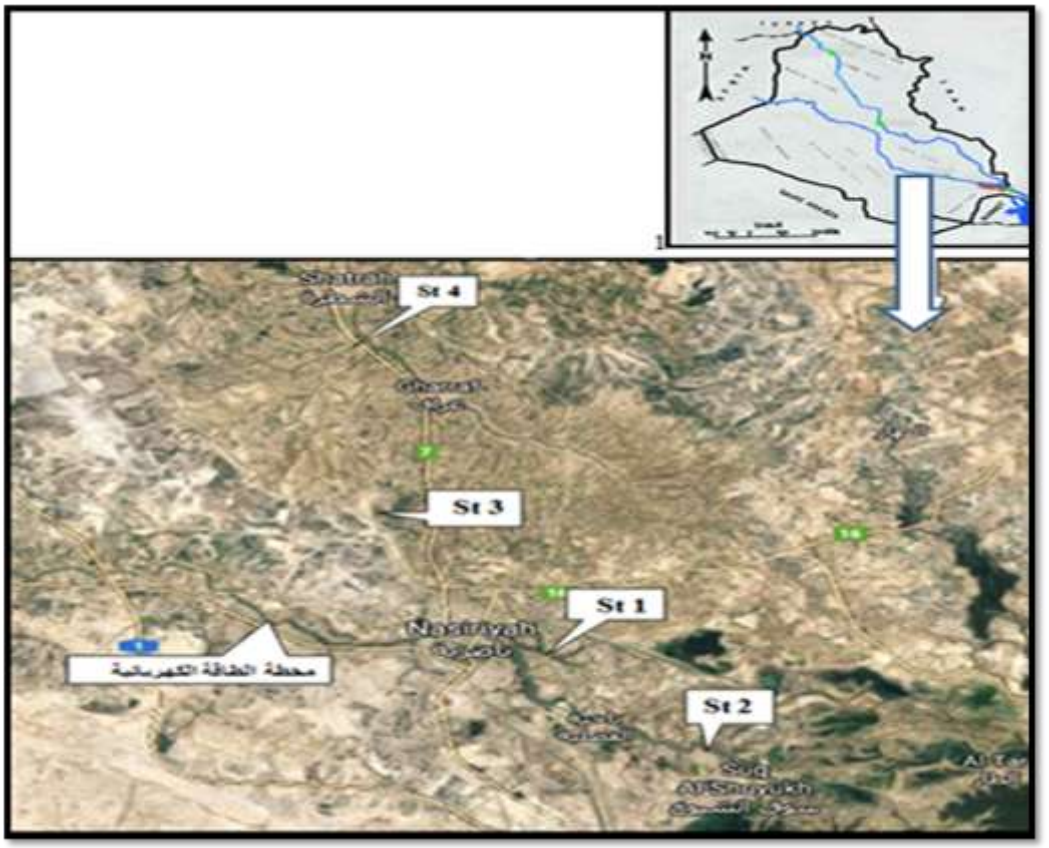

Image 2-1: Map showed the study stations

2.2 Samples collection

Samples of water and plants were collected from the study stations during winter 2016. 5 liters of water were taken at a depth 30 cm from each station were collected by using polyethylene bottles with a capacity 5 L. The plant samples were collected from the same stations areas, then placed in plastic bags. All samples were transfered to the laboratory.

2.3 Extraction of Trace element

2.3.1 Extraction of trace elements in water

The water samples were digested using the method (APHA 1995) . Firstly, 50 ml of a Water sample was transfered into a 100 ml standard flask ; then 5 ml of concentrated Nitric acid was added. The sample was placed on a hot Plate Until it dried completely and white salt is appeared , finally, the white salt was dissolved with few drops of dilute hydrochloric acid 0.5N ,and the solution transfered to a volumetric flask (50 ml), the volume was completed to the mark with distilled water. The samples became ready to measure in atomic absorption spectrophotometric

The trace elements concentrations in water samples were determined by using flame atomic absorption spectrophotomer (PG-990).

2.3.2 Extraction of trace elements in plants

The plants were dried at the room temperature ; then grinded and sieved with 40 micron diameter sieve. Trace elements in plants were extracted according to the method of Barman et al., 2000. Firstly, 1 gm of a plant samples were taken; then 5 ml of the mixture of concentrated Nitric acid and concentrated Perchloric acid (1 : 4) were added , the mixture were left for 30 minutes. The mixture was placed on a hot plate until it become clear. Finally, the clear solution was filtered , transferred to a standard flask (25ml) and diluted to the mark with distilled water. The sample bcame ready to measure in atomic absorption spectrophotometric.

The trace elements concentrations in plant samples were determined by using flame atomic absorption spectrophotomer (PG-990).

2. 4 Statistical analysis

The results were analyzed statistically using the analysis of variance (SPSS-10), to find the values of standard deviation and correlation coefficient between trace element concentrations in water and plants

3. Result and Discussion

3.1. Trace elements in water

Table 3-1 and Figure 3-1 show the concentration of trace elements for the water samples.It can be observed from the table (3-1) and figure (3-1) that the trace elements concentrations in water can be arranged as follows: Cr > Pb > Cu > Zn > Cd> Ni. The concentrations of Cu , Cr , Ni and Cd were exceeded the allowed limits for irrigation, while the means of Zn and Pb were within limits, the reason for the high concentration of trace elements in the water samples is the presence of many sources of polluted water such as waste and sewage water, and the use of agricultural fertilizers.Inaddition to the pesticides in agricultural areas adjacent to the water of the studied stations. This agrees with the results of [12,18,19]. The increase in the concentration of trace elements in this study water indicates to the danger using this water for irrigation.

Table 3-1 :Concentrations of the trace elements in the water samples (ppm)

Station	Cu	Pb	Zn	Cr	Ni	Cd
St 1	1.910	2.831	1.603	4.643	0.342	0.918
St 2	1.925	3.423	1.631	3.605	0.343	0.867
St 3	1.493	2.947	1.388	4.258	0.334	0.837
St 4	1.419	3.008	1.913	3. 821	0.345	0.895
Mean	1.687	3.052	1.634	4. 082	0.341	0.879
Standard deviation	0.268	0.258	0.216	0.462	0.005	0.035
The allowed maximum Limit [20]	0.2	5	2	0.1	0.2	0.01

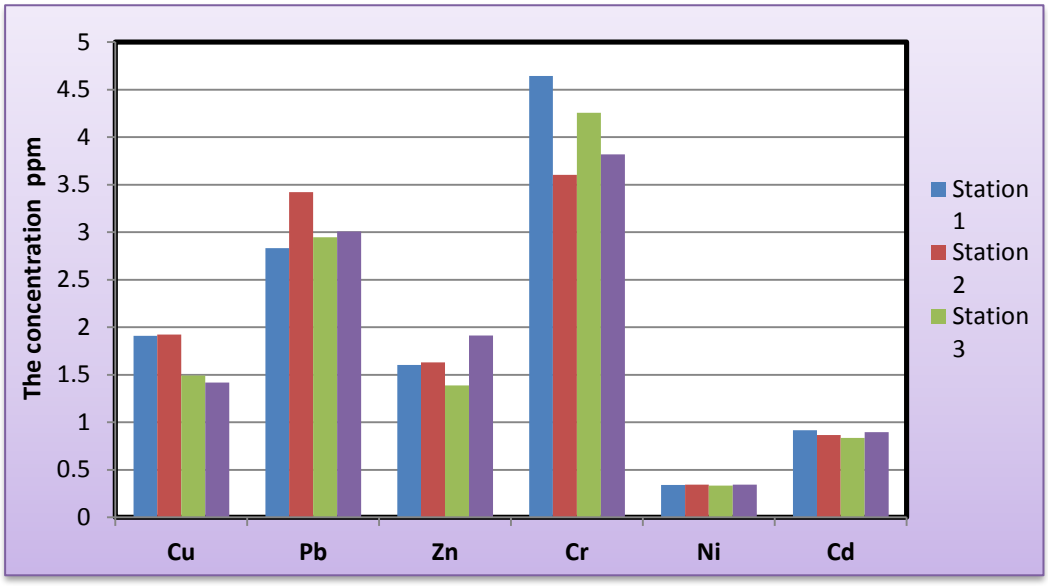

Figure 3-1: Concentrations of the trace elements in the water samples (ppm)

3.2 Trace elements in plants

Table 3- 2 and Figures 3-2 ,3-3, 3-4,3-5,3-6 and 3-7 show concentrations of trace elements in A. graveolens, L. sativum, and R. sativus plants It can be seen from the Table (3-2) and Figure (3-1) that the trace elements concentrations in A. graveolens plant can be arranged as follows: Cr > Cu> Zn > Pb > Cd> Ni , in L. sativum plant : Cu > Zn> Cr> Pb > Cd> Ni and in R. sativus plant: Cu > Cr > Zn > Pb > Cd> Ni. The means of Pb, Zn and Cr in the studied plants were exceeded the allowed limits of trace elements in vegetables but other elements within limits. The highest concentration of lead in A. graveolens plant is 1 .930 ppm while its concentration in L. sativum and R. sativus plants are 1.724 and 1.559 ppm respectively.This indicate the high susceptibility of plants especially A. graveolens plant to obsorb this element even with its few concentrations in irrigation water .This is in agreement with result of [14]. The water

polluted with waste should not be used to irrigate the A. graveolens plant for ability this plant on collect and store the elements in its different parts.Lead is a harmful element that moves from the plant to the consumer body of the human and animal through the food chain and does not contribute lead any vitality function of the body.Lead harms and affects in human health, it causes the red blood cells break and reduce the cognitive development and intellectual performance in children. It also causes heart and blood vessels diseases in adults [21]. The highest concentration of chromium in A. graveolens was 3.440 ppm while this concentration in L. sativum and R. sativus plants were 2. 789 and 2. 483 ppm respectively. Chromium tripl eare important for human health but very small amounts. Recent studies show that chromium plays a key role in liberating insulin into the cell, as it is beneficial for diabetics and is essential for the metabolism of fat, carbohydrates and protein in the body [22]. The high concentration of chromium causes impaired immune system efficiency and change in genetic material and also causes lung cancer and death [23]. The highest concentration of Cadmium in L. sativum plant is 0.750 ppm while its concentration in A. graveolens and R. sativus plants are 0.715 and 0.679 ppm respectively. Cadmium is a highly toxic element and accumulates mainly in the kidneys and liver [24]. Cadmium promotes kidney failure, skeletal damage, and reproductive defects [25]. The high concentration of lead, chromium and cadmium elements in A. graveolens, L. sativum and R. sativus plants is back for irrigation their plants with pollutted water with these elements. This is confirmed by the statistical analysis of the correlation coefficient between lead, chromium and cadmium concentration in A. graveolens , L. sativum and R. sativus plants and their concentrations in water, positive

correlation was found between the concentration of chromium in A. graveolens plant and its concentration in water (r =0.173), positive correlation with cadmium (r=0.283) and positive correlation with lead element (r =0.158) (Table 3-3). Also positive correlation was between concentrations Lead, chromium and cadmium in L. sativum plant and its concentrations in water (r=0.368) for the lead element ,(r=0.404) for the chromium element and (r=0.678) for the cadmium element (Table 3-4) ,positive correlation was found between lead, chromium and cadmium concentrations in R. sativus plant and its concentration in water (r =0.034) for lead element,(r= 0.489) for the chromium element and(r= 0.845) for the cadmium element (Table 3-5).This agrees with the study [26].

Table 3- 2: Concentrations of the trace elements in the plants (ppm) dry weight (mean ± standard deviation)

The plant	Cu	Pb	Zn	Cr	Ni	Cd
A. graveolens	± 3.191 3.288	± 0.464 1 .930	±2.850 0.633	± 1.016 3. 440	± 0.004 0.375	0.715±0.064
L. sativum	± 3.555 4.745	± 0.339 1.724	± 3.213 1.225	± 1.436 2. 789	± 0.006 0.375	±0.031 0.750
R. sativus	± 4.175 4.677	± 0.127 1.559	± 2.348 0.389	± 0.783 2. 483	±0.005 0.373	±0.039 0.679
WHO/ FAO [27]	73	0 .3	100	2 .3	67	**0. 2**

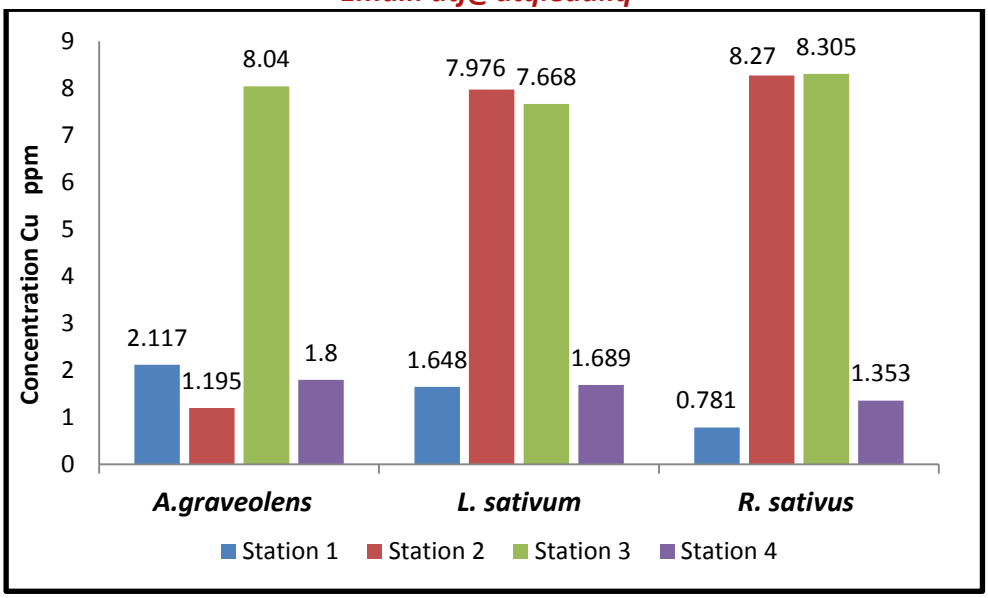

Figure 3-2 : The concentration of copper in the plants (ppm) dry weight.

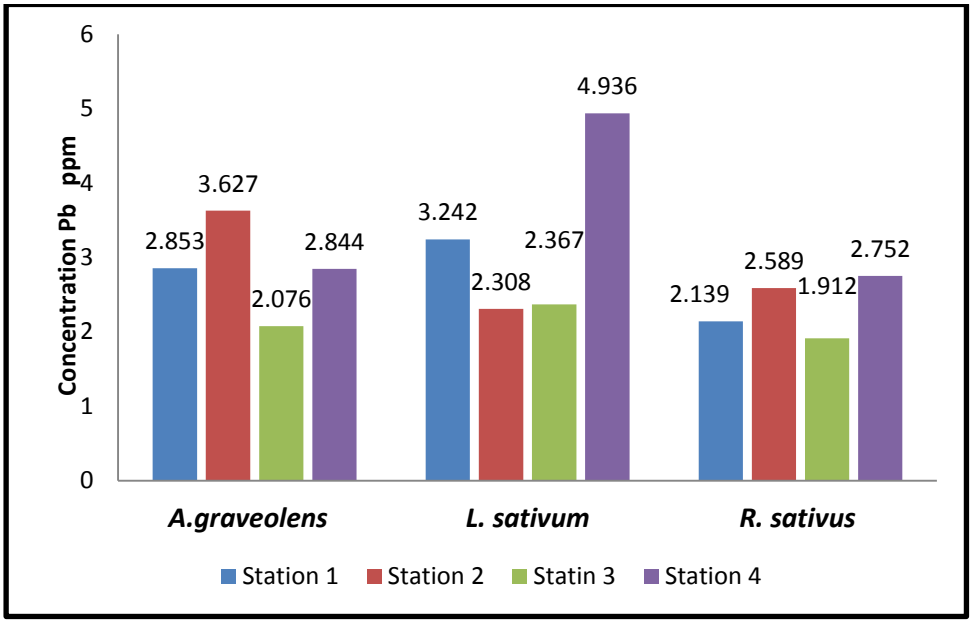

Figure 3-3 : The concentration of lead in the plants (ppm) dry weight

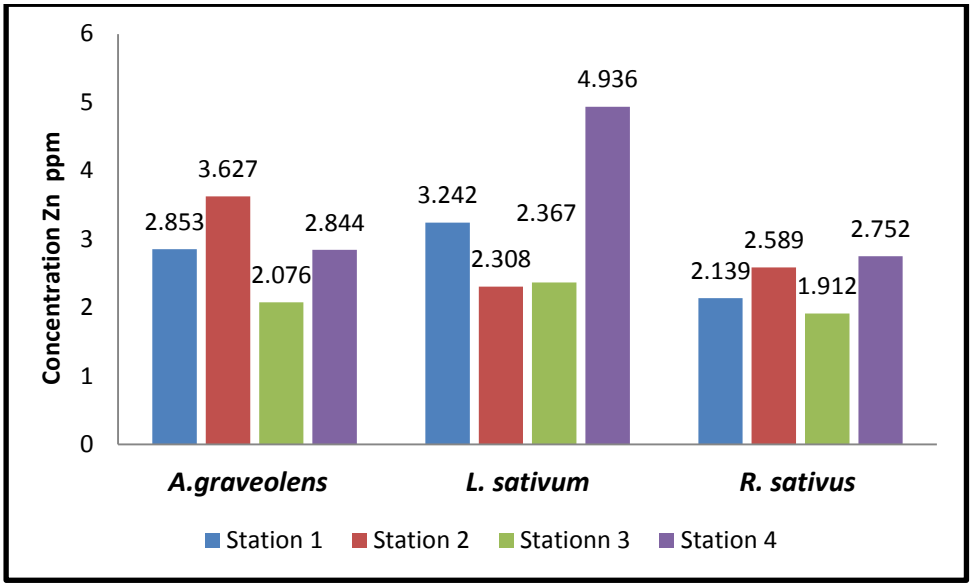

Figure 3-4 : The concentration of zinc in the plants (ppm) dry weight.

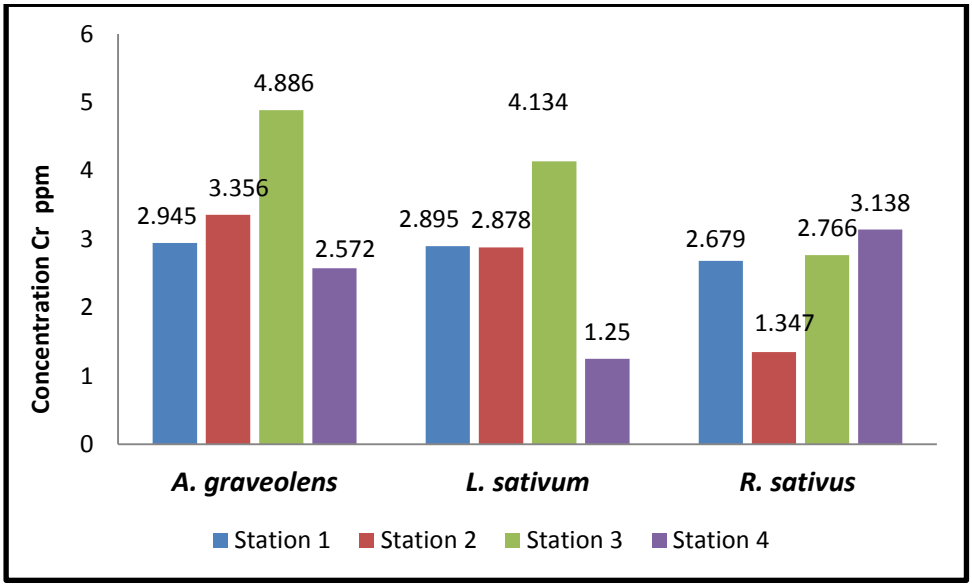

Figure 3- 5 : The concentration of chromium in the plants (ppm) dry weight.

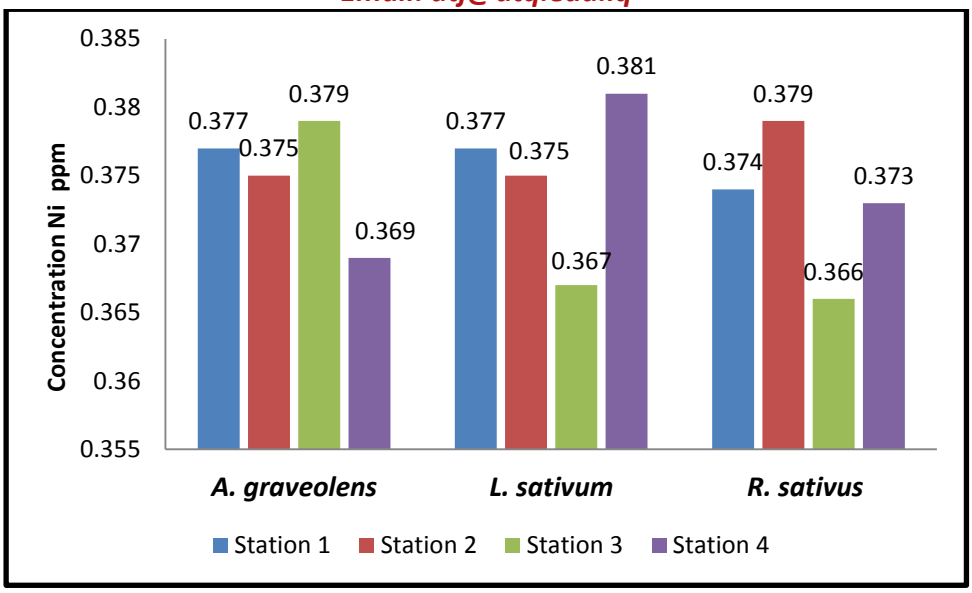

Figure 3-6: The concentration of nickel in the plants (ppm) dry weight.

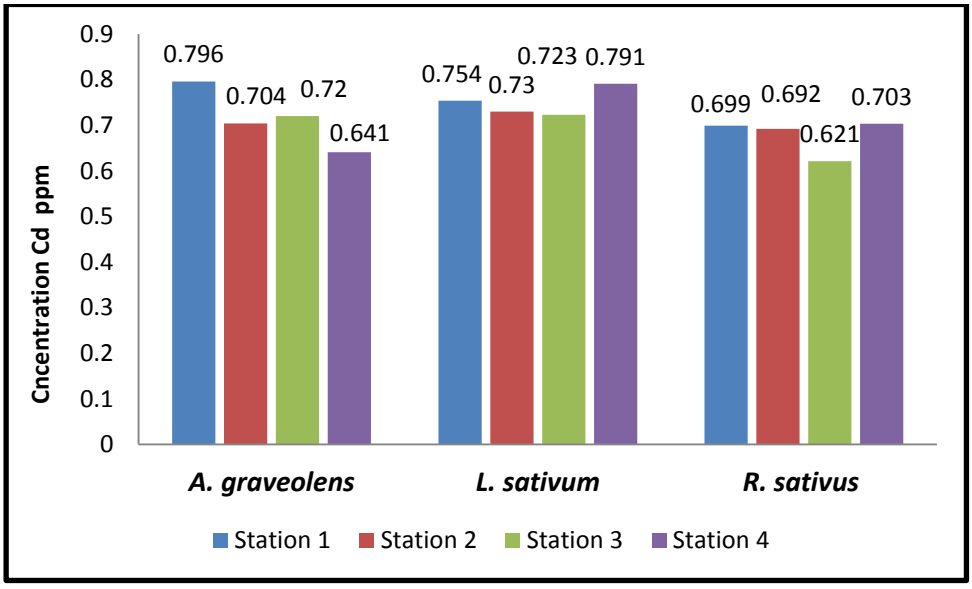

Figure 3- 7 : The concentration of cadmium in the plants (ppm) dry weight.

Table 3-3: The correlation coefficient between the trace elements in water and A. graveolens plant

***A . graveolens* plant**							
	Variables	**Cu**	**Pb**	**Zn**	**Cr**	**Ni**	**Cd**
The water	**Cu**	-0.499	0.536	0.662	-0.218	0.368	0.669
	Pb	-0.385	0.158	0.754	-0.045	-0.179	-0.391
	Zn	-0.747	-0.910	0.455	-0.887	- 0.974	-0.591
	Cr	0.354	0.599	-0.573	0.173	0.566	0.802
	Ni	-0.964	-0.661	0.758	-0.968	-0.799	-0.295
	Cd	- 0.727	- 0.245	0.349	-0.870	-0.409	0.283

Table 3- 4 : The correlation coefficient between the trace elements in water and L. sativum plant

***L. sativum* plant**							
	Variables	**Cu**	**Pb**	**Zn**	**Cr**	**Ni**	**Cd**
The water	**Cu**	0.115	0.832	-0.514	0.353	0.082	-0.390
	Pb	0.622	0.368	-0.347	-0.016	0.029	-0.306
	Zn	-0.646	-0.675	0.872	-0.986	0.940	0.908
	Cr	-0.399	0.151	-0.089	0.404	-0.227	-0.086
	Ni	-0.569	-0.287	0.621	-0.814	0.961	0.713
	Cd	-0.886	-0.194	0.583	-0.545	0.824	0.678

Table 3- 5 : The correlation coefficient between the trace elements in water and R. sativus plant

***R. sativus* plant**							
	Variables	**Cu**	**Pb**	**Zn**	**Cr**	**Ni**	**Cd**
The water	**Cu**	0.052	-0.779	-0.041	-0.726	0.698	0.397
	Pb	0.607	0.034	0.543	-0.864	0.662	0.181
	Zn	-0.633	0.736	0.896	0.218	0.483	0.810
	Cr	-0.413	-0.536	-0.767	0.489	-0.476	-0.213
	Ni	- 0.585	0.380	0.875	-0.127	0.799	0.975
	Cd	- 0.913	0.005	0.335	0.241	0.464	0.845

4. Conclusion

1-The concentrations of Cu , Cr , Ni and Cd in water were exceeded the allowed limits for irrigation, this indicates to this water is not suitable for irrigation. The order of trace elements concentrations in water Cr > Pb > Cu > Zn > Cd> Ni .

2-The concentrations Pb, Cr and Cd in plants (A. graveolens , L. sativum and R. sativus) were exceeded the allowed limits of trace elements in vegetables but other elements within the allowed limits.

3- The order of trace elements concentrations in A. graveolens plant Cr > Cu> Zn > Pb > Cd> Ni , in L. sativum plant Cu > Zn> Cr> Pb > Cd> Ni and in R. sativus plant Cu > Cr > Zn > Pb > Cd> Ni .

4- The high concentration of Pb,Cr and Cd in the plants is due to irrigation this plants with pollutted water with these elements. This is asserted by the statistical analysis of the correlation coefficient between Pb, Cr and Cd concentrations in the plants and their concentrations in water .

References

1- Agah , H.; Leermakers, M.; Fatemi, S. M. R. and Baeyens, W. (2009). Accumulation of trace metals in the muscles and liver tissues of five fish species from the Persian Gulf.Environ. Monit.Assess. 157: 499-514.

2- Uzun , I . and Guzel , F. (2000) . Adsorption of some heavy metal ions from aqueous solution by Activated carbon and comparison of precent adsorption results of activated carbon with those of some other adsorbents . Turk. J. Chem. 24: 291-297.

3- Veselov,D.;Kudoyarova,G;Symonyan,M.and Veselov,S.(2003). Effect of Cd on ion up take,Transpiration and cytokinin.contenet in wheat seedlings.J Bulg plant physiol. 353-359 .

4- Lovett-Doust, J. ; Schmidt, M. and Lovett- Doust, L. (1994). Biological assessment of aquatic pollution .areview with emphasis on plants as biomonitors Biol, Rev. 69:147-186.

5- Anonymous. (1998). Health Guide Line For The Use Of Waste Water in Agricalture and Aquacult-ure. Report of WHO Science Group. WHO. Geneva, Switzerla. Tech. Rep. Sci. 778, 10.

6-Codex Alimentarins Commission (FAO/WHO). (2001). Food Additives and Contaminats ,Joint FAO/WHO Food Standards Program. ALLNORM 01/12A. 1-289.

7 –Sadek, A. H and Kamel, K. F.(2008). Monthly Variations in Concentrations of Trace elements of Waters from Al-Garaf, one of the Main Branches of Tigris Rivere. partment of Fisheries and Marine Resources.College of Agriculture, University of Basrah.

8-AZita, B. H. and Seid, A. M. (2008). Investigation of heavy metals up take by vegetable crops from metal – contaminated soil. Warld Academy of Sciece, Engineering and Technology. 43(1): 56-58.

9 -Alkam, F.M.(2002). Concentration of some trace elements in the water and plants of the Diwaniyah River - Al Gharraf - Al Qadisiyah journal - Pure Sciences. 7 (4): 190- 196.

10- Salman, J.M. (2006). Environmental study of potential pollution in the Euphrates River between the Indian Lake and the Kufa .Doctorate thesis , Iraq, College of of Science , University of Babylon.

11- Bushra, A. G. (2013). The Effect of Sewage water Treatment in Some Physical, Chemical and Bacteriological of Euphrates River Near the City Center of Nasiriyah, Southern Iraq.Master Thesis, College of Science, Dhi Qar University.

12- Afaq, T.F. (2012) .Study of the effect of Thermal energy of power plant effluents upon the concentration of some trace elements in water, sediment and two aquatic plants species in Euphrates River near the center of Al -Nassyria city south Iraq. Master Thesis, College of Science, Dhi Qar University.

13-Mariam,A.A. (2015). Evaluation Pollution in the soil and some vegetative plants with the trace elements located on the water table corridor resulting from the Baiji refinery. Journal University of Kirkuk - scientific studies. 160: 10-176 .

14- Asen, H.A.; Ibrahim,O.S.; Jihad, T.M. (2015). A study of the effect of treated wastewater by sedimentation and filtration methods in the

accumulation of trace elements in celery plants. Journal of the University of Kirkuk , scientific studies. 10: 58-71**.**

15- Ghufran, F.J.; Riad , H.A. (2010). Evaluation of Pollution of Heavy Elements in Agricultural Land in Diyala Bridge. Department of Construction and Construction , University of Technology . Iraqi Journal of Market Research and Consumer Protection. 2 (3).

16-ROPME (Regional Organization For the Protection of the Marine Environment) (1983). Manual of oceanographic observation and pollutants analysis methods. AL – Safat, Kuwait. ROPME, P.O. Box 26388, 13124.

17-Thomas(2007). O. Burgess C. UV-Visible spectrophotometry of water and wastewater. Elsevier B.V. Netherlands.

18- Raed,S.A. (2004). Water characteristics in the Shatt al-Arab and the general estuary and their levels of pollution with some heavy elements. Doctorate thesis, College of Agriculture, University of Basra.

19- Alia, H. T. (2012). An environmental study of L. Ceratophyllum demersum. and its role in removing cadmium from the water of the river Euphrates in the city of Nazareth. Master thesis , College of Education, Dhi Qar University.

20-Ayers, R. S., and D. W. Westcot.(1985). "Water Quality for Agriculture." Irrigation and Drainage Paper no. 29, Rev. 1. Rome: Food and Agriculture Organization

21-Mahalakshmi, M.; Balakrishnan,S.; Indira,K. and Srinivasan, M. (2012). Characteristic levels of heavy metals in canned tuna fish. Journal of Toxicology and Environmental Health Sciences. 4(2): 43-45.

22-Schauss,A.G.(1994).Minerals and human health.The relation for optimal and balanced elementtracelevels.Nut.Rev.,52:367-375.

23-Ahmed ,I.T. and Abd Almoneim. (2012). Heavy elements sources and damage to the environment. Center for promising research in biological control and agricultural information, Qassim University .

24-Duruibe, J.O. ; Ogwuebu, M.O.C. and Egwurugwu, J.N. (2007). Heavy metal pollution and human biotoxic effects. Internat.J .Phys.Sci.2(5):112-118.

25-Rahimi, E.; Hajisalehi, M.; Kazemeini, H. R.; Chakeri, A.; Khodabakhsh, A.; Derakhshesh, M.; Mirdamadi, M.; Ebadi, A. G.; Rezvani, S. A, and Kashkahi, M. F. (2010). Analysis and determination of mercury, cadmium and lead in canned tuna fish marketed in Iran. African Journal of Biotechnology. 9 (31): 4938-4941

26-Durdana, R. H.; Shahnaz, I. and Shaikh, G. H. (2007). Assessment of the level of trace metal in commonly edible vegtables locally available in themaret of Karachi city .Pak.J.Bot.39(3) : 747-751.

27-Anonymous. 2001. Codex Alimentarius Commission (FAO/WHO). Food additives and contaminants-Joint FAO/WHO Food Standards Programme. 2001,ALINORM 01/12A. 1-289.

دراسة تحليلية لبعض العناصر النزرة في الماء والنباتات باستخدام مطيافية الامتصاص الذري في محافظة ذي قار

ا.م.د.ساجد حسن كزار **حوراء جاسب بخيبخ**

الخلاصة :

اجريت الدراسة الحالية لتقدير تراكيز ستة من العناصر النزرة (النحاس , الرصاص, الخارصين , الكروم , النيكل والكادميوم) في الماء ونباتات (الكرفس Apium graveolens والرشاد Lepidium sativum والفجل Raphanus sativus) والتى جمعت خلال شتاء 2016 من مناطق مختلفة في محافظة ذي قار واستخدم جهاز مطياف الامتصاص الذري اللهبي في تقدير تراكيز العناصر المدروسة . بلغت معدلات تراكيز العناصر (النحاس , الرصاص , الخارصين , الكروم, النيكل والكادميوم) في الماء (1.687 , 3.052, 1.634, 4. 082, 0.341, 0.879) ppm على التوالي وبلغت معدلات تراكيزاها في الكرفس (3.288 , 1.930, 2.850 , 3. 440 , 0.375 , 0.715) ppm وزن جاف على التوالي وفي نبات الرشاد (4.745 , 1.724, 3.213 , 2. 789 , 0.375 , 0.750) ppm وزن جاف على التوالي وفي نبات الفجل (4.677 , 1.559 , 2.348 , 2. 483 , 0.373 , 0.679) ppm وزن جاف على التوالي . ان اغلب تراكيز العناصر النزرة في مياه الدراسة تجاوزت الحدود المسموح بها لمياه الري, و في نباتات الكرفس والرشاد والفجل تجاوزت عناصر (Cd , Pb , Cr) الحدود المسموح بها التى حددتها منظمة الغذاء والزراعة FAO ومنظمة الصحة العالمية WHO .

الكلمات المفتاحية : العناصر النزرة , الماء , الكرفس, الرشاد , الفجل, مطيافية الامتصاص الذري.

University of Thi-Qar Journal Vol.14 No.3 SEP 2019
Web Site: https://jutq.utq.edu.iq/index.php/main
Email: utj@utq.edu.iq

Investigation of Refrigerant R134a Two Phase Flow Heat Transfer in Vertical Heat Exchanger Channel

Abdullah Adel Ibrahim[a] ,Ahmed J. Hamad[b] and Johain J. Faraj[c]

[a], [b], [c],Engineering Technical College-Baghdad, Middle Technical University, Emails: [a], (Abdullah.adel59@yahoo.com)

[b], (elhamad@mtu.edu.iq)

[c], (Johaintech@mtu.edu.iq)

Abstract

Two phase flow boiling heat transfer and pressure drop in the vertical evaporator tube section of refrigeration system have been experimentally investigated using refrigerant R134a as a working fluid. The objective of the present work is to investigate experimentally the effect of heat flux, mass flux, vapor quality and saturation temperature on refrigerant flow boiling heat transfer characteristics in the evaporator of refrigeration system. These investigated parameters have significant impacts to enhance the thermal performance of the evaporator. The experimental investigations were conducted in smooth copper tube with inner diameter 5.8 mm and 600 mm length under different test conditions. The test conditions considered in this study were, for heat flux of 7.718-32.78 kW/m^2, mass flux of 97.3-148.7 kg/m^2.s , saturation temperature of -

20.58 to -15.68 ˚C and vapor quality of 0.3-1. It can be concluded from the results that, the average heat transfer coefficient at relatively greater mass flux 148.7 kg/m^2.s was higher in range of 21% compared to other mass fluxes at constant test conditions. The relatively higher value of heat transfer coefficient was observed at heat flux 32.78 kW/m^2 with average increase of 19% compared to the relatively lower value 23.38 kW/m^2. The enhancement in local heat transfer coefficient at saturation temperature -15.68˚C was higher by about 12% than that for the relatively lower temperature -20.58˚C. The effect of increase in mass flux and heat flux on pressure drop in the evaporator tube was about 9% and 7.5% respectively.

Key Words: Heat transfer, Flow boiling, Pressure drop, Heat flux.

الخلاصة

تم في هذه الدراسة اجراء استقصاء عملي لمعامل انتقال الحرارة وانحدار الضغط خلال غليان مائع ثنائي الطور في حالة الجريان لمائع التثليج R-134a في مقطع أنبوب عمودي لمبخر منظومة تبريد تحت ظروف تشغيل مختلفة. الهدف من هذا العمل هو التحقيق التجريبي في تأثير الفيض الحراري والفيض الكتلي وجودة البخار ودرجة حرارة التشبع على خصائص نقل حرارة غليان تدفق المبرد في المبخر لنظام التبريد . ظروف الاختبار التي اعتمدت في هذه الدراسة كانت، للفيض الحراري 7.718-32.78 كيلوواط\متر مربع، وللفيض الكتلي 97.3-148.7 كغم\متر مربع. ثانيه ودرجة حرارة التشبع للمائع -20.58 الى 15.58 درجة مئوية ونسبة الجفاف للبخار0.3 - 1. نفذ باستخدام جهاز فحص لمنظومة تبريد سعة 310 واط والذي تم تصميمه وتصنيعه خلال العمل الحالي. نفذت الدراسة العملية على مقطع فحص لمبخر وهو عبارة عن أنبوب عمودي املس بقطر داخلي 5.8 مليمتر وطول 600 مليمتر. اظهرت النتائج بان قيم الفيض الحراري والفيض الكتلي ودرجة حرارة التشبع للمائع كان لها تأثير واضح على خصائص انتقال الحرارة لغليان المائع في حالة الجريان مقارنة بالتأثير الضعيف لنسبة جفاف بخار المائع الداخل. معدل معامل انتقال الحرارة عند اكبر فيض كتلي نسبيا 148.7 kg/m^2.s كان اعلى بحدود 21% مقارنة مع قيم الفيض الكتلي الاخرى عند ظروف اختبار ثابته. اعلى قيمه لمعامل انتقال الحرارة قد لوحظت عند الفيض الحراري 32.78 kW/m^2 مع معدل زيادة بحدود 19% مقارنة مع ادنى قيمة نسبيا 23.38 kW/m^2. مقدار التحسين في معامل انتقال الحرارة الموقعي عند درجة حرارة التشبع -15.68˚C كان اعلى بنسبة 12% مما هو عليه عند ادنى درجة حرارة نسبيا -20.58˚C. تأثير الزيادة في الفيض الكتلي والفيض الحراري للمائع على قيم انحدار الضغط في انبوب المبخر كان بحدود 9% و 7.5% على التوالي.

الكلمات المفتاحية: نقل الحرارة ، تدفق الغليان ، انخفاض الضغط ، تدفق الحرارة.

1. Introduction

Boiling is the process of a substance phase change from liquid into vapor by the increase of heat. Due to its ability to transfer heat at a very low temperature, boiling heat transfer is vital in many industrial applications such as, power stations, refrigeration and air conditioning systems, cooling of lasers, cooling of electronics, nuclear reactors and other high heat flux applications [1]. Dissimilar types of boiling can be classified according to the geometric situation and to the mechanism in process. [2]. Boiling can be classified into, pool boiling and flow boiling. Boiling is called pool boiling in the lack of bulk fluid flow. Boiling is called flow boiling in the presence of bulk fluid flow [3]. The flow boiling heat transfer process was investigated by many researchers in many thermal components and energy systems. **Chen et al. [4]** , studied the two-phase flow patterns in vertical small diameter tubes 1.10, 2.01, 2.88 and 4.26 mm with refrigerant R134a as the working fluid. Various flow pattern maps were presented at different pressures. The results showed that the Churn-annular and slug churn boundaries depend on diameter and pressure, while the dispersed bubble-churn and bubbly-slug were less affected by diameter and pressure**. Xiaorong et al. [5]**, investigated experimentally the boiling heat transfer in two stainless steel tubes with diameter 4.26 mm and 2.01 mm respectively using refrigerant R-134a. The range of mass flux 100 – 500 kg/m^2.s, pressure 8 – 14 bar, quality up to 0.9 and heat flux 13 – 150 kW/m^2.The results showed that for the 4.26 mm tube when the vapor quality was less than about 40% to 50%, the heat transfer coefficient increases with heat flux and system pressure but did not change with vapor quality. **Mahmoud et al. [6],** conducted a comparison between experimental flow boiling heat transfer results obtained using two different tubes of 150mm length**,** a seamless cold drew stainless steel tube of 1.1 mm inner diameter and 1.16 mm inner diameter welded stainless steel tube, with vertically upwards flow direction. The operating conditions considered were, for a mass flux of

300 kg/m^2.s, system pressure 8 bar, inlet sub-cooling 5K and up to 0.9 exit quality. The results presented the variation of local heat transfer coefficient with local quality at different conditions and investigated the effect of tube inner surface roughness on the heat transfer characteristics. **Ali et al. [7],** studied experimentally the flow boiling heat transfer in a stainless steel mini channel of 1.70 mm internal diameter and a heated length of 220 mm using R134a as a working fluid. The test conditions were for saturation temperatures of 27°C and 32°C, mass flux from 50 kg/m^2 s to 600 kg/m^2.s, and heat flux ranged from 2 kW/m^2 to 156 kW/m^2. The results show that the heat transfer coefficient increases with the increase of wall heat flux, while mass flux and vapor quality have no significant effects. Increasing the system pressure enhanced the heat transfer coefficient, and the heat transfer coefficient is reduced as dry out is reached. **Emily et. al. [8],** conducted experiments to compare the flow boiling heat transfer and pressure drop results between the refrigerant R134a and refrigerant R245fa, in a vertical stainless steel tube with an inner diameter of 1.1 mm and a heated length of 150 mm. The results show that the pressure drop of R245fa is higher by up to 300% compared to that of R134a at similar conditions. While the effect of mass flux and heat flux on the local flow boiling heat transfer coefficient was different. Heat transfer coefficients of R245fa showed a greater dependence on vapor quality. **Fang [9]**, proposed a new correlation to predict the R134a two-phase flow boiling heat transfer based on the experimental data from 19 published papers. The new correlation takes advantage of the newly defined dimensionless number (Fa) proposed by Fang which is highly related to flow boiling heat transfer. The new correlation also shows high prediction accuracy for other refrigerants such as CO2, R22, R410a and R236fa. **Mancin et al. [10]**, investigated the flow boiling heat transfer and pressure drop for refrigerant R134a inside a small micro-fin tube with an internal diameter of 3.4 mm. The experimental facility is developed to study both single and two-phase heat transfer processes. The experimental measurements were carried out at different test conditions. The results show that the flow boiling heat transfer is controlled by the two well-known phase change heat transfer mechanisms, nucleate boiling and two-phase forced convection. At a heat flux of 10 kW/m^2, the dry out

phenomenon doesn't occur at any mass velocity. The results also show the effects of the vapor quality and mass velocity on the frictional pressure gradients. **Wei Li et al. [11],** conducted the saturated flow boiling experiments to investigate the influence of surface wettability on the hydraulic and thermal transport performance in a rectangular micro channel with deionized water as the working fluid. Parametric experimental studies were carried out with the inlet vapor quality varied from 0.03 to 0.1 and the wall heat fluxes from 4 to 20 W/cm^2 and mass fluxes ranging from 120 to 360 kg/m^2.s. Results indicated that, a reduction in heat transfer was observed for the bared silicon wafer surface with increased inlet vapor quality and heat flux. The objective of the present work is to investigate experimentally the effect of heat flux, mass flux, vapor quality and saturation temperature on flow boiling heat transfer coefficient and pressure drop of refrigerant R-134a in the evaporator vertical test section. These investigated parameters have significant impacts to enhance the thermal performance of the evaporator in the refrigeration system.

2. Experimental Setup

The experimental setup is consisting of hermetic compressor with 125W capacity, water-cooled condenser, refrigerant flow meter, capillary tube, pre-heater, post-heater and test section which simulates the evaporator of the refrigeration system. Two visualization sections are installed at inlet and outlet of the test section with 150 mm length glass tube of the same internal diameter of the test section as shown in **Fig.1** and **Fig.2**. The evaporator section in the test rig system is represent a vertical smooth copper tube with an inside diameter of 5.8 mm, wall thickness of 1.05 mm and 600 mm length. Electrical heater is used to simulate the thermal load applied on the evaporator section using a 350 W heating wire with length of 2.5 m. The thermocouples are fixed with equal distance on the test section and the tube was wrapped with insulation material to minimize the heat loss caused by convection and radiation heat transfer to the ambient. The heat flux was regulated by varying the input electrical power using variable power supply (variac). The inlet and outlet of the

evaporator tube are connected with two transparent tubes of 5.8 mm inner diameter and 150 mm length to visualize the flow pattern as shown in **Fig.3.**

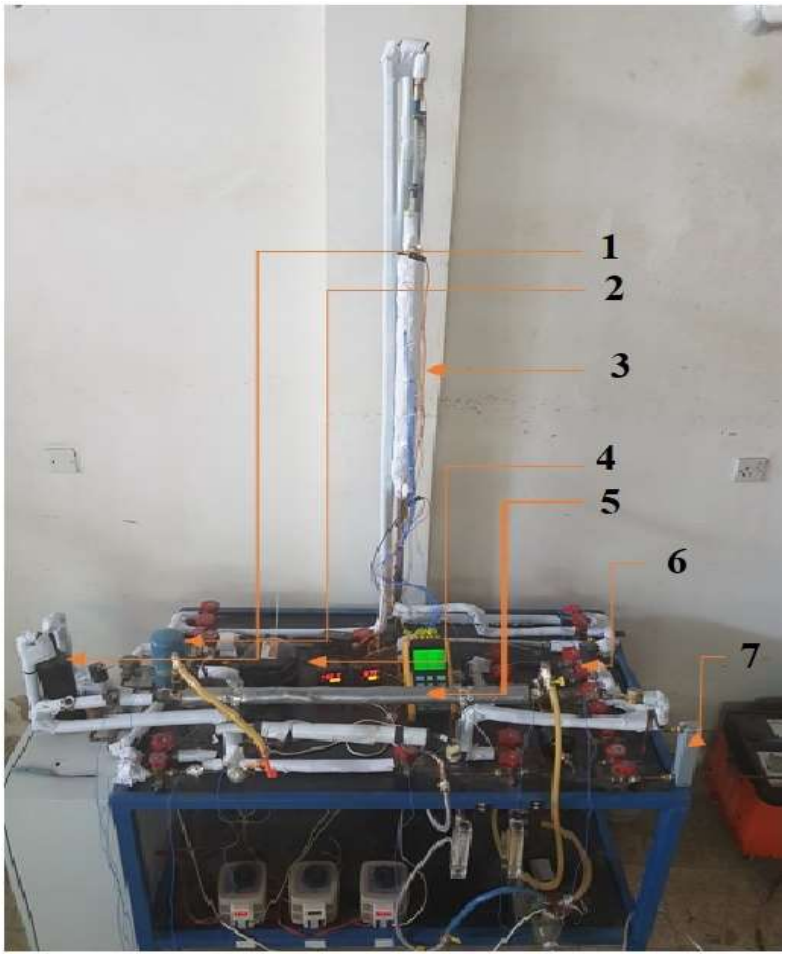

Item	Description
1	Accumulator
2	Oil Separator
3	Evaporator
4	Compressor

5	Condenser
6	Capillary Tubes
7	Flow Meter

Fig 1. Test Rig.

3. Theoretical Analysis

The heat transfer rates supplied by the electric coil to the outside wall surface of the copper tube in the evaporator section and preheater ($\dot{Q}_{ev}$, $\dot{Q}_{pre}$) are calculated by:

$$\dot{Q}_{ev} = V \cdot I \cdot \eta \quad (1)$$

Where (η) is the heating coefficient that reflects the efficiency of the heat transfer process in the test section which is based on the electrical power input ($P_{el.i}$) to the heater coil and determined by the following equation:

$$\eta = \frac{\dot{m} \cdot (h_o - h_i)}{P_{el.i}} \quad (2)$$

The heat flux supplied from the inside wall surface of the evaporator tube (q_{ev}) to the refrigerant is calculated by:

$$\dot{q}_{ev} = \frac{\dot{Q}_{ev}}{\pi \cdot di \cdot L_{ts}} \quad (3)$$

The local heat transfer coefficient of the refrigerant flow boiling in the test section (evaporator tube) is calculated by **[2]**:

$$h_z = \frac{\dot{q}_{ev}}{T_{w.i} - T_{ref}} \quad (4)$$

$T_{w.i}$. T_{ref}: Inner wall and refrigerant saturation temperatures at each axial position (z) along the test section tube (˚C).

For each axial location (z) along the test section tube, the external wall temperature T_{wo} was assumed to be the average of measured temperatures around the tube cross section and calculated by:

$$T_{wo} = \frac{T_{w.t} + T_{w.b}}{2}$$
(5)

$T_{w.t}$, $T_{w.b}$: The external wall temperatures at the top and bottom of the test section tube respectively (˚C).

The mean inner wall temperature at each position (z) ($T_{wi.z}$) is calculated using one dimensional heat conduction across tube wall by:

$$T_{wi.z} = T_{w.o} - \dot{Q}_{ev} \cdot R_w$$
(6)

Thermal resistance R_w of the test section tube is calculated by:

$$R_w = \frac{Ln\left(\frac{d_o}{d_i}\right)}{2\,\pi \cdot k_{cu} \cdot L_z}$$
(7)

The local saturation temperature $T_{sat.z}$ at each position (z) along the test section tube is calculated based on local saturation pressure $P_{sat.z}$ which is expressed by:

$$P_{sat.z} = P_{i.ev} - \Delta p \cdot \frac{L_z}{L_{ts}}$$
(8)

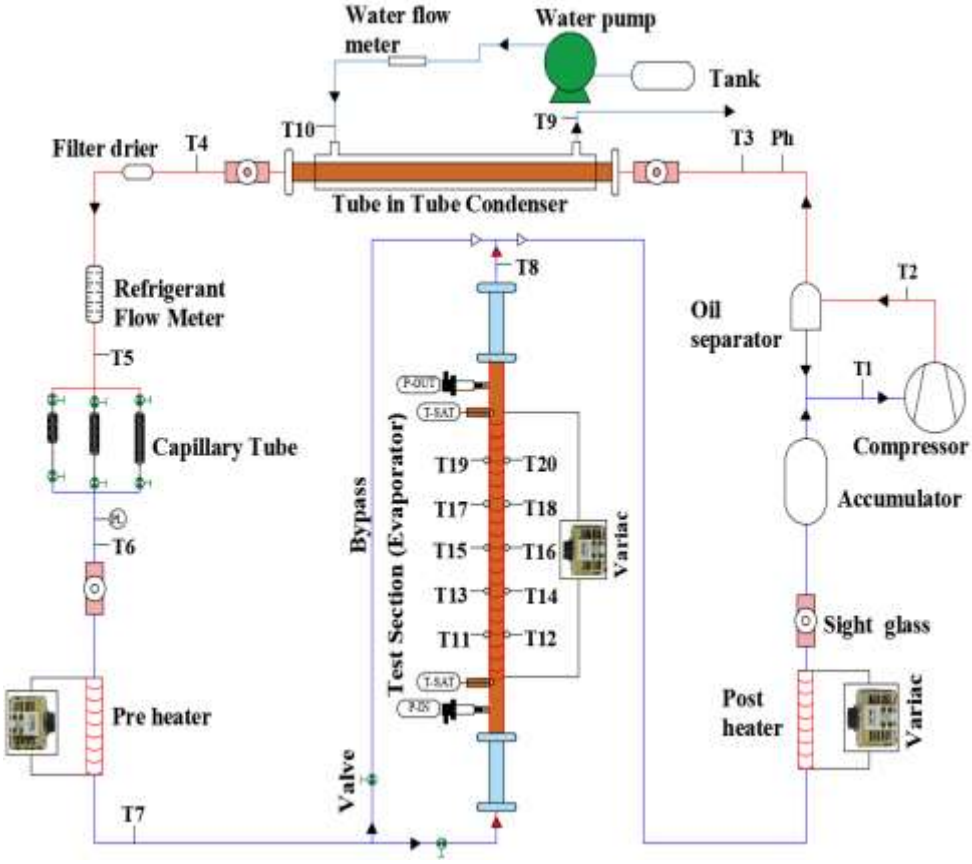

Fig 2. Schematic diagram of the test rig.

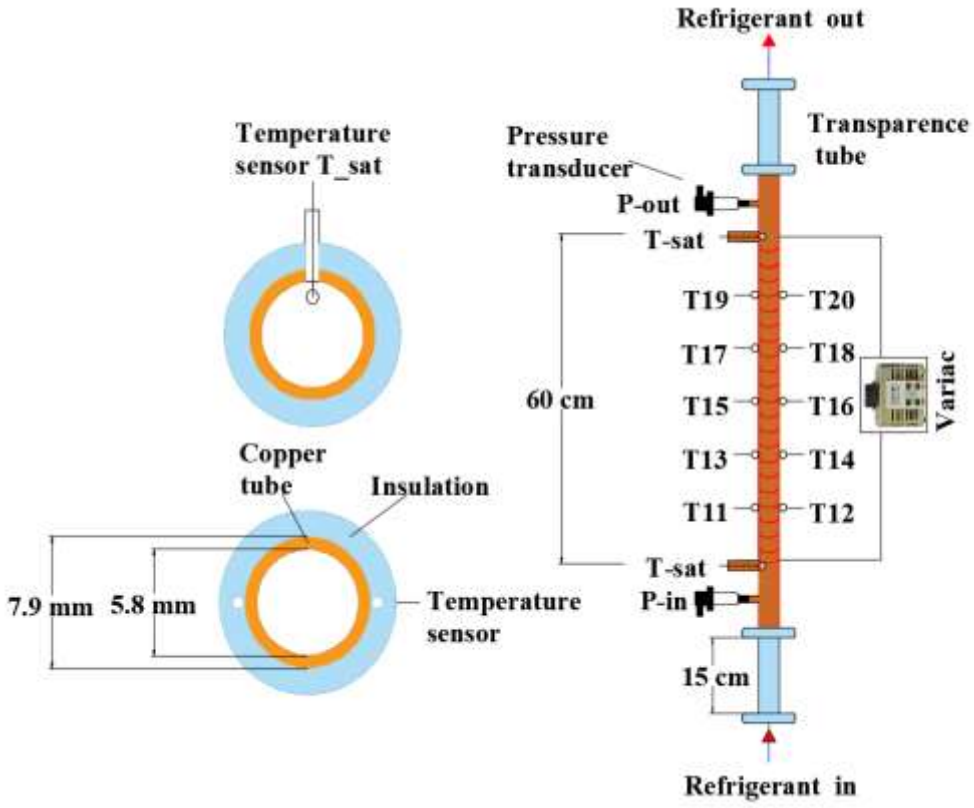

Fig 3. Schematic diagram of the test section (evaporator tube).

Where: $P_{i.ev}$ is the refrigerant pressure at inlet of the test section, Δp is the refrigerant pressure difference between inlet and outlet of the test section.

The vapor quality at the inlet of the test section tube (x_i) is expressed in term of the local enthalpy as follows **[13]**:

$$x_i = \frac{h_i - h_{l.i}}{h_{fg.i}} \quad (9)$$

The specific enthalpy of the refrigerant at the inlet of the test section $h_{i.ts}$ represents the specific enthalpy of the refrigerant at the outlet of

preheater, which can be determined by applying an energy balance on the preheater as follows:

$$h_{i.ts} = h_{i.pr} + \frac{\dot{Q}_{pr}}{\dot{m}}$$

(10)

Vapor quality (dryness fraction) of the refrigerant at each position (x_z) is calculated by using a linear relation along test section length:

$$x_z = x_i + \Delta x \cdot L_z$$

(11)

Vapor quality difference Δx of the refrigerant between inlet and outlet of the evaporator tube can be expressed by:

$$\Delta x = \frac{x_o - x_i}{L_{ts}}$$

(12)

Outlet vapor quality of the refrigerant in the test section tube is calculated by:

$$x_o = \frac{h_{o.ts} - h_{l.o}}{h_{fg.o}}$$

(13)

Outlet specific enthalpy of the refrigerant in the test section tube $h_{o.ts}$ is determined by applying an energy balance on the test section:

$$h_{o.ts} = h_{i.ts} + \frac{\dot{Q}_{ev}}{\dot{m}}$$

(14)

Total pressure gradient in the test section tube is calculated by **[1]**:

$$-\frac{dp}{dz} = -\frac{\Delta p}{L_{ts}}$$

(15)

$$\Delta p = \Delta p_{fr} + \Delta p_m + \Delta p_{st}$$

(16)

Where:

Δp: Total pressure drop of the refrigerant flow in the test section tube (kPa) which is determined experimentally using the following equation:.

$$\Delta p = P_{o.ev} - P_{i.ev} \quad (17)$$

Δp_{fr} : Frictional pressure drop of the refrigerant flow due to shear at the tube surface and at the vapor-liquid interface in the test section (kPa).

Δp_m: Momentum pressure drop due to the acceleration of the two-phase refrigerant flow in the test section (kPa).

Δp_{st}: Pressure drop of the refrigerant flow due to the static pressure change in the test section tube (kPa) and can be calculated by [**12**]:

$$\Delta p_{st} = [\alpha\rho_v + (1-\alpha)\rho_l]gsin\emptyset \quad (18)$$

Where: $\emptyset$ is the angle of the evaporator tube with horizontal plane (90^o), and α is the void fraction which can be determined as per homogenous model [**12**] as follow:

$$\alpha = \left[1 + \left(\frac{1-x}{x}\right)\left(\frac{\rho_v}{\rho_l}\right)^{2/3}\right]^{-1} \quad (19)$$

Momentum pressure drop Δp_m is determined by:

$$\Delta p_m = G^2\left[\frac{v_v * x^2}{\alpha} + \frac{v_l(1-x)^2}{(1-\alpha)}\right] \quad (20)$$

Frictional pressure drop of the refrigerant flow Δp_{fr} is determined by:

$$\Delta p_{fr} = \Delta p - \Delta p_m - \Delta p_{st} \quad (21)$$

4. Results and Discussions

The experimental investigations of the refrigerant R134a flow boiling heat transfer coefficient and pressure drop in the evaporator test section are conducted within test conditions in the range of (7.718– 32.78) kW/m^2 for heat flux, (97.3 -148.7) kg/m^2 .s for mass flux, vapor quality (0.3 – 1) and saturation temperature (-20 to -15) °C as shown in the Table 1.

Table 1 Test conditions considered in the present study

No	Mass Flux (kg/m^2.s)	Heat Flux (kW/m^2)				
1	97.3	7.718	11.75	16.48	23.38	32.78
2	112.5	7.718	11.75	16.48	23.38	32.78
3	148.7	7.718	11.75	16.48	23.38	32.78
	Range of vapor quality: X = 0.3 – 1					
	Rang of evaporating temperature: -20.58 to -15.68					

4.1 Characteristics of Refrigerant Flow Boiling

The variation of heat flux with wall-refrigerant temperature difference of flow boiling for several mass fluxes 97.3, 112.5 and 148.7 kg/m^2.s is shown in **Fig 4**. It can be seen for the range of (15 - 33) °C temperature difference, the dominance of nucleate and forced convective contributions of flow boiling heat transfer was evident. The observed large heat fluxes in this region are attributed to the combined effect of liquid entrainment and evaporation. The variation of the vapor quality during refrigerant flow boiling process along the test section tube is shown in the **Fig 5** with fixed mass flux 112.5 kg/m^2.s and different heat fluxes. It can be observed that the vapor quality increases with the normalized tube length as a result of the phase change from liquid into vapor. The higher vapor quality was observed at relatively higher heat flux 32.78 kW/m^2.

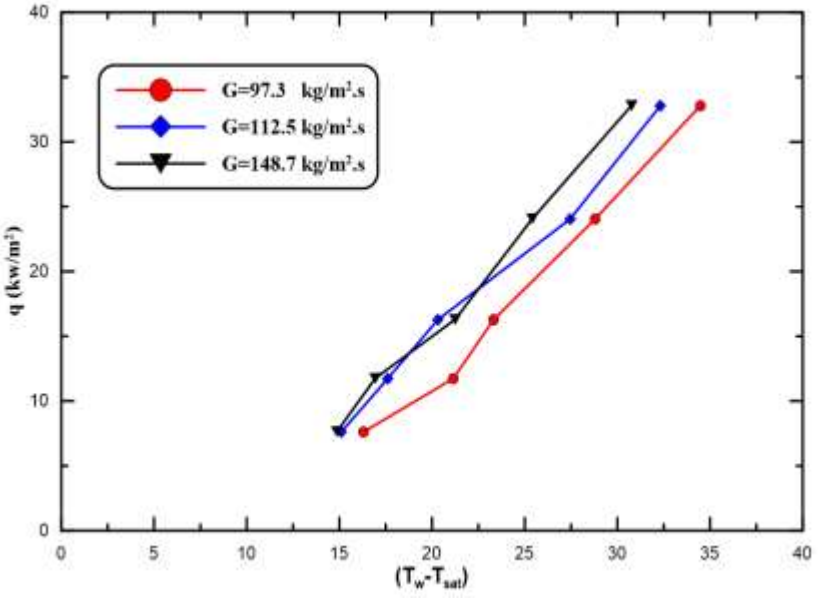

Fig 4. Variation of heat flux with wall-refrigerant temperature difference for various mass fluxes 97.3, 112.5 and 148.7 kg/m^2.s.

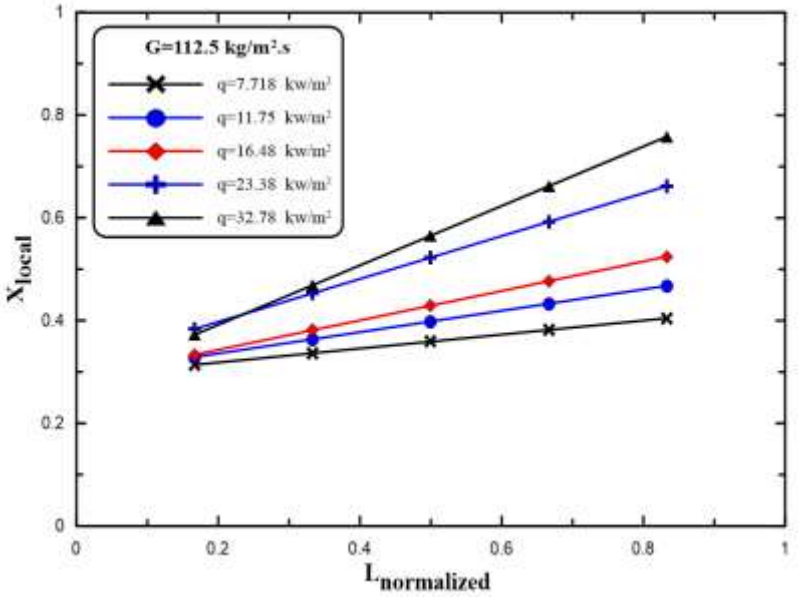

Fig 5. Refrigerant vapor quality as a function of the normalized length of the test section tube at G= 112.5kg/m^2.s and different heat fluxes.

4.2 Effect of Heat Flux on Heat Transfer

The effect of heat flux measured in the range of 7.718 to 32.78 kW/m^2 on flow boiling local heat transfer coefficient at fixed mass fluxes 97.3 and 148.7 kg/m^2.s is shown in **Fig 6** and **Fig 7**. It can be noticed that the heat transfer coefficient is higher at the low vapor quality and continuously decreases with vapor quality for all the values of heat flux due to the nucleate and convective boiling contributions at this ranges of vapor quality and difference of wall-refrigerant temperature. The heat transfer coefficient was directly proportional to heat flux and relatively higher value of heat transfer coefficient was observed at heat flux 32.78 kW/m^2. According to Newton's law of convection heat transfer, the increase in heat flux at constant tube surface-refrigerant temperature difference will enhance the value of heat transfer coefficient. A similar behavior of heat transfer coefficient can be observed for mass flux 148.7 kg/m^2.s in **Fig 7**.

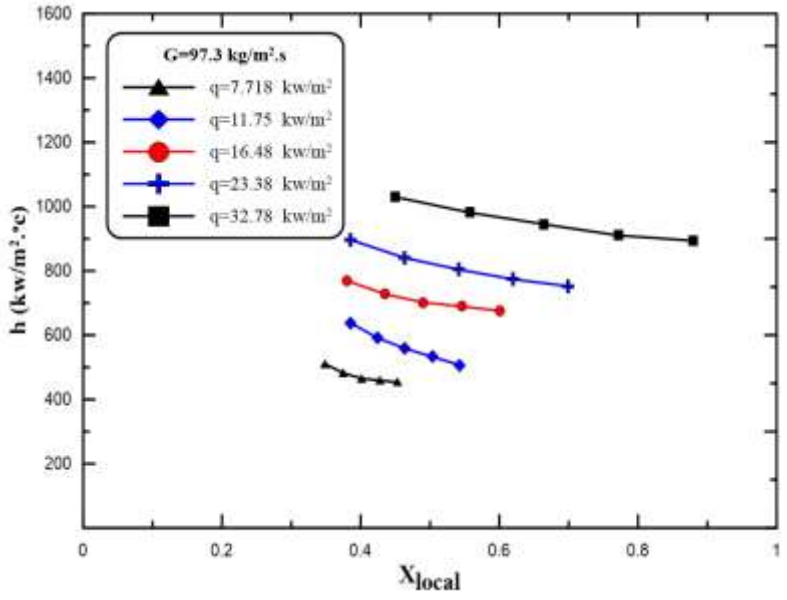

Fig 6. Effect of heat flux on local heat transfer coefficient for G= 97.3 kg/m^2.s.

4.3 Effect of Mass Flux on Heat Transfer

The variations of the flow boiling local heat transfer coefficient with vapor quality at fixed heat flux 11.85 kW/m^2 and various mass fluxes 97.3, 112.5 and 148.7 kg/m^2.s are shown in **Fig. 8** and **Fig.9** .The higher values of heat transfer coefficient can be observed at relatively greater mass flux 148.7 kg/m^2.s due to the heat transfer contribution of forced convective evaporation which depends on refrigerant mass flow rate. The same behavior of the heat transfer coefficient can be observed for heat flux 32.78kW/m^2 in **Fig.9**.

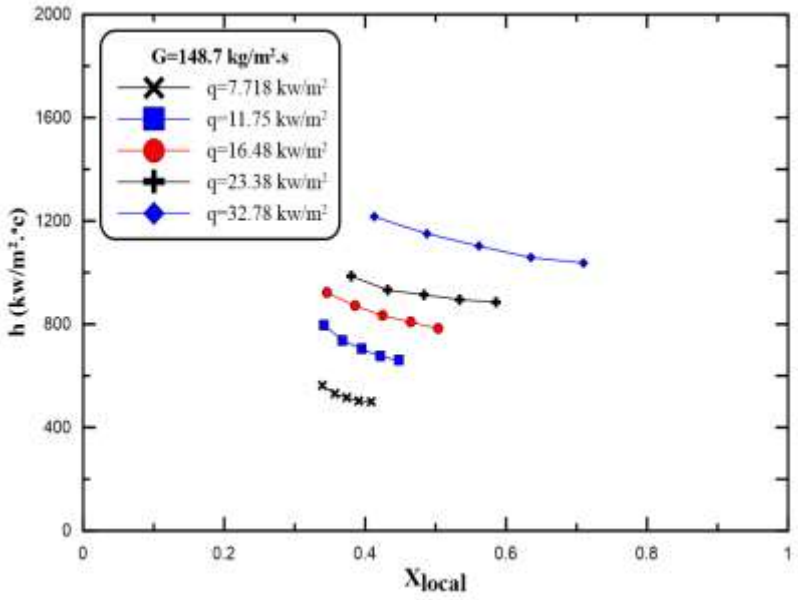

Fig 7. Effect of heat flux on the local heat transfer coefficient for G= 148.7 kg/m^2.s.

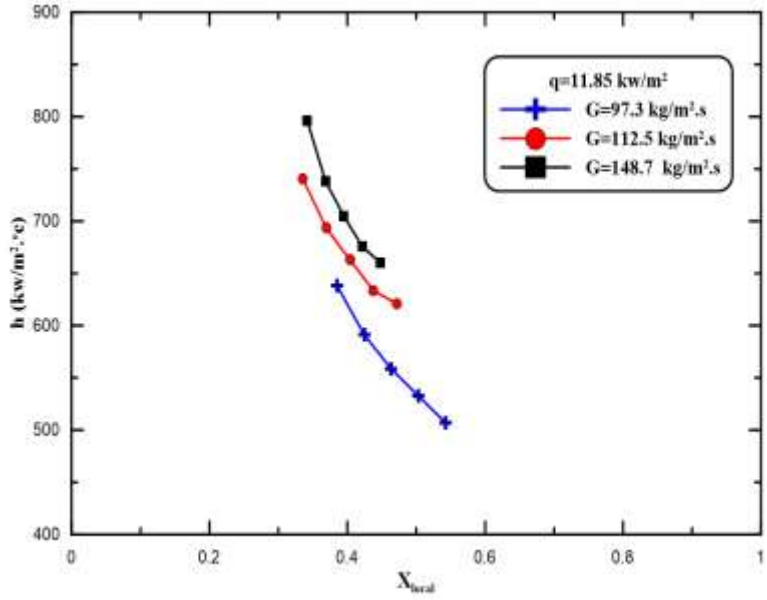

Fig 8. Effect of mass flux on the local heat transfer coefficient for q= 11.85 (kW/m^2)

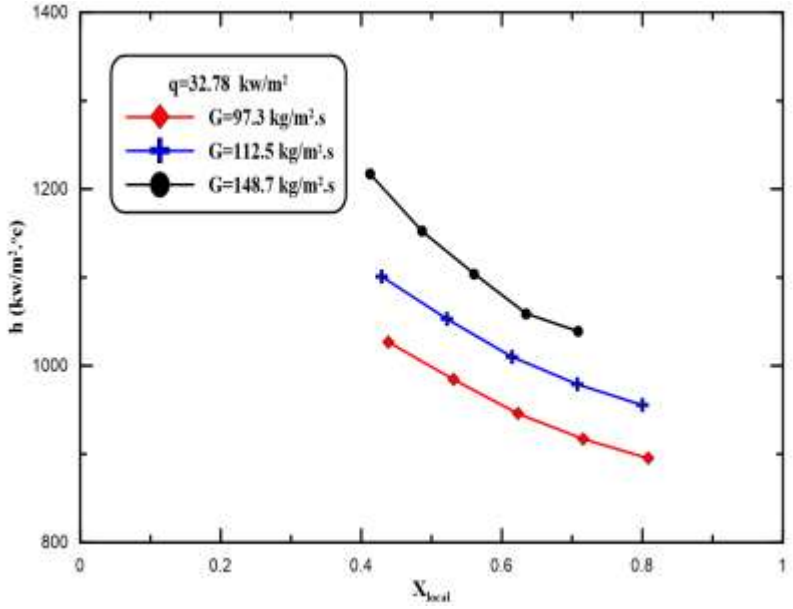

Fig 9. Effect of mass flux on the local heat transfer coefficient for q= 32.78 kW/m^2.

4.4 Effect of Inlet Vapor Quality and Saturation Temperature on Heat Transfer

The effect of R-134a inlet vapor quality on local heat transfer coefficient inside the evaporator tube at a constant heat flux 32.78 kW/m^2 and mass flux 112.5 kg/m^2.s is depicted in **Fig.10**. Three different values of the inlet vapor quality 0.3881, 0.3567, and 0.3357 were tested. It can be observed that the local heat transfer coefficient increases with inlet vapor quality along the evaporator tube due to the dominance of forced convective boiling at relatively higher inlet vapor quality. The effect of R-134a saturation temperature on local heat transfer coefficient at constant heat flux 16.48 kW/m^2 is illustrated in **Fig.11**. Three different values of saturation temperature -20.58˚C, -17.31˚C, and -15.68˚C were tested. The increase of saturation temperature leads to a significant increase in local heat transfer coefficient as a result of decrease in wall-refrigerant temperature difference at constant test conditions in accordance with Newton law of cooling. The enhancement in local heat transfer coefficient at temperature -15.68˚C was 12% higher than the relatively lower saturation temperature of -20.58˚C.

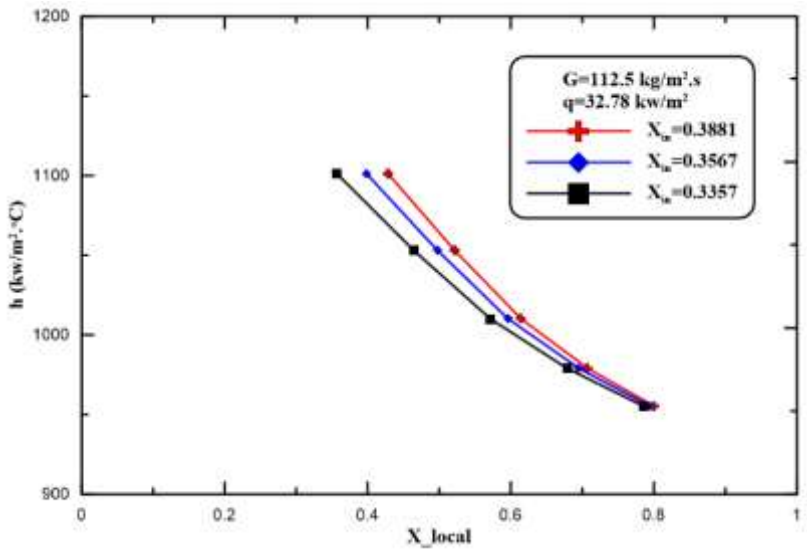

Fig 10. Variation of heat transfer coefficient with refrigerant inlet vapor quality at q= 32.78 kW/m^2 and G= 112.5 kg/m^2.s.

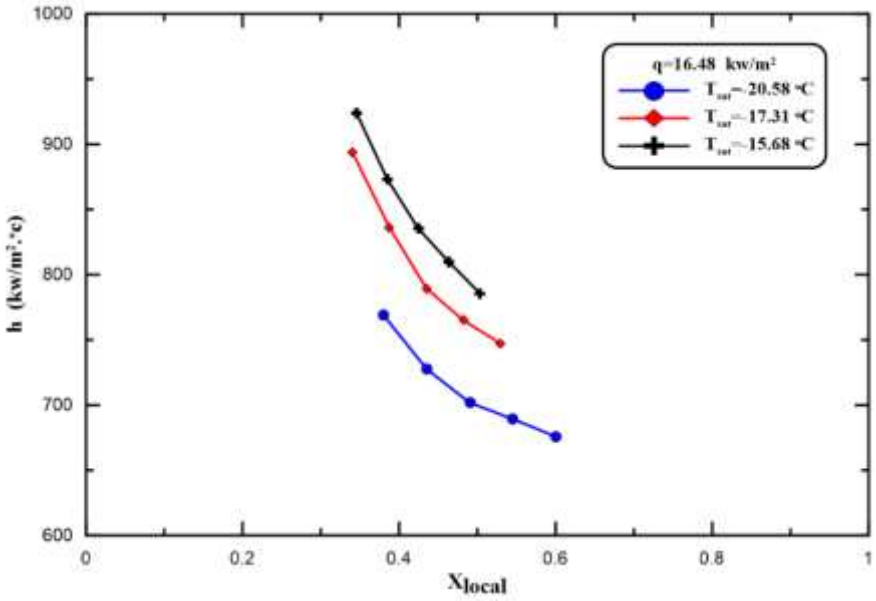

Fig 11. Effect of saturation temperature on local heat transfer coefficient for q= 16.48 kW/m^2

4.5 Effect of Heat Flux and Mass Flux on Pressure Drop

The variations of pressure drop of the refrigerant flow boiling with vapor quality in the evaporator tube can be attributed to three sources, friction of fluid with tube surface, momentum change of the flow in the tube and static pressure change. The experimental results of two-phase flow boiling show that the frictional pressure drop increases with the increase in mass flux as shown in **Fig. 12** and with heat flux as shown in **Fig. 13** at constant test conditions. The increase in mass and heat fluxes enhance the refrigerant flow velocity and then leads to rise in frictional pressure drop along the evaporator tube.

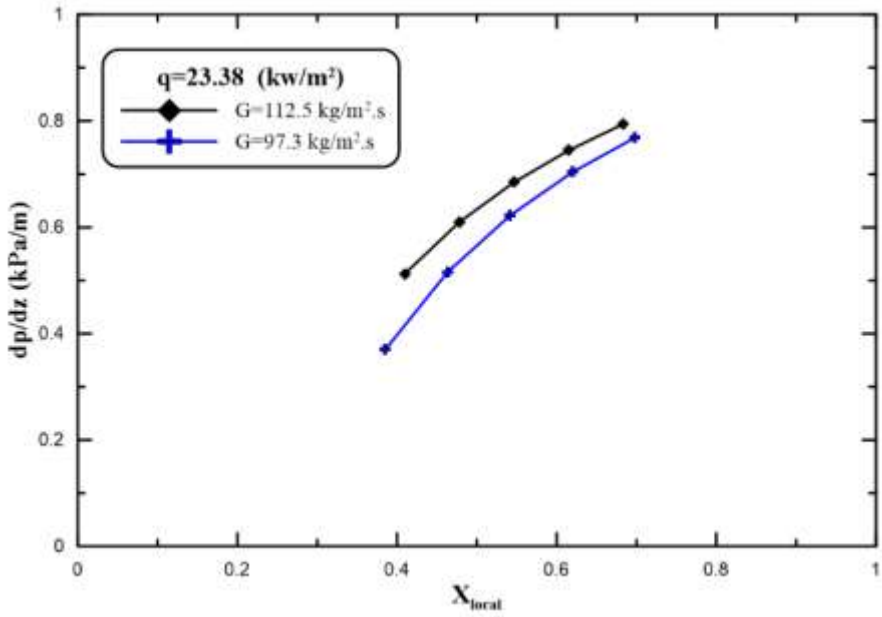

Fig. 12 Pressure drop variation as a function of vapor quality for q= 23.38 kW/m^2.

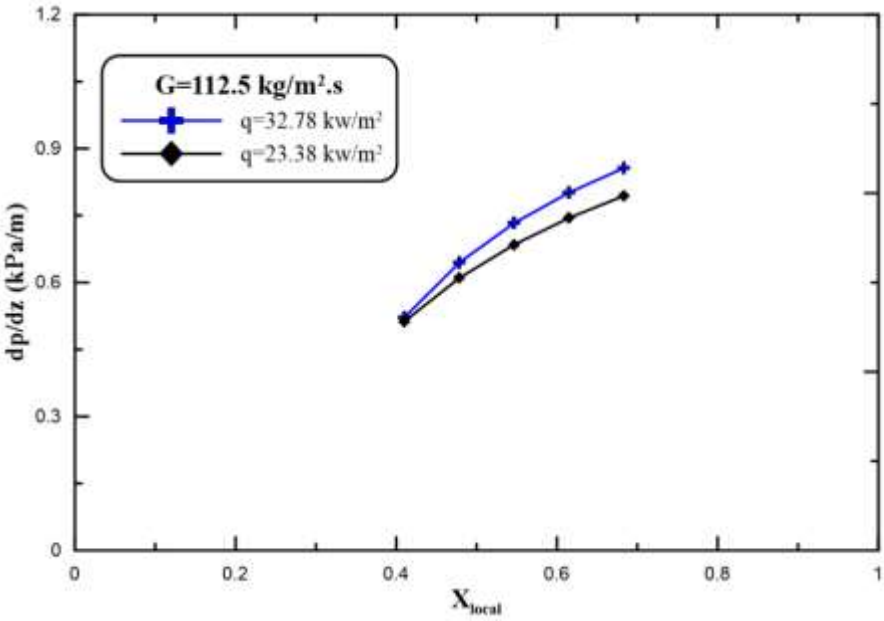

Fig 13. Pressure drop variation as a function of vapor quality for G=112.5 kg/m^2.s.

The Comparison between the current work results and Ong [14] results show a similar trend as illustrated in **Fig. 14**. The deviation in value of heat transfer coefficient is resulted from the difference in tube dimensions and operating conditions.

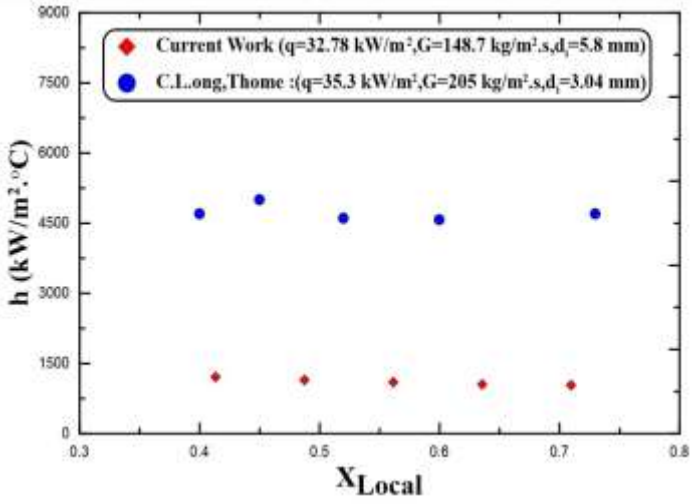

Fig 14. Comparison between the current work results and Ong **[14]** results.

5. CONCLUSIONS

1. The local heat transfer coefficient was directly proportional to the refrigerant mass flux, where the average heat transfer coefficient at relatively greater mass flux 148.7 kg/m^2.s was 21% higher than other mass fluxes at similar test conditions.
2. The relatively higher value of heat transfer coefficient was observed at heat flux 32.78 kW/m^2 with an average increase of 19 % compared to the relatively lower value of heat flux 23.38 kW/m^2.
3. The enhancement in local heat transfer coefficient was about 6% for inlet vapor quality 0.3881 compared to the relatively lower value 0.3357%.
4. The enhancement in local heat transfer coefficient at temperature -15.68˚C was approximately 12% higher than that for the relatively lower saturation temperature -20.58˚C.
5. The effect of increase in mass flux and heat flux on pressure drop was approximately 9% and 7.5% respectively.

NOMENCLATURE

d Diameter of the test section tube (m)
G Mass flux (kg/m^2.s)
g Gravity acceleration m/s^2
h Specific enthalpy (kJ/kg)
h_{fg} Latent heat of vaporization (kJ/kg.h)
h_z local heat transfer coefficient (W/m^2.˚C)
I Current (A)
k_{cu} Thermal conductivity of tube (W/m.˚C)
L Length of the test section tube (m)
Lz Length of tube subsection (m)
$\dot{m}$ Mass flow rate (kg/s)
p pressure (Pa)
$\dot{Q}$ Heat transfer (W)
$\dot{q}$ Heat flux (W/m^2)
T temperature (˚C)
V Voltage (V)
x Vapor quality, dimensionless

Subscripts:

b Bottom
ev Evaporator
fr frictional
i inlet
L Liquid
m Momentum
o Outlet
pr Preheater
ref Refrigerant
sat Saturation
t Top
ts Test section
v Vapor
w Wall

REFERENCES

[1] Martin Callizo, Claudi. "Flow boiling heat transfer in single vertical channels of small diameter" Diss. KTH, (2010).

[2] Anwar, Zahid. "Flow boiling heat transfer, pressure drop and dry out characteristics of low GWP refrigerants in a vertical mini-channel" Diss. KTH Royal Institute of Technology, (2014).

[3] Patel, Giteshkumar N. "CFD Simulation of Two-phase and Three-phase Flows in Internal-loop Airlift", (2010).

[4] Chen, L., Y. S. Tian, and T. G. Karayiannis. "Vertical upward flow patterns in small diameter tubes." (2005).

[5] Huo, Y., Tian S., and Karayiannis, T. G. "R134a flow boiling heat transfer in small diameter tubes." RT Edwards Inc., (2007).

[6] Mahmoud, Mohamed M., Tassos G. Karayiannis, and David BR Kenning. "Surface effects in flow boiling of R134a in microtubes." International Journal of Heat and Mass Transfer, 54, pp15-16, (2011).

[7] Ali, Rashid, Björn Palm, and Mohammad H. Maqbool. "Flow boiling heat transfer characteristics of a minichannel up to dryout condition." Journal of Heat Transfer 133.8 (2011): 081501.

[8] Pike-Wilson, Emily A., Mohamed M. Mahmoud, and Tassos G. Karayiannis. "Flow boiling of R134a and R245fa in a 1.1 mm diameter tube." ASME 2013 11th International Conference on Nanochannels, Microchannels, and Minichannels. American Society of Mechanical Engineers Digital Collection, (2013).

[9] Fang, Xiande. "A new correlation of flow boiling heat transfer coefficients based on R134a data." International Journal of Heat and Mass Transfer ,66, (2013).

[10] Mancin, Simone, Andrea Diani, and Luisa Rossetto. "R134a flow boiling heat transfer and pressure drop inside a 3.4 mm ID microfin tube." Energy Procedia, 45, (2014).

[11] Li, Wei, et al. "Effects of heat flux, mass flux and two-phase inlet quality on flow boiling in a vertical super hydrophilic microchannel", International Journal of Heat and Mass Transfer,119, (2018).

[12] Collier J. G. and J. R. Thome, "Convective boiling and condensation", Third ed., Oxford University press, pp. 176, (1994).

[13] Copetti, J. B., Macagnan, M. H., Zinani, F., and Kunsler, N. L., "Flow boiling heat transfer and pressure drop of R-134a in a mini tube: an experimental investigation", Experimental Thermal and Fluid Science, Vol. 35, pp 636-644, (2011).

[14] Ong, C. L., and J. R. Thome. "Macro-to-microchannel transition in two-phase flow: Part 2–Flow boiling heat transfer and critical heat flux." Experimental thermal and fluid science 35.6: 873-886. (2011).

University of Thi-Qar Journal Vol.14 No.3 SEP 2019
Web Site: https://jutq.utq.edu.iq/index.php/main
Email: utj@utq.edu.iq

Analysis of Composite Panels of Profiled Steel Sheet with Ferrocement by Using Finite Element Method

Prof. Dr. Nabeel Abdulrazzaq Jasim[(1)]

M. Sc. Mohammed Abd Al-baqer Jennam[(2)]

[1] University of Basrah, Department of Civil Engineering, Basrah, Iraq.

nabeel_ali58@yahoo.com

[2] Real-estate Registration Office, Ministry of justice, Iraq.

mohammedcivilll11@gmail.com

Abstract

This paper concerns with the application of finite element technique to the nonlinear analysis of the behavior of profiled steel sheet ferrocement (PSSF) composite panels. The composite panels were analyzed using nonlinear three dimensional finite element models. The constitutive models of the nonlinear material behavior for ferrocement matrix, PSS, and steel wire mesh were used. ANSYS version 16.1 program code was used to analyze the three dimensional model. Ferrocement was modeled by using the 8-noded isoperimetric brick elements (SOLID65) with three degrees of freedom, while the profiled steel sheet was modeled as SHELL181 element with four-node element with six degrees of freedom at each node: translations in the x, y, and z directions, and rotations about the x, y, and z-axes. A nonlinear spring element, COMBIN14, was used to represent the mechanical connectors, while to simulate the adhesive epoxy layer solid element SOLID185 was

used. It was defined by eight nodes having three degrees of freedom at each node: translations in the nodal x, y, and z directions. The wire mesh reinforcement was modeled as a volume ratio distributed within the ferrocement brick elements. The analytical results of load-deflection response have been compared with available experimental works.

Keywords: Ferrocement, Composite Panel, Finite Element modeling, PSSF.

1-Introduction

The last years had shown significant steps in research in order to develop ferrocement as an active building material. Ferrocement is a form of reinforced concrete made of wire mesh and mortar, which has unique values of serviceability and strength. It can be constructed from easily available materials and it does not require a large number of skilled workers. It has many applications and uses in the area of low-cost houses, agriculture, and industry [1].

In civil engineering construction, different materials can be arranged in optimum geometric configuration,with the aim that only the desirable property of each material will be utilized by virtue of its designated position. The structure is then known as a composite structure. Composite structures combine two or more materials in a unit structure to provide tangible benefits and a versatile solution to suite different applications. A composite system reduces the unnecessary and unwanted material properties, such as weight and cost, without sacrificing required capacity. A structure can be considered composite only so far as the various components are connected to act as a single unit. The structural performance depends on the extent to which composite action can be

achieved. Composite structures, in general, have a higher stiffness and a higher load bearing capacity when compared with their non-composite counterparts. Hence the composite sections have got smaller section depth [1].

In the last 30 years several approaches have been used for the analysis of ferrocement structures, but the first use of finite element technique to analyze such structures was done by Prakhya and Adidan [2], who analyzed ferrocement slabs using rectangular hetrosis elements. Bin-Omer et al. [3] presented a computational model based on the Timoshenko beam finite element formulation using quadratic isoparametric elements with 3 degrees of freedom to analyze flanged ferrocement beams. Boshra Aboul-Anen et al. [4] used ANSYS software with Eight-node solid isoparametric element to represented ferrocement slab to study the composite action between the ferrocement slabs and steel sheeting. The objective of this paper is to develop a non-linear finite element model to simulate the behavior of profiled steel sheet ferrocement (PSSF) composite panels. The validity and calibration of the theoretical formulations and the program used is judged through comparison of analytical results with experimental data.

2- Modeling of (Profiled steel sheet with ferrocement) composite panels system

Three dimensional finite element modeling technique was used to investigate numerically the behavior of (PSSF) panels that were tested experimentally under the effect of static load [An Experimental Study of Composite Panels of Profiled Steel Sheet with Ferrocement, Which will

be published later]. The software ANSYS finite element program version 16.1, Implementing ANSYS Parametric Design Language (APDL), is used in this analysis.

One of the main advantages of ANSYS is the integration of the three phases of finite element analysis: pre-processing phase, solution phase and post- processing phase. Pre-processing routines in ANSYS define the model, subdivide the problem into nodes, elements, and apply loadings and boundary conditions. Displays may be created interactively on a graphics terminal as the data are input to assist the model verification. Post-processing routines may be used to retrieve analysis results in a variety of ways. Plots of the structure deformed shape and the stress or strain contours to be obtained [5].

Nonlinear finite element analysis is adopted in the present study in order to investigate the behavior of the experimentally tested composite panels. ANSYS, including a variety of routines, allows for the implementation of specific material models to represent the profiled steel sheet, ferrocement, mechanical connectors, and epoxy adhesive layer, and boundary conditions.

2-1 Modeling of Profiled Steel Sheet

Profiled steel sheet is modeled, in this study, with SHELL181 element. It is used for analyzing thin to moderately thick shell structures. It is a four-node element with six degrees of freedom at each node: translations in the x, y, and z directions, and rotations about the x, y, and z-axes, as shown in Figure (1).

SHELL181 is well-suited for linear elastic, elastoplastic, creep, hyperelastic, and nonlinear material properties. Change in shell thickness is accounted for in nonlinear analyses. In the element domain, both full and reduced integration schemes are supported. The thickness of this element can be considered as a constant or varying smoothly over the area of the element by considering various values of the thickness at its four nodes. This element may be used for layered applications for modeling composite shells or sandwich construction. The basic formulation of this element was explained in the ANSYS 16.1 theoretical manual [6].

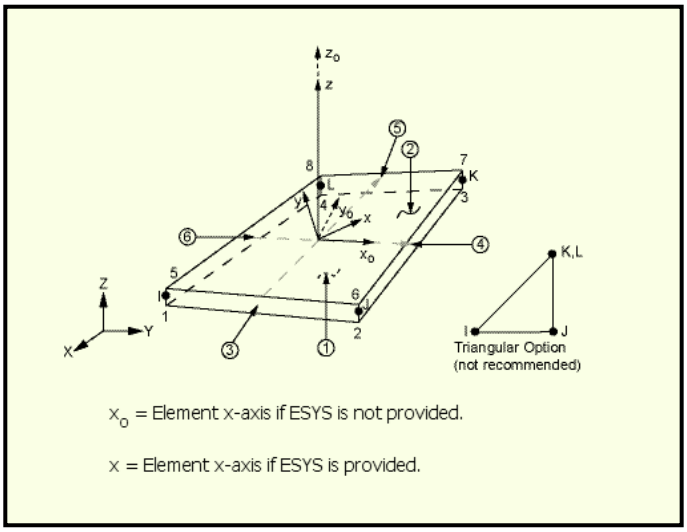

Figure (1) Geometry of Shell 181 (three- dimensional shell element) [6]

2-2 Modeling of Ferrocement Slab

The choice of the proper element is very important matter in the finite element formulation. For a reinforced concrete idealization, the element type depends upon the geometry of the structure and the number of independent space coordinates necessary to describe the problem. In

the present study, SOLID65 three-dimensional reinforced concrete brick element, Figure (2), is used to model the ferrocement slab.

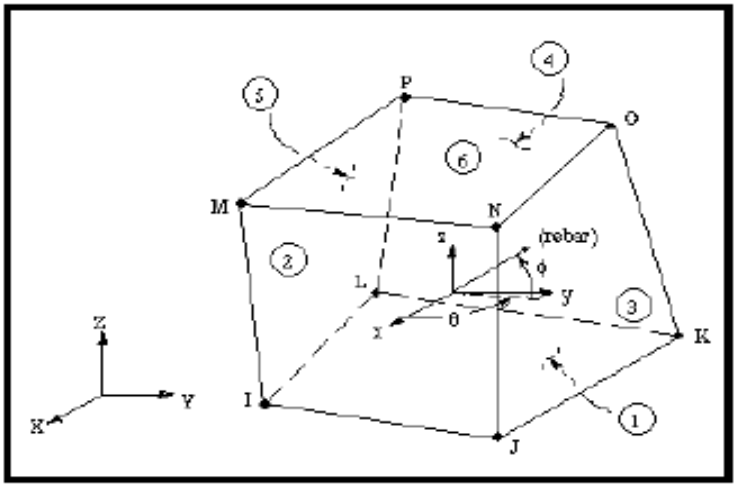

Figure (2) SOLID65-3D Reinforced concrete element [6]

SOLID65 can be used for the three-dimensional modeling of solids with or without reinforcing bars (rebars). The element is defined by eight nodes having three degrees of freedom at each node, translation in the x, y, and z directions. The element is capable of cracking in tension, in three orthogonal directions, crushing in compression, and plastic deformation. The rebars are capable of tension and compression, but not shear. They are also capable to reveal plastic deformation. The most important aspect of this element is the treatment of nonlinear material properties [5]. SOLID65 allows the presence of four different materials within each element; one matrix material and a maximum of three independent reinforcing materials. The matrix material is capable of directional integration point cracking and crushing besides incorporating plastic and creep behavior [7].

2.3 Representation of Wire Mesh

The steel is assumed to be distributed over the concrete element, with a particular orientation angle θ, Figure (3). A composite-reinforcement constitutive relation is used in this case. To derive such a relation, perfect bond must be assumed to occur between the concrete and the steel.

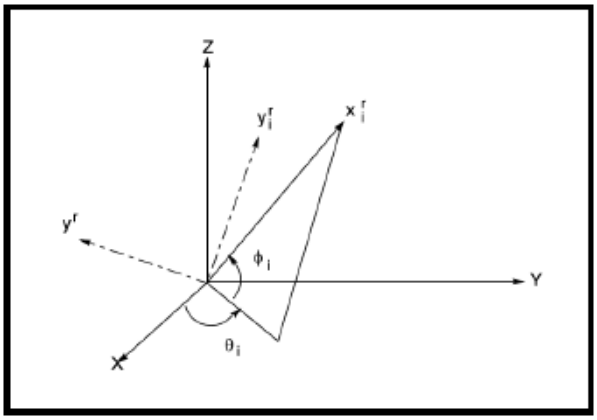

Figure (3) Reinforcement orientation for distributed model

2.4 Modeling of Mechanical Connectors

A nonlinear spring element, COMBIN14 in ANSYS, is used to represent the mechanical connectors behavior. COMBIN14 has longitudinal or torsional capability in 1-D, 2-D, or 3-D applications. The longitudinal spring-damper option is a uniaxial tension-compression element with up to three degrees of freedom at each node: translations in the nodal x, y, and z directions. No bending or torsion is considered, as shown in Figure (4).

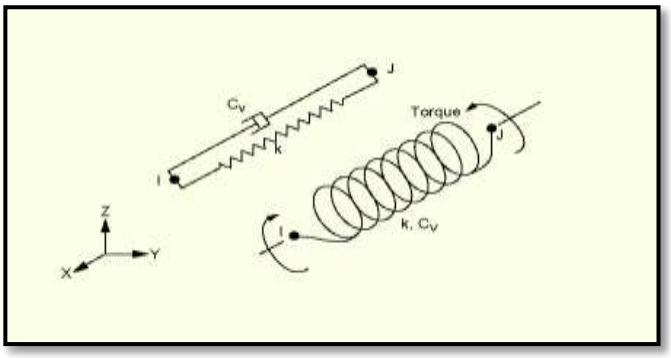

Figure (4) Geometry of Combin14

2.5 Modeling of Epoxy Adhesive Layer and interface surface

Two methods can be used to simulate the epoxy adhesive layer. In this study it is represented by using solid element SOLID185, (the element is used for the 3-D modeling of solid structures. It is defined by eight nodes having three degrees of freedom at each node: translations in x, y, and z directions as shown in Figure (5) [6].

3- Finite Element Formulation

The three–dimensional body in the finite element analysis is represented by a finite number of elements and a finite number of nodes that are identified on each element, where the elements are to be joined. The equilibrium equation for a nonlinear structure in a static equilibrium is derived using the principle of virtual work. This principle states that if a general structure in equilibrium is subjected to a system of small virtual displacements within a compatible state of deformation, the virtual work due to the external action is equal to the virtual strain energy due to the internal stress [8].

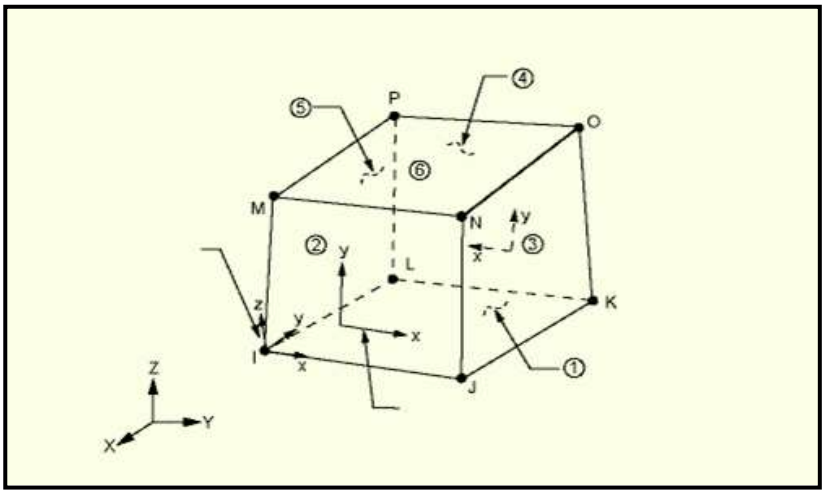

Figure (5) Geometry of Solid185 (three- dimensional solid element)

In the analysis of the composite (PSSF) elements, the behavior of a nonlinear material is due to the continual and sudden change in the element stiffness which arises from cracking, crushing of ferrocement, and yielding of steel sheet. These represent the main sources of the nonlinearity. A combined incremental-iterative technique is used to solve the nonlinear problem. Modified Newton-Raphson method is used where the stiffness matrix is updated at the second iteration of each load increment.

4- (PSSF) Composite panels and Materials

The geometry and the details of cross section for composite panels are shown in Figure (6). The composite PSSF panels were prepared with dimension of (0.71x2.0) m and tested under the action of line load at mid-span. All the tested PSSF composite panels comprise of single ferrocement panel connected on one side of the profiled steel sheet. The thicknesses of the ferrocement used are (10, 20,40) mm, and the thickness

of the profiled steel sheet is (0.8) mm for all specimens. The composite panel specimens were fabricated by connecting the precast ferrocement segments on the ribs of PSS. Mechanical connectors and other suggested method of connection by using epoxy adhesive resin alone and epoxy adhesive resin in additional to mechanical connecters were examined. A summary of the materials properties of the selected specimens are listed in Table (1).

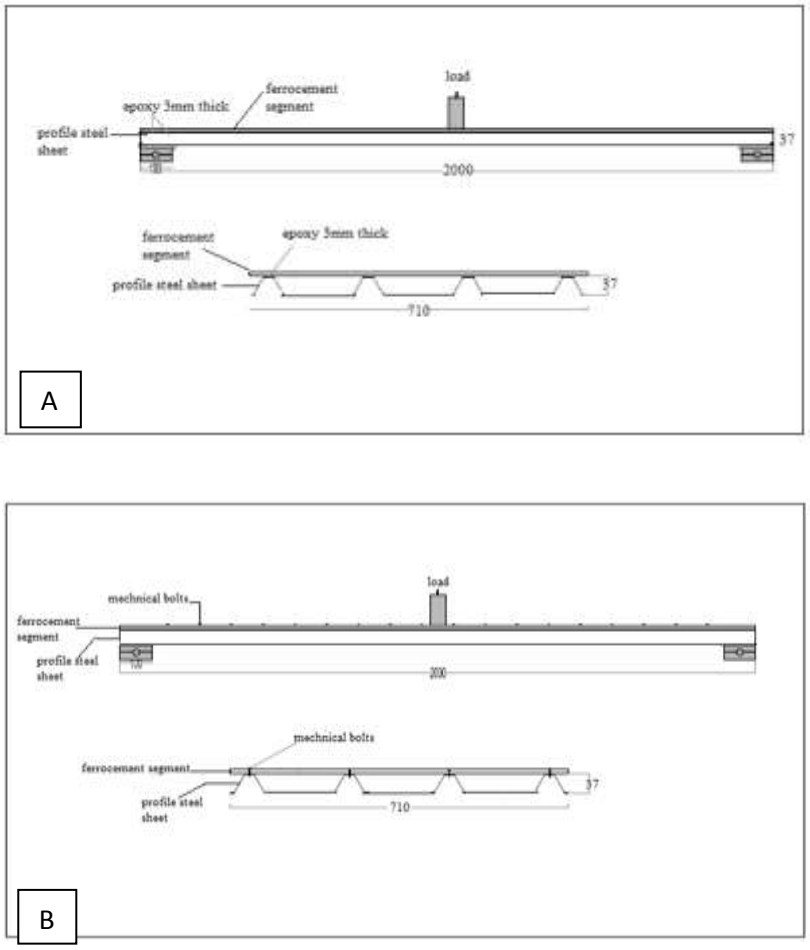

Figure (6) Typical PSS with ferrocement Panel Connected by (A) Epoxy Adhesive (B) Mechanical Fasteners.

Table (1). Materials properties

Materials	properties	value
Mortar	Young's modulus (MPa)	30000
	Compressive strength (MPa)	35 ,45
	Poisson's ratio	0.2
	Flexural strength *fr* (MPa)	5.5
	Crushing Strain,	0.0035
Steel Mesh	Diameter, mm	1
	Grid size, mm	12.5 x 12.5
	Young's modulus, MPa	92000
	Yield stress, MPa	415
Profiled Steel Sheet	Elastic Modulus(MPa)	200000
	Density(kg/m3)	7850
	Poisson's ratio	0.3
	Yield strength(MPa)	230
Epoxy Adhesive Resin	Density l/cm3	1650
	Poisson's ratio	0.4
	Elastic Modulus MPa	3300
Mechanical Connectors	Bolt Diameter (mm)	10
	Stiffness (N/mm)	5000

5- RESULTS AND DISCUSSION

A nonlinear finite element analysis has been carried out to analyze the composite PSSF panels. The analysis is performed by using ANSYS finite element computer program (Version 16.1). The ability of the method to simulate the behavior of this type of composite systems is demonstrated through the analysis of the tested panels. The results obtained by using finite element method are compared with the experimental results in terms of the load-deflection behavior and ultimate load values. The validity and accuracy of this method are examined.

The model was implemented by employing the ANSYS Parametric Design Language (APDL), implied in ANSYS software program. The implementation was started with the definition of the element types, element real constants, material properties and the geometry of the composite panel. Then, the mesh, coupling and linkage (connection) between the elements were added. After this step was completed, the solution processor was used to define the analysis type and analysis options, applying loads and boundary conditions, specifying load step options, and then initiating the finite element solution and calculating the deflection, stresses and strains at integration points of created small elements.

5-1 Mesh Size

An important step in the finite element modeling is the selection of the element mesh size. A convergence of results is obtained when an adequate number of elements is used in a structure. In the present study, and for best convergence, the overall span of each panel is divided into 80

elements (in y-direction). The composite panel cross section (in z-direction) is divided into one element for the ferrocement. In x-direction, the ferrocement panel is divided depending on the cross section of the profiled steel sheet. The rib flange and trough flange of PSS is divided into two and six elements, respectively, and the web into one elements. A typical discretization of the composite system is shown in figure (7) and figure (8). Three dimensional 8-noded brick element with three dof at each node is selected to represent the ferrocement, whereas three dimensional 4-noded shell elements with six dof at each node is selected to represent the PSS, and 8-noded brick element with three dof at each node is selected to represent the epoxy adhesive resin. Combine14 element with longitudinal capabilities is chosen for the modelling of bolt and in addition to this, surface to surface contact elements were introduced between the PSS and ferrocement elements to constitute the contact and sliding between these elements and for preventing the elements from piercing one another. Displacement boundary conditions are needed to constrain the model to get a unique solution. The support was modeled in such a way that a roller was created. The translations UZ and UY on a single line of nodes on the left supporting plate were given values of zero. While, the right supporting plate was restrained with a single line of nodes in z-direction only. By doing this, the panel will be allowed to rotate at the support. The external applied load represented by the plate in the actual experimental tests is modeled by an eight-node solid element, Solid185, at the mid span location. The application of the loads up to failure was done incrementally as required by the newton-Raphson procedure. Therefore, the total applied load was divided into a series of load increments (load steps).

5-2 Ultimate load

The ultimate loads of the PSSF composite panels obtained by the finite element analysis are summarized along with the corresponding experimental values in Table (2). Comparison between the results of finite element method and the experimental values of ultimate load shows reasonable agreement. For the three methods of connections, the predictions by the finite element method are very close to corresponding experimental values of ultimate loads

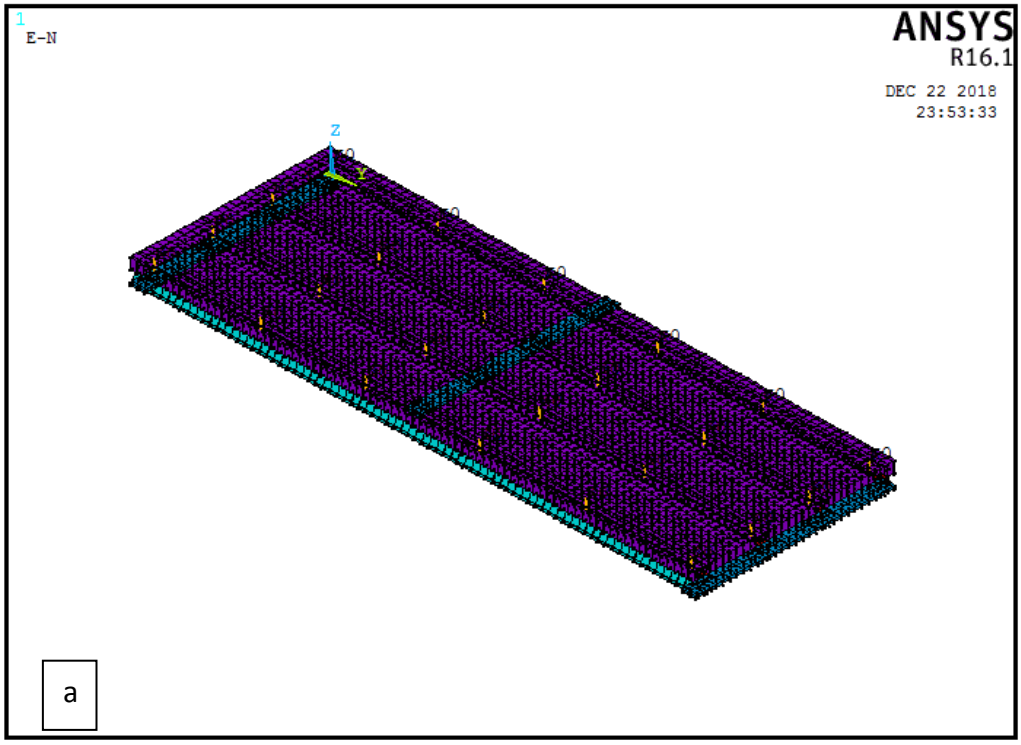

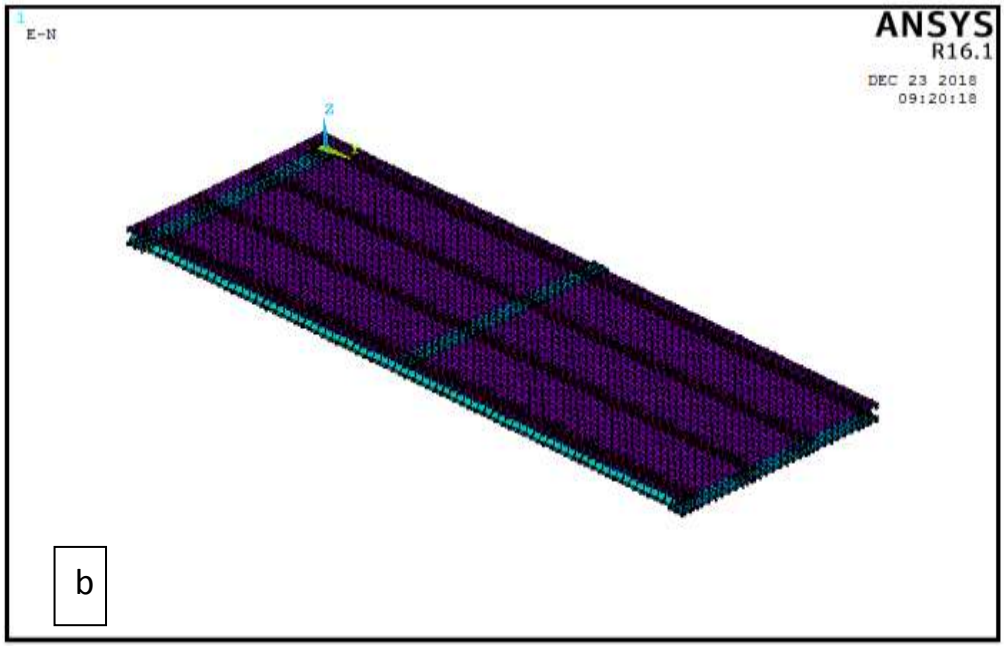

Figure (7) Finite Element Modeling of Composite Panels

Connected by: (a) mechanical fasteners (b) epoxy

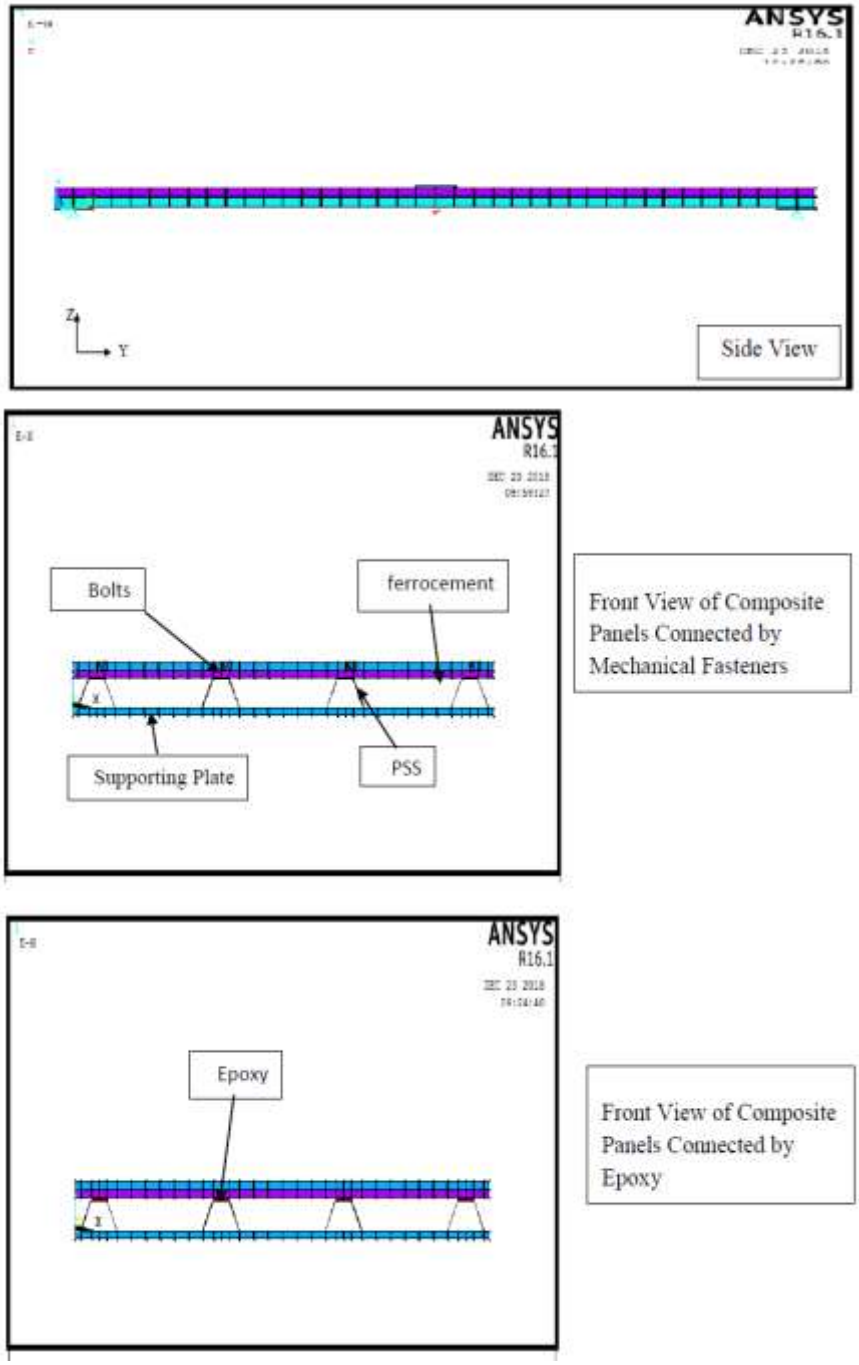

Figure (8) Discretization of Tested Composite Panels

Table (2):Results of ultimate loads

No.	Designation	Type of Connection	Spacing of bolts (mm)	Ultimate Load (kN)		$\frac{F_{FEA}}{F_{EXP}}$
				(F_{exp})	F_{FEA}	
1	2s1 (s=100)	Bolts	100	6	5.94	0.99
2	2s1 (s=50)	Bolts	50	7.9	7.8	0.98
3	2s`1 (s=200)	Bolts	200	4.9	4.5	0.91
4	2s`1 (s=100)	Bolts	100	6.3	6	0.95
5	2s`1 (s=50)	Bolts	50	8.6	7.9	0.92
6	3s1 (E+s=150)	Epoxy and bolts	150	11	9.9	0.9
7	3s1 (E)	Epoxy	-	10.2	9.3	0.91
8	3s`1 (E+s=200)	Epoxy and bolts	200	10.5	9.64	0.92
9	3s2 (s=150)	Bolts	150	11.68	11.40	0.97
10	3s2 (s=75)	Bolts	75	13.6	13.1	0.96
11	4s2 (s=150)	Bolts	150	12.5	12	0.96
12	5s2 (s=150)	Bolts	150	13.5	12.4	0.92
13	3s`2 (E+s=380)	Epoxy and bolts	380	16.3	15.8	0.97
14	4s`2 (E)	Epoxy	-	15.7	15.6	0.99

15	5s`2(E+s=380)	Epoxy and bolts	380	16.65	16.25	0.97
16	5s4(E+s=380)	Epoxy and bolts	380	27.5	24.2	0.88
17	6s4 (E)	Epoxy	-	27	24.1	0.89

The symbols in Designation (2s1 , 2s`1) mean :

2; The number (2) indicates the number of layers of wire mesh.

S; Ferrocement panel with compressive strength of 35 MPa.

1; The number (1) indicates the thickness of ferrocement panel in cm.

S` ; Ferrocement panel with compressive strength of 45 MPa.

E ; Epoxy.

s; spacing of bolts in mm

5-3 Mid-span Deflection

The vertical deflections at the centre of bottom face of the composite panel for all tested panels were measured. The load versus deflection curves obtained from the finite element method together with the experimental plots are presented in Figures (9) to (15) which show in general a good agreement. The values from the finite element models were calculated at the same locations of the experimental measurements.

It can be noted from these figures and from Table (2) that the finite element solutions are in good agreement with the experimental results throughout the entire behavior.

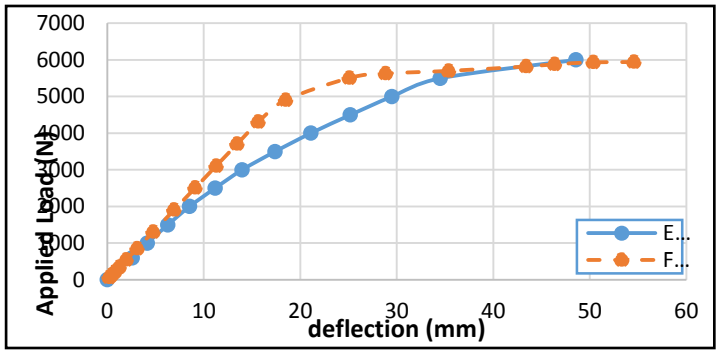

Figure (9) Mid-span Deflection Versus Applied Load for Composite panel 2S1 (S=100).

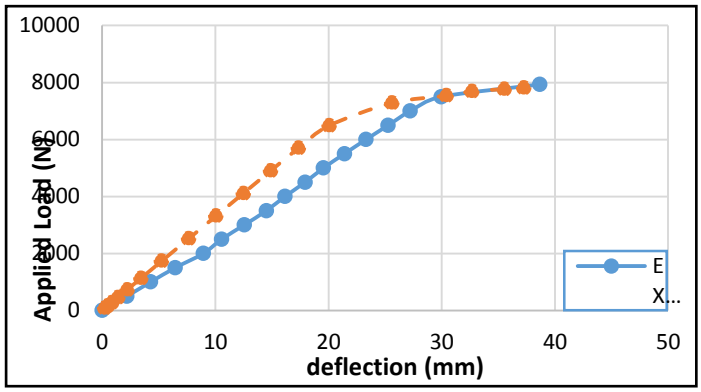

Figure (10) Mid-span Deflection Versus Applied Load for Composite panel 2S1(S=50)

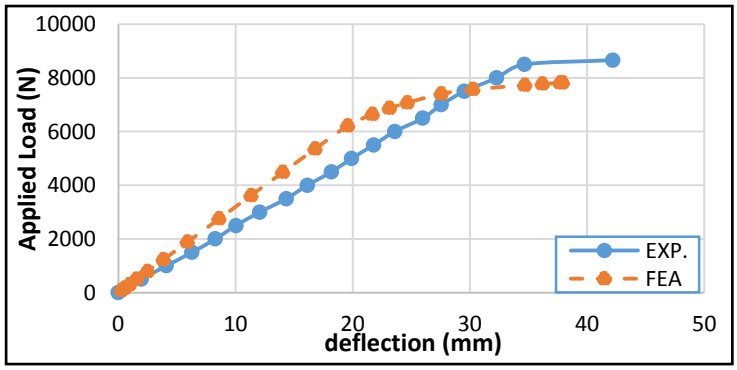

Figure (11) Mid-span Deflection Versus Applied Load for Composite panel 2S`1 (S=50).

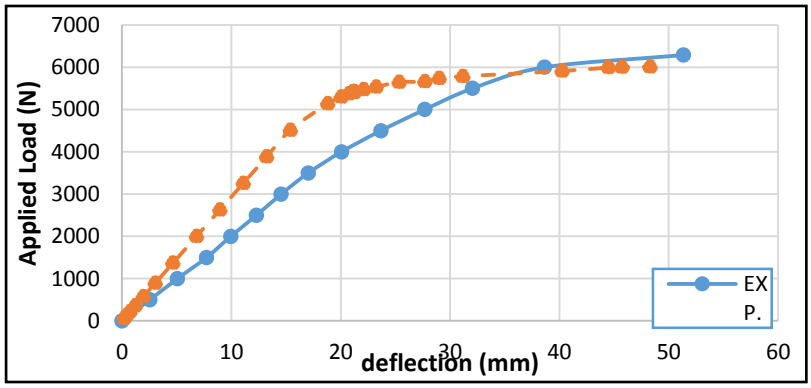

Figure (12) Mid-span Deflection Versus Applied Load for Composite panel 2S`1 (S=100).

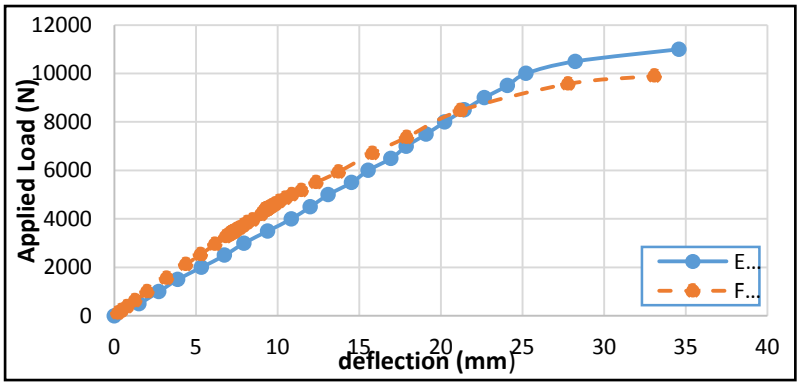

Figure (13) Mid-span Deflection Versus Applied Load for Composite panel 3S1 (E+S=150).

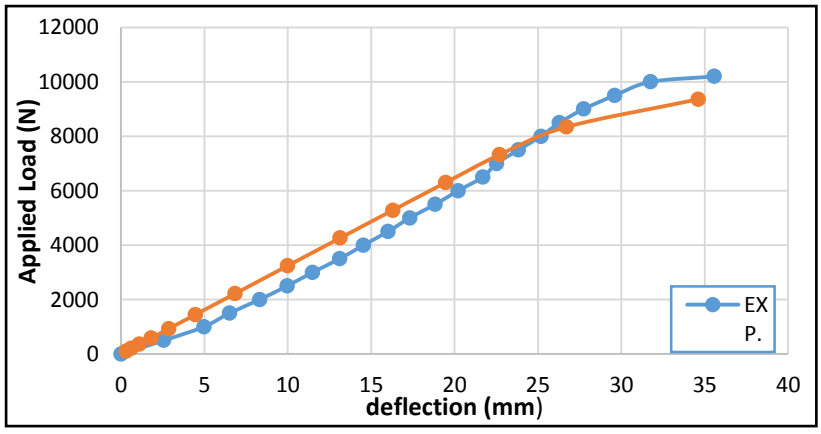

Figure (14) Mid-span Deflection Versus Applied Load for Composite panel 3S1 (E).

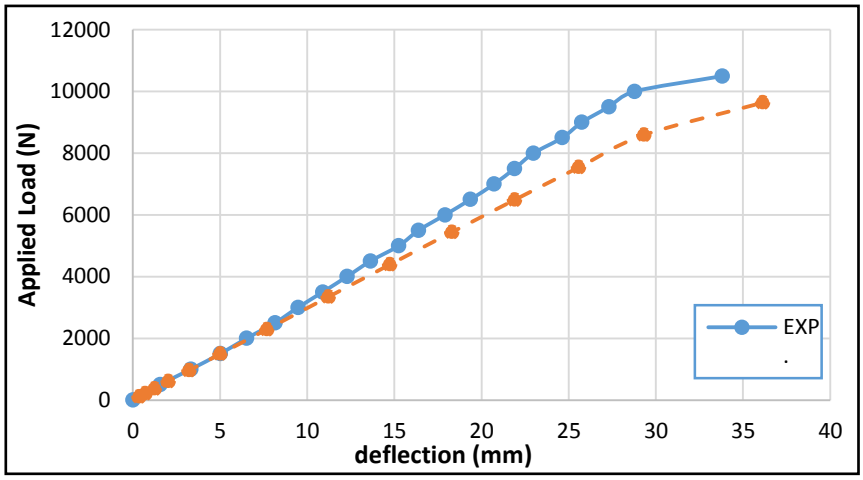

Figure (15) Mid-span Deflection Versus Applied Load for Composite panel 3S`1 (E+S=200).

6- Conclusions

In the nonlinear finite element analysis, the (ANSYS version 16.1) program is used with the following elements; three dimensional 8-noded brick element (SOLID65) to represent the ferrocement, three dimensional 4-noded shell elements (SHELL181) to represent the PSS and 8-noded brick element (SOLID185) for the epoxy adhesive resin. Combine14 element with longitudinal capabilities is chosen for modelling of bolts, and in addition to this the surface to surface contact elements are introduced between the PSS and ferrocement elements to constitute the contact and sliding between these elements and for preventing the elements from piercing one another. Acceptable agreement with the experimental results are obtained by this model. The average value of ratios of results of the finite element method to experimental results for ultimate load is 94%. Also the relationships of load-mid-span deflection are coincident.

References

1- Bouazaouia L., Jurkiewiezb B., Delmasa Y., and Lia A., "Static Behavior of A Full-Scale Steel - Concrete Beam with Epoxy-Bonding Connection", Journal of Engineering Structures, Vol. 30, February 2008, pp. 1981-1990.

2- Prakhya K. V. G. and Adidam, S. R." Finite Element Analysis of Ferrocement Plates ", J. Ferrocement, No.17, 1978, pp. 313-320.

3- Bin-OMAR, A. R. H.H. Abdel- Rahman, G. J. Al-Sulaimani, " Nonlinear Finite Element Analysis of'Flanged' Ferrocement Beams ", Computers & Structures, Vol. 31, No. 4, 1989, pp. 581-590.

4- Boshra Aboul-Anen, Ahmed El-Shafey, and Mostafa El-Shami, " Experimental and Analytical Model of Ferrocement Slabs " , International Journal of Recent Trends in Engineering,Vol.1,No.6,May2009, pp. 25-29.

5- ANSYS, " Basic Analysis Guide", ANSYS Release 16.1, Inc, Copyrite ©2012.

6- ANSYS, " ANSYS Modelling and Meshing Guide", ANSYS Release 16.1, Inc, Copyrite ©2012.

7- Willam, K. J. and Warnke, E. P., "Constitutive Model for the Triaxial Behavior of Concrete", Proceedings, International Association for Bridge and Structural Engineering, Vol. 19, ISMES, Bergamo, Italy, 1975, pp.174.

8- Mottram, J. T., and Show, C. T., "Using Finite Elements in Mechanical Design". First Edition, McGrew-Hill Company, UK,1996.

University of Thi-Qar Journal Vol.14 No.3 SEP 2019
Web Site: https://jutq.utq.edu.iq/index.php/main
Email: utj@utq.edu.iq

تحليل الالواح المركبة من صفائح الفولاذ المضلعة والمربوطة بألواح الفيروسمنت باستخدام العناصر المحددة.

أ. د . نبيل عبد الرزاق جاسم [1]

م. محمد عبد الباقر جنام [2]

[1] أستاذ، قسم الهندسة المدنية، كلية الهندسة- جامعة البصرة، العراق.

[2] ماجستير هندسة مدنية، وزارة العدل ، العراق.

المستخلص:

يتضمن هذا البحث استخدام تقنية العناصر المحددة في التحليل الغير الخطي لسلوك الألواح المركبة المصنوعة من صفائح الفولاذ المضلعة والمربوطة بالواح الفيروسمنت. واستخدمت علاقات السلوك اللاخطي للفيروسمنت و صفائح الفولاذ المضلعة و شبكة التسليح. وتم اعتماد برنامجANSYS version 16.1 لتحليل النموذج الثلاثي البعد، و جرت نمذجة الفيروسمنت باستخدام عناصر من نوع SOLID 65 بثمانية عقد ونمذجة صفائح الفولاذ المضلعة بعناصر SHELL181 بأربعة عقد فقط. استخدم COMBIN14 لتمثيل سلوك البراغي المعدنية، ولمحاكاة طبقة الايبوكسي اللاصقة استخدام عنصر صلب SOLID185. أما شبكة التسليح فقد تمت نمذجتها كنسبة من الحجم ضمن عناصر الفيروسمنت.و تم افتراض ترابط تام بين الفيروسمت وشبكة التسليح .ووجد بان نماذج العناصر المحددة تعطي قيم للأحمال القصوى وللإزاحات ذات اتفاق جيد مع النتائج المختبرية.

University of Thi-Qar Journal Vol.14 No.3 SEP 2019
Web Site: https://jutq.utq.edu.iq/index.php/main
Email: utj@utq.edu.iq

Privacy Preserving Scheme for Online Image Sharing

Suhad Abbas Yassir
Southern Technical University, Shatra Technical Institute, Iraq
Suhadabbas@yahoo.com
سهاد عباس ياسر
الجامعة التقنية الجنوبية/ المعهد التقني الشطرة

Abstract:

This paper presents a privacy protection solution for online photo share by obscuring faces in images, which keeps persons anonymous. The proposed system contains two modules. The first is the face detection module to identify region of interest (ROI) which is faces. The second is a face encryption module, which encrypts the ROI pixels using keys so that the access to the faces is restricted. The face detection module uses skin color detector in YCbCr color space to detect skin areas in the image. Also, to overcome the illumination problems in color images, two color constancy methods were adopted for color correction and lighting of the input images. The edges of the image are utilized to separate the faces segments from the background or object that have similar skin color. Morphological operations such as erosion are applied to remove small areas and hole filling to remove any holes in the binary segments. In addition, the correct faces are located by using a set of features. The face encryption module uses two chaotic logistic maps. One map is used for shuffling the face area pixels and another map is used for encrypting the pixels. Both shuffling and encryption are done using a keys. The face detection was tested on Caltech face database and showed a high detection rate and can localize face under different illumination conditions. The experiments on face encryption showed satisfactory results in various tests in terms of key space, PSNR, MSE and entropy analysis.

Keywords: face detection; image encryption; photo sharing; privacy; chaotic cryptography

الملخص:

تقدم هذه الورقة حلاً لحماية الخصوصية لمشاركة الصور عبر الإنترنت من خلال إخفاء الوجوه في الصور ، والتي تبقي الأشخاص مجهولين. يحتوي النظام المقترح على وحدتين. الأول هو وهي الوجوه. والثاني هو وحدة تشفير (ROI) وحدة الكشف عن الوجوه لتحديد منطقة الاهتمام باستخدام المفاتيح بحيث يكون الوصول إلى الوجوه ROI الوجه ، والتي تقوم بتشفير بكسلات للكشف عن YCbCr مقيدًا. تستخدم وحدة الكشف عن الوجوه كاشف لون البشرة في مساحة لون مناطق الجلد في الصورة. أيضا ، للتغلب على مشاكل الإضاءة في الصور الملونة ، تم تبني طريقتين لثبات اللون لتصحيح الألوان وإضاءة الصور المدخلة. تُستخدم حواف الصورة لفصل مقاطع الوجوه عن الخلفية أو الكائن ذي لون البشرة المماثل. يتم تطبيق العمليات المورفولوجية مثل التعرية لإزالة المساحات الصغيرة وملء الثقب لإزالة أي ثقوب في الأجزاء الثنائية. بالإضافة إلى ذلك ، توجد الوجوه الصحيحة باستخدام مجموعة من الميزات. تستخدم وحدة تشفير الوجه خريطتين لوجستيتين فوضويتين. يتم استخدام خريطة واحدة لخلط وحدات بكسل مساحة الوجه ويتم استخدام خريطة أخرى لتشفير وحدات البكسل. تتم كل من خلط ورق اللعب والتشفير للوجه وأظهر معدل اكتشاف Caltech باستخدام مفاتيح. تم اختبار كشف الوجه في قاعدة بيانات مرتفعًا ويمكنه توطين الوجه تحت ظروف إضاءة مختلفة. أظهرت التجارب على تشفير الوجه نتائج مرضية في اختبارات مختلفة من حيث المساحة الرئيسية.

الكلمات المفتاحية: كشف الوجه؛ تشفير الصور مشاركة الصور؛ خصوصية؛ التشفير الفوضوي

1. Introduction

Due to the increased development of information technology and the widespread of digital contents, images can be frequently transmitted and stored over networks [1]. Users can use online social network (OSN) to share their images which includes Facebook and Twitter or image sharing platforms such as Flicker and Instagram. In Facebook, for instance, there are about 1.2 billion active user daily and near 300 million uploaded images every day [2]. The shared images can be easily browsed, downloaded or even used in inappropriate goals [3]. Secure image delivery is therefore becoming a great demand [4]. Encryption of images is a vital method for protecting image privacy in online communications. Many studies focused on protecting the privacy of image such as Lin et.

al [5]. He proposed a privacy protection system that can be used in mobile phones. It consists of three stages which are face detection, face recognition and face encryption. In the face detection state, the authors adopt the skin color mode which is based on YCbCr color to detect the faces. Then, for face recognition, facial features are extracted using local binary patterns (LBP) method. Extracted facial features are used as key for encryption and decryption. In the encryption stage, a special lookup table embedded with face features is used to hide the face area. Experimental results show that the proposed system can demolish the face details and the encryption time is fast. Cutillo et. al. [6] presented a method of protecting user privacy of images in online social networks (OSN). Firstly, all faces in in the images are automatically obscured and then if the user meets the access policy rule of a co-worker the co-worker's face in the image can be revealed, otherwise the face also is hidden. Experimental tests show that the proposed system scheme can protect the user's faces in OSN environment. Lawrence et. al. [7] came up with privacy protection technique based on skin color, principle component analysis (PCA) and DES algorithm. For face detection stage, the authors convert the input image into NCC color model to identify skin color and refined the resulting segments to localize the faces. The PCA is applied on the detected face to extract the feature vectors that used as encryption key. The detected face regions are encrypted using DES algorithm. Experiments tests show that the proposed system can detect and hide face area of the images. Khashan et. al. [8] proposed an encryption scheme for protection the privacy of images. The scheme has two stages which are face detection and face encryption. In the face detection step, the authors used OpenCV Haar cascade classifier to identify the face region in the input image. Next, Blowfish algorithm with 128-bit key is used to encrypt the detected faces in the image. Experimental results show that the proposed encryption scheme has a better encryption time in comparison to full encryption and it is suitable for real-time application. Zhang et. al. [9] presented a secure system for photo sharing and searching for mobile phones. The proposed system has several options, one of them is face obscuring choice. In that option, the user can choose the face area automatically or manually for preparing to

encryption. Then, the user has three options to encrypt the face area. The first choice (Mask) replaces the face pixels with zeros. The second choice (P3) encrypts the high frequency parts of the DCT coefficients. The third choice (Blur) uses a filter box to blur the face area. Experimental results indicate a fast communication and low computation overhead. He et. al. [10] proposed a secure image sharing technique based on encrypting region of interest (ROI) in the image. The proposed technique consists of two stages: ROI detection and distortion of ROI. In the ROI detection stage, the system can either automatically detect ROI such faces or manually by user. Next, the ROI encryption uses a key to encrypt DCT coefficients to hide detected ROI. The authors used 19,000 images to test the system performance. The tests showed that the system is effective for privacy protection and require small computation time. Li et. al. [11] presented a privacy protection scheme for secure image sharing in instant messaging platforms. The proposed system composed of three main stages. In first stage (face recognition); the system performs face recognition for all the faces in the input image. The second stage (face hiding) encrypts each recognized face with generated random key. The final stage (message dispatching) is used to send the encrypted images along with the encryption keys to the receivers. Performance analysis of the proposed system found that it is suitable for instant messaging system. In this paper, a privacy protection scheme for images is introduced. It divides the image into two parts: privacy part or referred to region of interest (ROI) and non-privacy part. The ROI is identified using face detection module that is based on skin color detection. Then, the localized faces is scrambled using two chaotic maps.

2. YCbCr Color Space

In YCbCr, Colors are represented in terms of luminance (Y channel) and chrominance (Cb and Cr channels) [12]. The linear transformations between RGB and YCbCr is expressed in Eq. (1).

$$\begin{aligned} Y &= (0.2989 * R) + (0.5866 * G) + (0.1145 * B) \\ C_b &= (0.1688 * \mathrm{R}) - (0.3312 * \mathrm{G}) + (0.5 * \mathrm{B}) \\ C_r &= (0.5 * \mathrm{R}) - (0.4184 * \mathrm{G}) - (0.0816 * \mathrm{B}) \end{aligned} \quad (1)$$

3. Logistic Chaotic Map

Logistic map is one of the simplest chaos functions that have been studied extensively for cryptographic systems [13]. The logistic map function can be expressed in Eq. (2).

$$X_{n+1} = ax_n \times (1 - X_n) \quad (2)$$

Where X(n) is the initial value that can be in interval (0,1) and (a) is the control parameter that lies in (0,4). The logic map behavior is shown in Fig. 1.

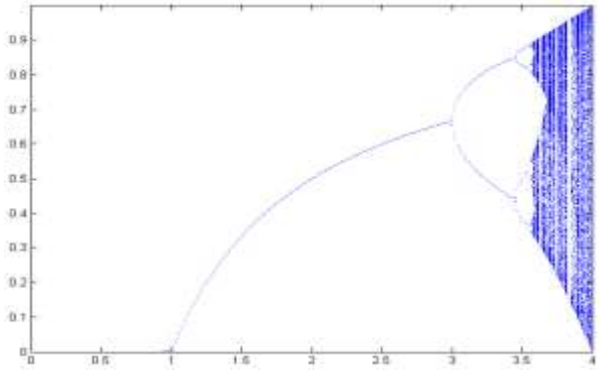

Fig. 1. Logistic map bifurcation [14].

4. Proposed System Layout

The proposed scheme consists of two main stages which are face detection and face encryption. The overall structure is illustrated in Fig 2.

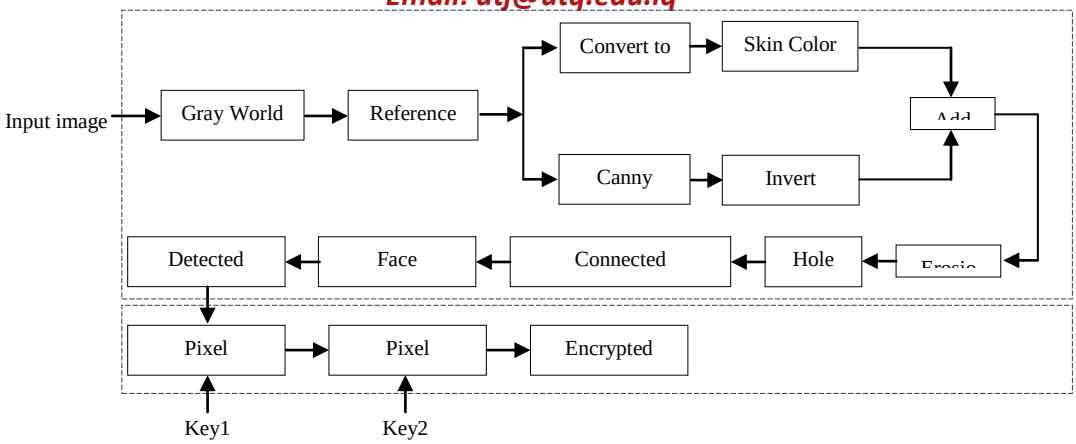

Fig. 2 Layout of the proposed privacy protection scheme

5. Face Detection

This section will discuss the different procedures in detail for the proposed face detection schemes.

5.1. Gray World Assumption

The skin color is usually affected by light condition in image which can lead to color deviation of the real skin color. Color constancy algorithm called Gray World Assumption (GWA) is used to perform color correction in images [15]. The GWA method can be defined in Eqs. (3-6).

$$R' = R \times \frac{K}{R_{average}} \quad (3)$$

$$G' = G \times \frac{K}{G_{average}} \quad (4)$$

$$B' = B \times \frac{K}{B_{average}} \quad (5)$$

$$K = \frac{R_{average} + G_{average} + B_{average}}{3} \quad (6)$$

Where $R_{average}$, $G_{average}$ and $B_{average}$ represents the mean of each color channel of the image. Fig. 3 shows the result of applying GWA on an image.

(a) (b)

Fig. 3 Gray World (a) Original image (b) Gray World image

5.2. Reference White

To detect faces under different lighting conditions, reference white scheme is utilized for illumination compensation. In this scheme, the top 5% of luminance values in the image is considered as the reference white in case of the number of pixels, is satisfactorily large (> 100). The RGB channels of the original image are adjusted so that the average gray value of the reference white pixels is scaled to 255 [16]. Reference white can be calculated according to Eqs. (7-8).

$$M_{top} = \sum_{i=l_u}^{255} i \times f_i / \sum_{i=l_u}^{255} f_i \quad (7)$$

$$X_{new} = X_{old} / M_{top} \times 255, where\ X \in \{R, G, B\} \quad (8)$$

Where i ∈ [*lu*,255] be the top 5% gray levels, *fi* is the pixel number with gray level *i* in an image. Reference white results is shown is Fig. 4.

Fig. 4. Reference white (a) Original image (b) Reference white image

5.3. Skin Color Detection

Skin color model can be constructed using a variety of color spaces, the YCbCr color model is the most common one [17]. To build this model, a set of skin patches is used for training the system. It consists of 110 images that have about (91,674) skin pixels. A sample of skin patches is shown in Fig. 5.

Fig. 5 Variety of skin patches

Each sample is converted to YCbCr color space. The mean and covariance between Cb and Cr is computed for all skin samples as shown in Eq. (9) and (10).

$$\sigma = \frac{1}{n}\sum_{k=1}^{n} x_k \quad (9)$$

$$\sum = \frac{1}{n}\sum_{k=1}^{n}(x_k - \sigma)(x_k - \sigma)^T \quad (10)$$

Where n is the number of skin samples, x_k is the vector representing the kth sample and σ and Σ are the mean vector and covariance matrix of the gaussian probability distribution function. The resulting probability density skin model can be represented by Eq. (11) and skin color distribution is illustrated in Fig. 6. Algorithm 1 explains the skin color training model.

$$p(x) = \frac{1}{(2\pi)^{\frac{d}{2}}|\Sigma|^{1/2}} \times exp\left\{-\frac{1}{2}(x-\sigma)\Sigma^{-1}(x-\sigma)^T\right\} \quad (11)$$

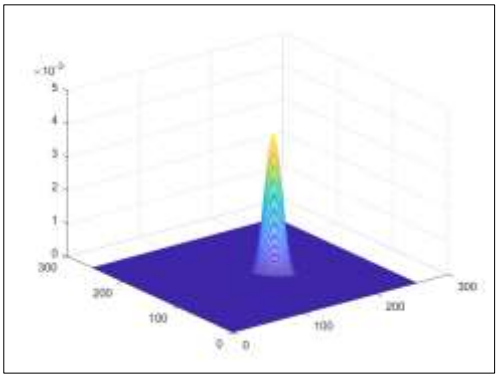

Fig. 6. Gaussian distribution in YCbCr color

Algorithm (1) skin color training

Input: RGB skin image sample
Output: Cbmean, Crmean and CbCrCov

1: Begin

2: Set Cb_sum ⇦ 0

3: Set Cr_sum ⇦ 0

4: Set N ← number of image samples

5: Loop k from one to the N

6: Set Img ← traing_img(k)

7: Set Cb(k) ← 0.1688 ×R- 0.3312×G+0.5 × B

8: Set Cr(k) ← 0. 5 ×R – 0.4184×G - 0.0816 × B

9: Set Cbmean ← Cbmean + Cb(k)

10: Set Crmean ← Crmean + Cr(k)

11: End k loop

12: For i from one to N

13: Set ← Sum_all = sum_all + (Cb(i) – Cbmean) × (Cr(i) – Crmean(i))

14: End For i

15: Set CbCrCov ← Sum_all / N

16: End

Applying equation (11) will result in grayscale image which is called skin likelihood image. Using thresholding process, it will be transformed into binary image with only 0 and 1. Fig. 7 shows the

resulting binary image of input image. Algorithm 2 shows the skin color detection function.

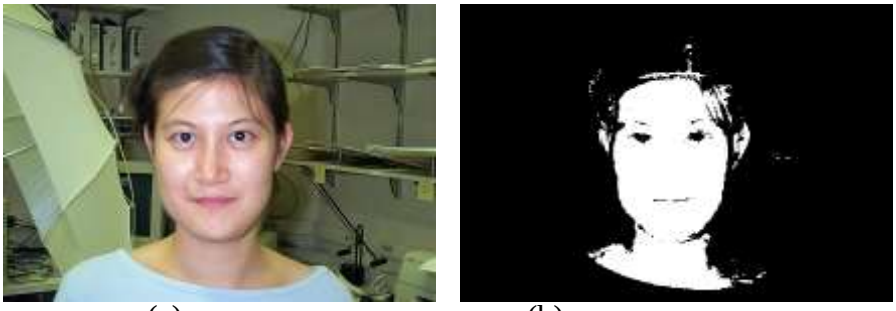

(a) (b)

Fig. 7. Skin color detection (a) input image (b) skin region in binary

Algorithm (2) skin color detection

Input: RGB image, Cbmean, Crmean and CbCrCov
Output: Binary Image

Begin

Set Col ← Number of Image Columns
Set Row ← Number of Image Rows
Set T ← Threshold
For i from one to Col
For j from one to Row
Set Cb ← 0.1688 ×R- 0.3312×G+0.5 × B
Set Cr ← 0. 5 ×R – 0.4184×G - 0.0816 × B
Set x ← [(cb-bmean); (cr-rmean)]
Set skinlikelihood (i,j) ← exp(-0.5 × x^T × inv(brcov) × x)
End i Loop
End j Loop
For i from one to Col
For j from one to Row
If Set skinlikelihood (i,j) > T
Bin_img(I,j) = 1
End if
End i Loop
End j Loop

End

5.4. Edge image with skin image combination

The most common face detection algorithms that are based on skin color can function well in case of images containing non-skin color background or the persons are wearing non-skin color cloths. An image containing similar skin color backgrounds or cloths can lead to identifying the entire region as skin segment [18] as shown in Fig. 8a. In such case, the candidate face region may merged with the background or any object with same skin color. Therefore, it is necessary to use a mechanism that it is able to separate the candidate face region from background region for easy face localization. To solve this issue, the edges of the image is combined with resulting binary image of the skin detector as in Fig. 8b.

(a) (b)

Fig. 8. (a) face segment connected with background (b) face segment disconnected from background

5.5. Morphological operations

Morphological operation such as erosion and hole filling are utilized for the skin area that are loosely connected. The morphological erosion is used to ensure that any is not connected to any other object or background in case of being not fully detached [19]. Then, morphological hole filling is applied to fill any holes found in the detected skin segments [20]. Next, connected component labeling is used for the resulting binary image to label all clustered pixels group [16] for further analyzing to determine whether it is face region or not as shown in Fig. 9.

Fig. 9 binary labeled image

5.6. Face Verification

This step is used to verify the labeled face segments in the binary image. It is an essential one as it filers the resulting face segments and

detects the correct face segments. Fig. 9 shows a binary image after applying the verification step. Usually, the verification process consists of several features which eliminate non-face segments including:

- **Area:**

The area refers to the number of pixels in a specific segment. Small segments are eliminated that which have area less than 5% of the total image as illustrated in Fig. 10.

Fig. 10. Face verification

- **Aspect ratio:**

The aspect ratio represents the maximum width of the face segment divided by the maximum height [21]. Any segment within the values of 0.5 to 0.9 is considered as a face segment according to the experiments.

- **Extent:**

The extent is calculated by Eq. (12). It was found that the extent between the range 0.5 to 0.9 is identified as face segments.

$$\text{Extent} = \frac{Area}{l1\ l2} \quad (12)$$

Where l1 and l2 are the maximum width and height respectively.

- **Ellipse Area:**

The elliptical area is computed according to Eq. (13). Experiments showed that ellipse area of segment between is 1.04 to 0.5 considered a face segment.

$$\text{Ellipse area} = \frac{4A}{\pi l1 l2} \quad (13)$$

After the face is detected, a boundary box coordinates is sent for the next stage which is face encryption.

6. Face Encryption

The localized faces in the image are passed into encryption stage. This stage performs the encryption by two methods which are pixel permutation followed by pixels encryption. Both steps use chaotic logistics maps to perform these tasks. The encryption steps are described as the follows:

Step 1: Input the detected face area coordinates in the image, key1,key2,

Step 2: Apply pixel permutation using chaotic logistic map as follows:

- Convert the face area image box into a 1D array of M×N.
- Generate chaotic sequences of length M×N using chaotic logistic map; key1 is used as the initial value and key2 used as the control parameter.
- Chaotic numbers are sorted in ascending order.
- Obtain the permutated face image box by mapping the value position of the face box to its corresponding index position in the sorted chaotic logistic map sequence.
- Convert the resulting face image sequence into a 2D array of (M×N).

The face permutation is explained in Algorithm 3.

Algorithm (3) Face area shuffling

Input: RGB image, Face coordinates, key1, key2
Output: Shuffled face

Begin

Set r ← key1
Set X(0) ← key2
Set Counter ← 0
Loop n from 0 to Number of image pixels
Set X(n+1) ← r × X(n) × (1-X(n))
Set Map(Counter) ← X(n+1)
Counter ← Counter + 1
End n Loop
Sort Ascending Index () ← Map()
// Store face area into 1D arrays
Set initial counter ← 0
Loop i from 0 to image width
Loop j from 0 to image height
Set 1DRed(counter) ← Red(i,j)
Set 1DGreen(counter) ← Green(i,j)
Set 1DBlue(counter) ← Blue(i,j)
Set Counter ← Counter + 1
End j Loop
End i Loop
// Shuffle pixels
Loop k from 0 to Number of pixels
Loop j from 0 to Number of pixels
If Map(k) = Index(j) then
Set sRed(k) ← aRed(j)
Set sGreen(k) ← aGreen(j)
Set sBlue(k) ← aBlue(j)
End if
End j Loop
End k Loop

End

Step 3: Perform pixel encryption using chaotic logistic map as bellow:

- Generate chaotic sequences of length M×N using chaotic logistic map; key3 is used as the initial value and key4 is used as the control parameter.
- Perform XOR operation between random numbers and the localized face pixels.

The face encryption process is described in Algorithm 4.

Algorithm (4) Face area ciphering

Input: Shuffled face area, Face coordinates, key1, key2
Output: encrypted face

Begin
46: Set r ← key1
47: Set X(0) ← key2
48: Set Counter ← 0
49: Loop n from 0 to Number of image pixels
50: Set X(n+1) ← r × X(n) × (1-X(n))
51: Set Map (Counter) ← X(n+1)
52: Set Counter ← Counter + 1
53: End n Loop
54: Loop i from 0 to image width : Loop j from 0 to image height
55: Set cRed(i,j) ← sRed(i,j) XOR MapSin (Counter)
56: Set cGreen(i,j) ← sGreen(i,j) XOR MapSin (Counter)
57: Set cBlue(i,j) ← sBlue(i,j) XOR MapSin (Counter)
58: Set Counter ← Counter + 1
59: End j Loop: End i Loop

End

7. Experimental Results

This section will discuss the experimental results for the face detection and face encryption.

7.1. Face detection results

To test the performance of the proposed face detection scheme, the Caltech face database [22] is used. It contains 450 images that have different illumination levels and variety of facial expressions from various locations. The image size is 896x592 and each image have one face.

MATLAB 2017a software is used for programming with Core i7-6500U CPU.

Table (1)
Face detection results

Total Faces	Detected Faces	Detection Rate
450	391	86.88%

Face detection results are shown in Table 1. Form the table, it is noted that the face detection shows satisfactory results. Fig. 11 shows a sample of face detector results of the proposed method. It can be seen that the proposed method can respond to different skin colors and less sensitive to skin like background. The proposed method detection results are compared with two other schemes and it has higher detention rate as shown in Table (2).

Table (2)
Face detection comparison

Method	Detection rate
Ban et. al [23]	65.4%
Khac et. al [24]	79.08%
Proposed	86.88%

7.2. Encryption analysis

In this section, some security analysis of the proposed algorithm will be discussed in terms of key space analysis, mean square error, peak signal-to-noise ratio and information entropy analysis. Four images were used to test the proposed scheme, as shown in Fig. 12.

Fig. 12 Test images. Original images Image_134, Image_157, Image_181 and Image_332 left column and encrypted face images for the same images in the right column.

7.2.1. Key space analysis

A good encryption algorithm must be sensitive to the secret keys and the key space must also be large enough to make the brute-force attacks difficult for intruders. In the proposed scheme, the initial conditions and control parameters for the chaotic logistic maps can be used as keys. If the single key size is 10^{14}, then the key space can be up to 10^{56} which it is larger than 2^{128}.

7.2.2. Mean Square Error and Peak Signal-to-Noise Ratio

The mean square error (MSE) is a mathematical measure that refers to the average squared difference between the original face image and the encrypted face image. It is computed by adding up the squared differences of all pixels of the image. Then, it is divided by the total number of pixels. The peak signal-to-noise ratio (PSNR) is utilized to obtain the differences between the original face image and the encrypted one. The main benefit of using PSNR is to point out the encrypted face area noise level. MSE and PSNR are expressed by Eqs. (14) and (15) respectively:

$$MSE = \frac{1}{M \times N} \sum_{i=1}^{M} \sum_{j=1}^{N} [f(i,j) - \hat{f}(i,j)]^2 \quad (14)$$

$$PSNR = 10 \log_{10} \left[\frac{max_f^2}{MSE} \right] \quad (15)$$

where f(i,j) is the original face image; $\hat{f}$(i, j) is the encrypted face image; M, N are the two dimensions of the face box image; and max_f is the maximum value of an image f. Table 3 demonstrates the MSE and PSNR results for the encrypted face images.

Table (3)

MSE and PSNR values for the encrypted image samples

Image Name	MSE	PSNR
Image_134	5934.5421	10.4309
Image_157	6331.1624	10.1160
Image_181	7762.0603	9.2310
Image_332	6109.6332	10.2707

7.2.3. Entropy Analysis

Information entropy is used to measure the randomness of a source. The information entropy referred to as H(X) is shown in Eq. (16):

$$H(X) = \sum_i p(x_i) \log_2 \frac{1}{p(x_i)} \quad (16)$$

where $p(x_i)$ denotes to the probability of the pixel value (x_i). If the probability of occurrence of each pixel value is the same, then value of the entropy must be 8. This will be the maximum entropy for an encrypted face image that has true uniform pixel distribution. Therefore, the higher entropy value of an encrypted image means that the proposed encryption algorithm is resistant against the entropy attack. Table 4 demonstrates the entropy values for the red, green and blue of the encrypted face images.

Table (4)

Entropy values for encrypted face images

Image Name	Red	Green	Blue
Image_134	7.7512	7.7651	7.7109
Image_157	7.7857	7.7772	7.7612
Image_181	7.7926	7.7532	7.7097
Image_332	7.7741	7.7833	7.7849

8. Conclusions

In this paper, a privacy protection scheme is presented. The proposed scheme has two stages, which are face detection and face encryption. In the face detection stage, skin color model in the YCbCr is used to detect the skin regions. In addition, the edges of the image are combined with the binary image to separate the face segment from the background or any other skin-like object. Then, a set of features is used to

discard non-skin segments. In the face encryption stage, two chaotic logistics map is used. One map is used for pixel permutation and another is used for pixel encryption. Face detection test showed that the detection rate is high and it is able to detect face under different illumination conditions. The face encryption analysis showed that the key space is large, MSE is high, PSNR is low and entropy is close to optimal. Based on these results, it can be concluded that the proposed scheme can provide a privacy protection for the transmitted images in social networks and photo sharing platforms.

References:

[1] S. K. Rajput and A. Konidena, "PERFORMANCE ENHANCEMENT IN IMAGE ENCRYPTION USING AES," *Int. J. Innov. Adv. Comput. Sci.*, vol. 4, no. 1, pp. 16–19, 2015.

[2] M. A. H. Al-Hamami, "A Proposed Framework for Photos Copyright Protection in Facebook," *Int. J. Comput. Appl.*, vol. 162, no. 1, 2017.

[3] K. Liang, J. K. Liu, R. Lu, and D. S. Wong, "Privacy concerns for photo sharing in online social networks," *IEEE Internet Comput.*, vol. 19, no. 2, pp. 58–63, 2014.

[4] J. Chen, Z. Zhu, C. Fu, H. Yu, and L. Zhang, "An efficient image encryption scheme using gray code based permutation approach," *Opt. Lasers Eng.*, vol. 67, pp. 191–204, 2015.

[5] C.-Y. Lin, C.-C. Chang, Y.-H. Chen, and P. Prangjarote, "Multimedia Privacy Protection System for Mobil Environments," in *2011 Seventh International Conference on Intelligent Information Hiding and Multimedia Signal Processing*, 2011, pp. 133–136.

[6] L. A. Cutillo, R. Molva, and M. Önen, "Privacy preserving picture sharing: Enforcing usage control in distributed on-line social networks," in *Proceedings of the Fifth Workshop on Social Network Systems*, 2012, p. 6.

[7] L. Y. Deng, D. L. Lee, and Y. Liu, "Face Recognition Lock," in

2013 International Conference on IT Convergence and Security (ICITCS), 2013, pp. 1–2.

[8] O. A. Khashan, A. M. Zin, and E. A. Sundararajan, "Performance study of selective encryption in comparison to full encryption for still visual images," *J. Zhejiang Univ. Sci. C*, vol. 15, no. 6, pp. 435–444, 2014.

[9] L. Zhang, T. Jung, C. Liu, X. Ding, X.-Y. Li, and Y. Liu, "Pop: Privacy-preserving outsourced photo sharing and searching for mobile devices," in *2015 IEEE 35th International Conference on Distributed Computing Systems*, 2015, pp. 308–317.

[10] J. He *et al.*, "Puppies: Transformation-supported personalized privacy preserving partial image sharing," in *2016 46th Annual IEEE/IFIP International Conference on Dependable Systems and Networks (DSN)*, 2016, pp. 359–370.

[11] F. Li, J. Yu, L. Zhang, Z. Sun, and M. Lv, "A privacy-preserving method for photo sharing in instant message systems," in *Proceedings of the 2017 International Conference on Cryptography, Security and Privacy*, 2017, pp. 38–43.

[12] S. L. Phung, A. Bouzerdoum, and D. Chai, "Skin segmentation using color pixel classification: analysis and comparison," *IEEE Trans. Pattern Anal. Mach. Intell.*, no. 1, pp. 148–154, 2005.

[13] N. Bigdeli, Y. Farid, and K. Afshar, "A robust hybrid method for image encryption based on Hopfield neural network," *Comput. Electr. Eng.*, vol. 38, no. 2, pp. 356–369, 2012.

[14] J. D. D. Nkapkop, J. Y. Effa, J. Fouda, M. Alidou, L. Bitjoka, and M. Borda, "A fast image encryption algorithm based on chaotic maps and the linear diophantine equation," *Comput. Sci. Appl.*, vol. 1, no. 4, pp. 232–243, 2014.

[15] K. H. Bin Ghazali, J. Ma, and R. Xiao, "An innovative face detection based on skin color segmentation," *Int. J. Comput. Appl.*, vol. 34, no. 2, pp. 6–10, 2011.

[16] W.-C. Hu, C.-Y. Yang, D.-Y. Huang, and C.-H. Huang, "Feature-based face detection against skin-color like backgrounds with

varying illumination," *J. Inf. Hiding Multimed. Signal Process.*, vol. 2, no. 2, pp. 123–132, 2011.

[17] M. V Daithankar, K. J. Karande, and A. D. Harale, "Analysis of skin color models for face detection," in *2014 International Conference on Communication and Signal Processing*, 2014, pp. 533–537.

[18] Q. Huynh-Thu, M. Meguro, and M. Kaneko, "Skin-color extraction in images with complex background and varying illumination," in *Sixth IEEE Workshop on Applications of Computer Vision, 2002.(WACV 2002). Proceedings.*, 2002, pp. 280–285.

[19] Q. Liu and G. Peng, "A robust skin color based face detection algorithm," in *2010 2nd International Asia Conference on Informatics in Control, Automation and Robotics (CAR 2010)*, 2010, vol. 2, pp. 525–528.

[20] F. Y. Shih, S. Cheng, C.-F. Chuang, and P. S. P. Wang, "Extracting faces and facial features from color images," *Int. J. Pattern Recognit. Artif. Intell.*, vol. 22, no. 03, pp. 515–534, 2008.

[21] H.-J. Lin, S.-H. Yen, J.-P. Yeh, and M.-J. Lin, "Face detection based on skin color segmentation and SVM classification," in *2008 Second International Conference on Secure System Integration and Reliability Improvement*, 2008, pp. 230–231.

[22] W. Zhang, B. Yu, G. J. Zelinsky, and D. Samaras, "Object class recognition using multiple layer boosting with heterogeneous features," in *2005 IEEE Computer Society Conference on Computer Vision and Pattern Recognition (CVPR'05)*, 2005, vol. 2, pp. 323–330.

[23] Y. Ban, S.-K. Kim, S. Kim, K.-A. Toh, and S. Lee, "Face detection based on skin color likelihood," *Pattern Recognit.*, vol. 47, no. 4, pp. 1573–1585, 2014.

[24] C. N. Khac, J. H. Park, and H.-Y. Jung, "Face detection using variance based Haar-like feature and SVM," *World Acad. Sci. Eng. Technol.*, vol. 60, pp. 165–168, 2009.